HeliX

Ahead of the curve

Alfred Gessow Rotorcraft Center

Department of Aerospace Engineering

University of Maryland

College Park, MD 20740, USA

Elizabeth Weiner, Graduate Student

James Lankford, Graduate Student

Bharath Govindarajan, Graduate Student

Erik Levin, Graduate Student

Nishan Jain, Graduate Student

Jaime Reel, Graduate Student

Tejaswi Jarugumilli, Graduate Student

Dr. Inderjit Chopra, Faculty Advisor

Benjamin Jimenez, Graduate Student

Dr. J. Gordon Leishman, Faculty Advisor

Zachary Kaler, Graduate Student

Dr. V.T. Nagaraj, Faculty Advisor

Team Contact Information

Team Leader: Elizabeth Weiner – weiner.elizabeth.a@gmail.com

Bharath Govindarajan – bharathmg@gmail.com

Nishan Jain – nishan@umd.edu

Tejaswi Jurugumilli – Jtsn423@umd.edu

Benjamin Jimenez – bjimene1@umd.edu

Zachary Kaler – zakkaler@gmail.com

James Lankford – lankford@umd.edu

Erik Levin – erikdlevin@gmail.com

Jaime Reel – jreel@umd.edu

Dr. Inderjit Chopra – chopra@umd.edu

Dr. J. Gordon Leishman – leishman@umd.edu

Dr. V.T. Nagaraj – vnagaraj@umd.edu

AHS Design Team

Alfred Gessow Rotorcraft Center

University of Maryland

College Park, MD 20742, USA

To the American Helicopter Society,

The University of Maryland Graduate Team hereby grants permission to the AHS to distribute this design report as they see fit.

Thank you,

UMD Design Team

ACKNOWLEDGMENTS

The University of Maryland graduate team wishes to acknowledge the following people for their assistance and guidance throughout this design process:

Professors:

Dr. Inderjit Chopra – Gessow Professor, Director of Alfred Gessow Rotorcraft Center (AGRC), Dept. of Aerospace Engineering, University of Maryland, College Park

Dr. J. Gordon Leishman – Minta Martin Professor of Engineering, Dept. of Aerospace Engineering, University of Maryland, College Park

Dr. Vengalattore T. Nagaraj – Senior Research Scientist, Dept. of Aerospace Engineering, University of Maryland, College Park

Dr. Omri Rand – Shirley and Burt Harris Academic Chair, Technion Israel Institute of Technology, Technion City, Haifa, Israel

Dr. Sudarshan N. Koushik – Assistant Research Scientist, Dept. of Aerospace Engineering, University of Maryland, College Park

Dr. Wei Hu – Faculty Research Assistant, Dept. of Aerospace Engineering, University of Maryland, College Park

Dr. Derek A. Paley – Associate Professor, Dept. of Aerospace Engineering, University of Maryland, College Park

Industry Professionals:

Dr. Ashish Bagai – Program Manager, Tactical Technology Office, Defense Advanced Research Projects Agency

Charley Kilmain – Director, Rotor and Drive System Design, Bell Helicopter Textron, Inc.

Olav Kaarstein – President, Direct of Research and Development, NODIN Aviation AS

Craig Renier – Pilot, Trooper 3, Maryland State Police Command, Frederick Section

Pat Engel – ORO Manufacturing Company

Fellow Graduate Students:

CPT Daniel R. Brown, Ananth Sridharan, Joseph Schmaus, Juergen Rauleder, William Staruk, Harinder Singh, Pablo Sztein, Graham Bowen-Davies, Conor Stahlhut

Contents

List of Tables

List of Figures

Adherence to the RFP Requirements

General Requirements	Design Point	Section
Long range capable	MGTOW Ferry Range at 6,000 m, ISA+15°C of 3,373 km (with fuel reserves)	3.5
Minimum cruise speed = 240 kts (123.5 ms^{-1})	MGTOW V = 283 kts	3.4
Three crew members	Three crew member stations	18.1
Average climb rate of 2,000 ft min^{-1}	Capable of an average of 2,408 ft min^{-1} from 1,500–6,000 m, ISA+15°C	3.4
Fleet rescue capability	Easily configurable, avionics options, search and rescue simulation	18.1, 13.2, 19
High autonomy	Avionics, self-deployed wing extensions	13, 8.6.1
Minimum useful load of 6 tons	Vehicle MGTOW is sized using this requirement	2.2
MGTOW of 15 tons	MGTOW = 15.3 tons	2.2
Performance Index (PI)	PI = 11.2	4
Stress level assessment of dynamic and static component*	FEA analysis on transmission gearing and wing	9

* Requirement for the graduate category

Mission Requirements	Design Point	Section
Start and warm up in 15 minutes	Engine choice	7.1
Takeoff at 1,500 m, ISA+15°C	Can hover at MGTOW at 2,526 m, ISA+20°, FM = 0.71 at 1,500 m, ISA+15°C	3.3, 5
Minimum 240 kts cruise speed at 6,000 m, ISA+15°C (Missions 1, 3)	Mission 1: V = 283 kts Mission 3: V = 317 kts	3.4
Load/Unload: 2 tons relief aid in 1 hour, 6 wounded in 30 mins	Aft-loading ramp, dual-operating winch/hoist, quickly reconfigurable interior	18.3, 18.4
Capability of rescuing 6 wounded	Maximum 18 victim rescue, vibration suppressing stretchers, medical aid configuration	18.4

1 Vehicle Configuration and Selection

1.1 Introduction

In response to the 2013 AHS Student Design Competition Request for Proposal (RFP), the University of Maryland (UMD) Graduate Team proudly presents the *HeliX*.

Global awareness of weaknesses in disaster relief efforts has greatly increased, stressing the need for an improved rescue aircraft. Because of the dynamic and unpredictable operating environments at disaster sites, a vertical takeoff and landing (VTOL) aircraft is needed. Hurricane Katrina and the 2008 Sichuan earthquake were two starkly different natural disasters, requiring rescue efforts that revealed significant weaknesses in the capabilities of modern VTOL aircraft, and provided compelling evidence that a more effective disaster response was necessary. The UMD Graduate Team has designed a variable-diameter tiltrotor to excel in all of these disaster environments. Through the course of this report, the Team will show that the *HeliX* is a superior aircraft solution and a necessity in the vertical lift community.

The RFP has specified three separate missions that require the vehicle to be easily and quickly reconfigurable. Because of the nature of the requirements and the need for multi-role capability, a variable-diameter tiltrotor (VDTR) configuration was selected. The VDTR configuration has a higher technology readiness level (TRL) than compound helicopters, demonstrates success as a transport in demanding operating environments, and is primed for improvements to meet the configuration's full potential.

1.2 Mission Requirements

The RFP requires that the *HeliX* works as a part of a fleet, and that it completes three particular mission profiles to assert its versatility in critical life-saving situations.

1.2.1 Mission 1: Fast Deployment and Rescue Coordination – Aerial Triage

Because of the unpredictable nature of disasters, it is important to plan a course of action. The first mission that the *HeliX* must be able to perform is aerial triage. The RFP requires that the vehicle must takeoff at 1,500 m, ISA+15°C and then climb at an average rate of climb of 10.2 m s^{-1} (2,000 ft min^{-1}) to an altitude of 6,000 m, ISA+15°C. Once at this altitude, the vehicle must then accelerate to at least 240 kts (444 km hr^{-1}) and travel a total distance of 600 km (324 nm), minus the distance traveled during the acceleration and climb phases. Once the vehicle has reached its destination, it must descend to an altitude of 2,000 m and then perform a low-speed loiter at 120 kts (222 km hr^{-1}) for 2.5 hrs (equivalent to approximately 600 km). During this loiter period, the pilot and crew will assess the nature of the disaster to determine the extent of the help required, as well as share data and images with the relief operation commander, as discussed further in Section 19. After this assessment, the vehicle will again climb to 6,000 m and fly at a minimum airspeed of 180 kts (333 km hr^{-1}) back to base. With the information provided by the aerial triage team, the remainder of the fleet must be able to carry out the relief missions, as required.

1.2.2 Mission 2: Aid Distribution

The second mission that the *HeliX* must be able to accomplish is one of aid distribution. This mission consists of providing medical aid such as water, food, and clothing to the most serious victims. The RFP requires that the *HeliX* takeoff and climb from 1,500 m, ISA+15°C to 6,000 m, ISA+15°C, as before, but carrying 2 metric tons (4,409 lbs) of relief material. The aircraft must then fly for 600 km at a minimum speed of 180 kts, and once the destination has been reached, again descend to 2,000 m, ISA+15°C. The vehicle must then loiter at 80 kts (148 km hr^{-1}) to deliver the material. The crew is allowed one hour to distribute the aid as needed, after which the aircraft must again climb to

6,000 m, ISA+15°C and return to base at a minimum airspeed of 140 kts (259 km hr^{-1}).

1.2.3 Mission 3: Search and Rescue – Evacuation of Casualties

The third mission consists of evacuating the most seriously injured people to the operations base, where they can then be transported to nearby hospitals by other vehicles. This mission requires the vehicle to takeoff at 1,500 m, ISA+15°C, climb to 6,000 m, ISA+15°C, accelerate to 240 kts and travel approximately 600 km at this airspeed. Once at the destination, the vehicle will descend to 2,000 m, ISA+15°C and land. A minimum of six victims will be brought on board within a 30 minute timeframe, after which the aircraft will again takeoff and climb to 6,000 m and return to base at an airspeed of 240 kts.

1.2.4 Additional Considerations

Although the three missions are very different, there are a number of RFP requirements that are not explicitly stated within the individual mission descriptions, but are common to all three. During each mission, the crew will only consist of three. Additionally, the vehicle must be sized to have a minimum useful load of 6 tons (13,228 lbs), which will be discussed in detail in Section 2.2, to provide for a wide range of future missions.

The design driving factors for each mission were identified and assessed to determine what capabilities would ensure that *HeliX* exceeded all expectations during its missions. For example, Mission 1 requires that the vehicle have a minimum range of 1,800 km (972 nm), of which a two thirds is at an altitude of 6,000 m, ISA+15°C. As shown in Fig. 1.1, no current rotorcraft in this weight class is capable of exceeding this distance at mean sea level (MSL), let alone the altitudes specified in the RFP. After the vehicle sizing, as discussed in Section 2, the *HeliX* was shown to be capable of achieving a range of 1,819 km (with reserves) at MSL. Another factor with substantial influence in the design process was the vehicle speed. In Missions 1 and 3, the aircraft must achieve a minimum cruise speed of 240 kts. While the RFP emphasizes forward flight capability, it is noteworthy that none of the missions explicitly require any extended hovering flight time.

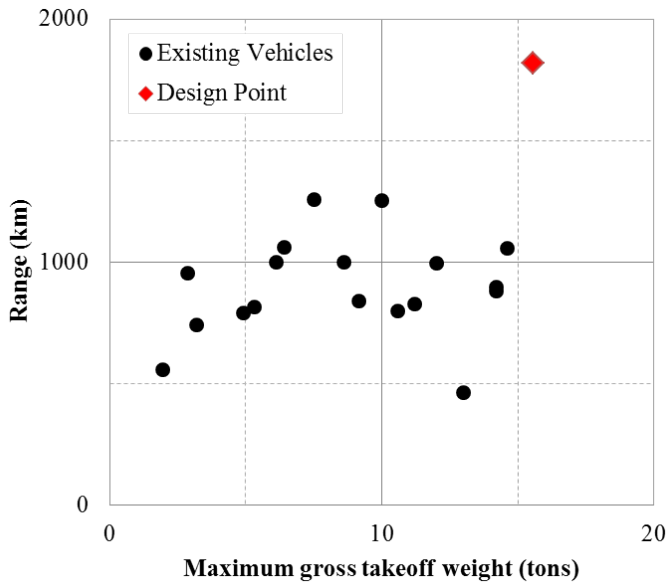

Figure 1.1: Range versus maximum gross takeoff weight for existing medium weight class VTOL platforms

1.3 Examination of Different Vehicle Configurations

In this section, the rationale for the selection of a VDTR concept to fulfill the requirements of the RFP is discussed, including thorough evaluation of alternative configurations. The key design requirements focused on the need for a high-speed vehicle capable of flying relatively long distances under hot-and-high conditions.

1.3.1 Conventional Helicopters

The first design considered was the conventional single main rotor (SMR) helicopter with a tail rotor, Fig. 1.2(a). The SMR offers the advantages of a low empty weight fraction, good endurance capabilities and mechanical reliability, and has relatively low production and maintenance costs. SMR helicopters, however, have poor range efficiency and limited forward speed. Forward speed is typically limited by retreating side blade stall and advancing side drag rise (compressibility effects). Because of the limitations on both speed and range, the SMR helicopter concept was not considered as a solution for meeting the requirements of this RFP.

(a) Sikorsky UH-60 Black Hawk

(b) Boeing CH-47 Chinook

Figure 1.2: Configuration examples: a) Conventional single main rotor helicopter b) Tandem helicopter

1.3.2 Tandem Rotor Helicopters

The tandem rotor configuration uses two rotors, with one situated at the front and the other at the rear of the helicopter, Fig. 2.2(b). These designs are typically used for carrying larger payloads because of their wide range of center of gravity travel. These helicopters generally have a low downwash, a low empty weight fraction, and a large amount of open cabin space. However, because of their relatively higher parasitic drag, which results in much lower cruise speeds and poorer fuel economy, this configuration was determined to be unsuitable for meeting the requirements of the RFP.

1.3.3 Compound Helicopters

When considering compound helicopters, the Team considered propulsive augmented configurations, like the Sikorsky X-2, as well as lift and propulsive augmented designs such as the Eurocopter X^3, see Fig. 1.3. While no compound helicopters are currently in full production, the apparent success of these two demonstrators has required a detailed examination of the potential of these configurations.

Implementing either lift or propulsive augmentation, or even both, allows these vehicle to fly much faster than a conventional SMR helicopter, but this speed comes at some cost. Compound helicopters tend to have a higher empty weight fraction and increased power requirements. In the case of the X-2, the higher forward speed is achieved by the pusher propeller. Retreating blade stall and drag divergence are avoided by slowing the rotor as well as implementing the Advancing Blade Concept (ABC). The ABC consists of two stiff contra-rotating rotors. Not only does this coaxial configuration eliminate the need for an anti-torque method (i.e., a tail rotor), it offloads the retreating blades at higher forward flight speeds because most of the lift is carried by the advancing sides of both rotors.

The Eurocopter X^3 uses wings to offload the rotor, the rotor also being slowed to avoid drag rise at higher airspeeds. Propulsion is achieved with the use of two tractor propellers, located on the wing of the vehicle, which also provide the necessary anti-torque and directional control.

Ultimately neither of these previous designs were chosen because of two major considerations: the lack of proven scalability, as well as the danger that ground level propellers pose to victims who are being evacuated, as required in Mission 3. Because this vehicle is being designed to be a search and rescue (SAR) aircraft with a crew of three, it would be safer to keep blades as far away from the ground as possible to minimize the danger to victims who may approach the vehicle unsupervised. Additionally, because of the size considerations of the design it was difficult to justify the scaling of a coaxial rotor design that had a low drag hub faring, and blades that were both large and stiff enough to avoid static droop and prevent inter-blade collisions.

(a) Sikorsky X-2 Demonstrator (b) Eurocopter X^3

Figure 1.3: Compound helicopter platforms: a) Thrust compounded b) Full compounded

1.3.4 Experimental Designs

Designs such as the AWI ”Project Zero” aircraft were also considered, but were not deemed suitable for the needs of the RFP because of the relatively high empty weight fraction and lack of proven mission capability. These types of designs, although novel and exciting for the rotorcraft community, are not at a technology readiness level where they could be considered viable to meet the requirements of this particular RFP.

1.3.5 Convertible Rotorcraft

The last design group considered were convertible rotor vehicles, such as tiltwing and tiltrotor concepts. The main advantage of these configurations is their ability to takeoff vertically like a conventional helicopter, and then transition into forward flight like an airplane. This capability allows for the aircraft to achieve much higher forward speed flights and operational altitudes than all of the other configurations previously discussed.

It was decided that because of the handling quality problems that are often associated with low-speed transition flight, as well as increased weight and complexity of rotating either the entire wing or even a portion of it, the tilt wing concept was not as strong a contender. The tiltrotor on the other hand, has proven to be a vehicle that can achieve higher airspeeds, and long flight ranges. Tiltrotors are unique in the sense that they fill a niche in the aircraft community and are well suited to perform missions that necessitate high cruise speeds, long range capabilities, and high altitude flight. Their added capabilities of vertical takeoff and hover allow them to operate in disaster situations where landing strips are unavailable. However, they are more mechanically complex and their design is also much more involved. In fact, there are many unique trades in their design, which will be discussed throughout this report.

The design of the *HeliX* goes above and beyond the capabilities of conventional tiltrotor designs with the use of two novel concepts: 1) A variable diameter rotor (VDR) which gives increased efficiencies in both hover and forward flight, and 2) outboard wing extensions (OWEs) that significantly increase the aspect ratio of the wing as well as provide additional lift.

1.4 Analytical Hierarchy Process and House of Quality

The most important questions the design team addressed at the beginning of the design process were: what are our customer needs and what design choices are necessary to meet those needs? To evaluate the different concepts and determine which configuration best satisfied the requirements of the RFP, the team went through a comprehensive analysis in which an Analytical Hierarchy Process (AHP) matrix and then a House of Quality diagram were generated.

Table 1.1: AHP prioritization matrix for configuration selection

Prioritization Matrix	Cruise speed	Range	Hover Efficiency	Vibration	Useful load Fraction	Reliability and Safety	Cost	Pilot Workload	Eigenvector
Cruise Speed	1.00	1.00	3.00	4.00	2.00	3.00	4.00	3.00	0.24
Range	1.00	1.00	2.00	4.00	2.00	3.00	4.00	3.00	0.23
Hover efficiency	0.33	0.50	1.00	3.00	0.50	2.00	4.00	2.00	0.13
Vibration	0.25	0.25	0.33	1.00	0.30	0.50	1.00	1.00	0.05
Useful Load Fraction	0.50	0.50	2.00	3.00	1.00	3.00	3.00	2.00	0.16
Reliability and Safety	0.33	0.33	0.50	2.00	0.33	1.00	3.00	1.00	0.08
Cost	0.25	0.25	0.25	1.00	0.33	0.33	1.00	0.33	0.04
Pilot Workload	0.30	0.33	0.50	1.00	0.50	1.00	3.00	1.00	0.08

The AHP is a technique that uses pair-wise comparisons between competing configuration choices to select the best option, both subjectively and objectively. Based on the RFP, seven different design criteria were chosen: speed, range, hover efficiency, vibration, useful load fraction, reliability, and cost. These criteria were compared to each other to determine their relative importance and these results are shown in Table 1.1. It should be noted that the outcome of this matrix does not reflect that any one of these figures of merit is unimportant.

Another way to visualize the ranking of these criteria is through a spider diagram, which is shown in Fig. 5(a). Each of the criteria is placed along one of the axes and the farther along the axis a point is placed, the more important it is. Based on this diagram, it is clear that both speed and range were considered highly important for the missions of this RFP. By applying the prioritization matrix to different vehicles, the team was able to objectively determine what vehicles would best achieve the goals set forth by the RFP. As shown in Fig. 1.4, after the ranking was complete, the full compound and convertible rotor platforms were very closely ranked. The spider diagram in Fig. 5(b) shows, however,

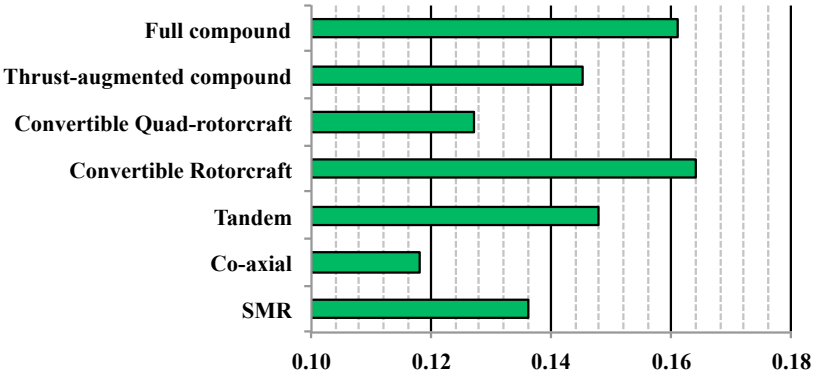

Figure 1.4: Normalized results of configuration selection using the Analytical Hierarchy Process

that the convertible platform ranked higher in both range and speed, the two most important design considerations in this case. Although the hover efficiency was better for the full compound design, factors such as useful load fraction for transport of relief material, and lower vibrations for more comfortable patient transport, confirmed the decision that a tiltrotor concept best met the requirements of this RFP.

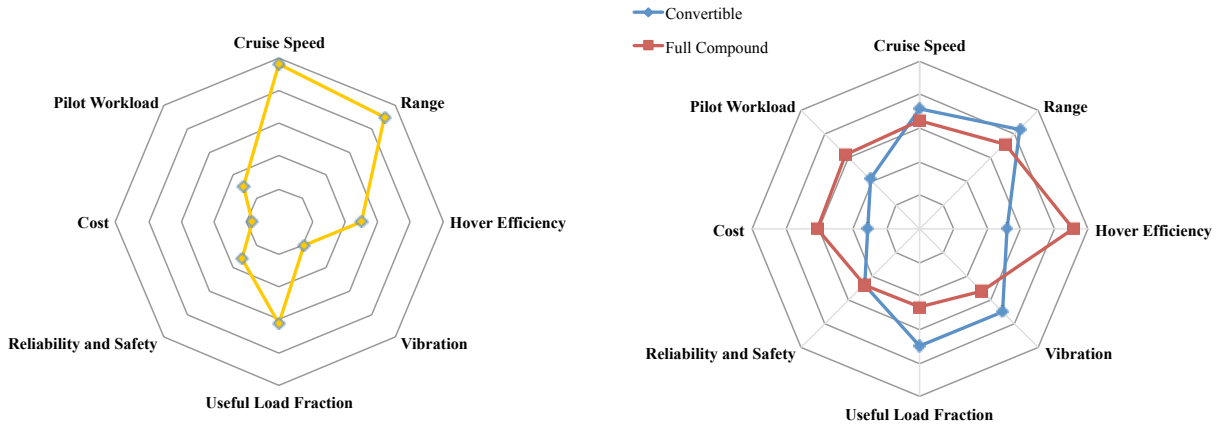

(a) Spider diagram for criteria ranking

(b) Spider diagrams for two configurations

Figure 1.5: Spider diagrams depicting relative importance of operational and vehicle needs

The House of Quality, shown in Fig. 1.2, considers the engineering design aspects that would be needed to meet the requirements of the RFP. This diagram allowed the team to focus on key concepts that had to be addressed during the design process.

Although no aspect of the design is unimportant, the HOQ matrix makes it clear that to best satisfy the customer, mechanical configuration factors such as engine type, transmission design, and avionics would play a critical role in the ability of the *HeliX* to meet the customer's needs. From an aerodynamic perspective, the wing and rotor design are also important. The design criteria that emerged from the AHP and HOQ matrices provided significant guidance throughout the course of the design.

Table 1.2: House of Quality matrix for configuration selection

			Aerodynamic Performance																Mechanical Configuration										Fuselage				Safety and Reliability			
															Blade design																						
			Empty weight fraction	Hub design		Disk loading	Power loading	CT/sigma	Autorotative index	Tip speed	Wing Design		Aerodynamic	Structural	Fuselage drag	Engine Type	Auxillary Fuel storage method	Transmission design	Avionics	Material Selection	Landing gear configuration	Vibration suppression devices	Loading/Unloading mechanism	Loading accessibility	Internal Cabin Design/Cabin Modularity	Fuselage Vertical Download	Cockpit design	HUMS	Crashworthy structure	MEDEVAC equipment				
		Weights (1-5)		Hub Drag	Hub Configuration																															
0 - No-Minimal relation 1 -Medium relation 2 - Highly Related																																				
Operational requirements	Hover at 3000 m, ISA + 20°C	5	1	0	2	2	2	1	1	2	2	1	1	1	0	0	1	0	0	0	0	0	0	0	0	0	0	0	0	0	0	0	52	11
	Range: 1800 km	5	2	0	0	0	0	0	0	1	2	1	1	1	0	2	2	2	0	0	2	0	0	0	0	0	1	0	0	0	0	0	0	0	0	0
	Cruise speed: 240 kts	5	0	0	0	1	2	2	0	2	2	1	1	1	0	0	2	2	0	0	2	2	0	0	0	0	1	0	0	0	0	0	0	0	0	0
	FF(cruise) at Max Density Altitude: 6000 m, ISA + 15°C	5	0	1	0	1	2	1	0	1	1	0	1	0	1	2	1	1	0	0	1	2	2	1	0	0	0	0	0	0	0	0	0	0	0	0
	Min Rate of Climb: 2000 ft/min	5	0	1	0	2	2	1	0	0	1	0	1	1	0	2	1	1	0	0	1	0	0	0	0	0	0	0	0	0	0	0	0	0	0	0
	Max TOGW: 15 tons	4	2	1	0	0	0	0	0	0	1	0	0	0	0	2	2	2	0	2	1	0	0	0	0	0	0	0	0	0	0	0	0	0	0	0
	Multi role capability	4	1	0	0	0	0	0	0	0	0	0	0	1	0	2	0	0	2	0	0	0	0	0	0	0	0	0	0	0	0	0	0	0	0	0
	Useful load: 6 tons	5	2	0	0	0	0	0	0	0	0	1	0	0	0	2	1	1	0	0	0	0	0	0	0	0	0	0	0	0	0	0	0	0	0	0
	Capable of takeoff within 15 minutes	5	0	0	0	0	0	0	0	0	0	0	0	0	0	2	2	1	0	2	0	0	1	0	0	0	0	0	0	0	0	0	0	0	0	0
	PAX: 3 crew + 6 wounded	5	0	0	0	0	0	0	0	0	0	0	0	0	0	0	0	0	0	0	0	0	2	1	0	2	1	0	0	0	0	0	0	0	0	0
	Load/unload supplies	5	0	0	0	0	0	0	0	0	0	0	0	0	0	0	0	0	0	2	0	0	2	0	0	0	0	0	0	0	0	0	0	0	0	0
	Ability to operate within a fleet	4	0	0	0	0	0	1	0	0	0	0	0	0	0	0	0	0	0	0	0	0	0	0	0	0	0	0	0	0	0	0	0	0	0	0
Design Considerations	Noise requirements	4	1	0	1	0	0	1	0	2	0	0	2	2	1	2	0	0	0	0	0	0	0	0	0	0	0	0	0	0	0	0	0	0	0	0
	Vibration levels	4	0	1	2	0	0	1	0	2	1	0	2	2	1	2	0	0	0	0	0	0	0	0	0	0	1	0	0	0	0	0	0	0	0	0
	Operation in devastated/ground inaccesible areas	4	0	0	0	2	0	1	0	0	0	0	1	1	0	0	1	0	2	1	2	0	1	0	0	0	0	2	0	2	1	0	18	27		
	SAR equipment and medical aid accommodation	5	2	0	0	0	0	0	0	0	0	0	0	0	0	0	1	1	2	2	1	2	2	1	2	0	0	1	0	0	2	0	26	25		
	Pilot workload	4	0	0	1	0	0	1	2	0	0	0	0	0	0	0	0	0	2	2	1	1	1	1	2	0	0	2	0	0	2	0	71	4		
Costs and development	Maintenance and operational costs	4	0	0	2	0	0	0	0	0	1	0	0	0	2	0	2	1	2	2	2	2	2	1	0	0	0	0	0	0	1	0	34	23		
	End of life recyclability	2	0	0	1	0	0	0	0	0	0	0	0	0	2	0	2	1	2	2	2	0	0	0	0	1	0	0	0	0	0	0	59	9		
	Manufacturing costs	2	0	0	2	0	0	0	0	0	1	0	2	2	0	2	1	2	1	2	1	1	1	0	1	0	0	0	0	0	0	0	31	24		
Safety	Autorotation capability	4	0	0	0	2	2	0	2	2	1	1	1	2	0	0	0	0	0	1	0	0	0	0	0	0	0	0	0	0	0	0	49	17		
	Crashworthiness	3	0	0	0	0	0	0	0	0	1	0	0	0	0	0	1	2	0	2	2	2	0	0	0	0	0	0	0	0	0	0	65	8		
	Survivability	3	0	0	1	0	0	0	0	0	1	0	0	0	0	0	1	0	0	2	2	0	0	0	0	0	0	0	0	1	0	0	52	11		
	Mean time between repairs/failures	2	0	0	2	0	0	0	0	0	0	0	2	2	0	0	2	0	2	1	1	1	0	0	0	0	0	0	0	2	0	0	82	3		
	Proximity awareness system	4	0*	0	0	0	0	0	0	0	0	0	0	0	0	0	0	0	0	0	0	0	0	1	0	0	0	0	0	0	0	0	51	13		
Rawscore		102	47	38	37	50	50	45	21	54	69	51	51	66	38	97	69	85	82	51	65	52	49	31	59	34	71	26	18	27						
Rank			18	20	22	15	15	19	26	10	5	13	7	20	1	5	2	3	13	8	11	17	24	9	23	4	25	11								

2 Tiltrotor Sizing

The *HeliX* was designed to achieve relatively high forward airspeeds as well as having good hovering efficiency with significantly lower power requirements at "hot-and-high" conditions compared to other rotorcraft in the same weight class. As a VDTR concept, the *HeliX* is a hybrid between a fixed-wing aircraft and a conventional helicopter. A modified sizing method based on Ticshchenko's original helicopter methodology [1] was used to size the *HeliX* to provide estimates of the vehicle weight and its power requirements. This sizing method was applied to the missions of the RFP with the most demanding flight requirements in terms of maximum gross takeoff weight (MGTOW), installed power, and fuel required. Trade studies were conducted to examine the merits of varying proprotor blade radius and aspect ratio, rotor disk loading, tip speeds, and number of blades. From these trade studies, an initial vehicle design was obtained.

2.1 Description of the Sizing Algorithm

Tishchenko's method is constituted of basic methodologies and algorithms centered around historic data that have been extensively validated for determining the size and weight of a helicopter. While this methodology is fairly general in its applicability to most rotorcraft concepts, several modifications were necessary to provide the flexibility needed to design tiltrotor configurations. The missions outlined in the RFP were first decomposed into mission segments, as shown in Fig. 2.1, and the sizing method was used to compute the power requirements and fuel quantity required to complete each segment of the defined mission. It was also necessary to account for the change in relevant equations for the power required in forward flight when in helicopter/hybrid mode (e.g., the loiter segment of Mission 1 and 2) or full airplane mode (e.g., the cruise segments of every mission).

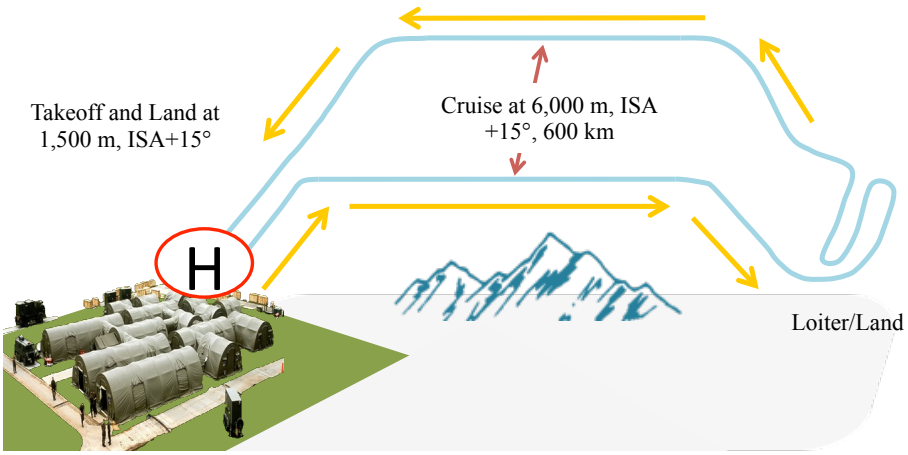

Segment	Requirement
1	Start and warm up at 1,500 m ISA+15°
2	Climb to 6,000 m, ISA +15°
3	Accelerate and cruise 600 km
4	Descend
5	Loiter/Land (mission specific)
6	Takeoff and/or climb
7	Accelerate and cruise 600 km
8	Descend and land

Figure 2.1: Generalized mission profile

The component weight equations in Tishchenko's method were replaced with the equations used in NASA Design and Analysis of Rotorcraft (NDARC) methodology [2]. The NDARC equations account for, amongst other things, wing-related items that are sized based, in part, on the structural stiffness requirements needed for propeller-based aircraft. This methodology also accounts for the spinner, which is used to reduce the hub drag in forward flight. A detailed list of the component weights comprising the aircraft empty weight are given in Section 11. Because the RFP does not require the installation of any specific engine, a "rubber" engine model was used and the engine characteristics were defined based on the AHS's 2007 student design competition RFP engine model [3]. The engine weights, specific fuel consumption, and the preliminary dimensions of the engine, were also obtained from the 2007 AHS RFP engine model.

A schematic of the design algorithm is shown in Fig. 2.2. The process is iterative and begins with the specification of particular mission requirements, including the desired range, payload, and cruise speeds, as well as the operational altitudes and atmospheric conditions. Estimated initial values of proprotor figure of merit, propulsive efficiency, transmission efficiency, engine installation losses, aspect ratios of the wing and blades, propotor disk loading, hover tip speeds, and number of blades are also required. These parameters are, however, changed during the design iterations to obtain the vehicle with the best efficiency in hover and forward flight, as explained in Section 5.

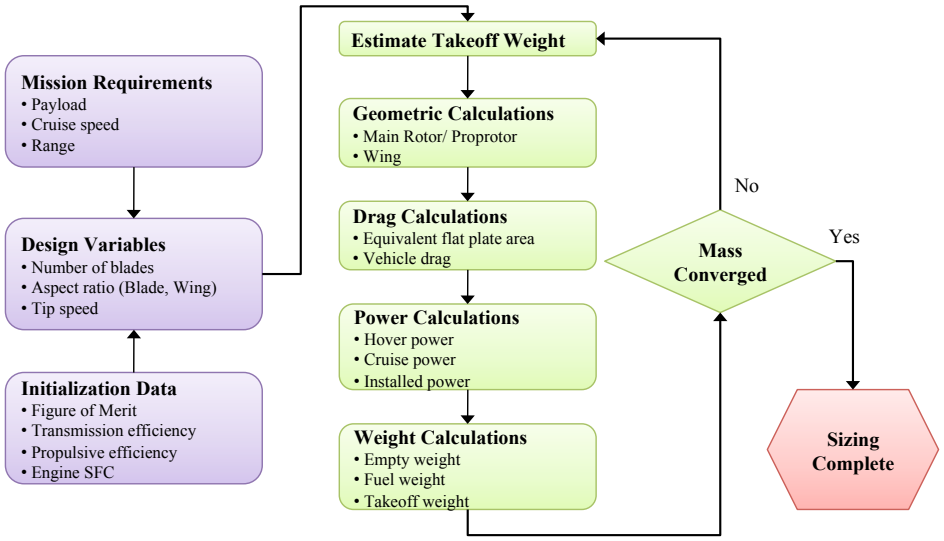

Figure 2.2: Flowchart for the vehicle sizing procedure

The steps in the sizing procedure, which is referred to as the UMD sizing methodology, are carried out as follows:

1. Mission requirements are specified and initial vehicle characteristics are provided.
2. An initial estimate is made for the MGTOW of the vehicle to be designed based upon historical data.
3. From the disk loading desired in hover, the proprotor diameter is calculated.
4. With the user defined blade aspect ratio and the proprotor diameter, the blade chord is computed.
5. The power required in hover is based on the MGTOW, disk loading, figure of merit, and the vertical download on the vehicle in hover.
6. The wing span is calculated based on geometric constraints, which include the proprotor diameter, an estimate for the fuselage width, and the necessary spacing between the proprotors and the fuselage for reasons of operational safety. With the aspect ratio of the wing defined, the wing chord is also determined.
7. The estimated parasitic drag area, discussed in Section. 3.1, in conjunction with the wing dimensions, are used to calculate the cruise power requirements. Because of the relatively high cruise altitude requirement specified in the RFP (density altitude of 6,515 m or 21,373 ft), the cruise power also determines the installed power available at mean sea level (MSL) ISA conditions.
8. Based on the power requirements in each segment of the mission, the total mass of fuel required is calculated, including IFR reserves (30 mins) based on FAR Sec. 91.167, Part(a)(3).
9. The empty weight equations are used to estimate the total empty weight.
10. The MGTOW obtained at the end of each iteration is used as a starting point for the next iteration.

The above procedure is repeated until convergence is obtained, based on the relative error between the initial and final value of the MGTOW. This procedure was carried out for all three missions of the RFP to determine the sizing of the vehicle.

Sizing results from the UMD sizing methodology were also validated by using NDARC directly. Inputs to NDARC consist of a sizing task followed by off-design mission descriptions for performance analysis. Mission 1, which was also the sizing mission, was used as the input in this case. Results from the UMD sizing method were found to agree closely with the results from NDARC; the values of empty weight, MGTOW, and the cruise power predicted by the UMD sizing methodology were within 5% of those from NDARC. These results established confidence in the UMD sizing methodology.

Once the aircraft was sized, NDARC was also employed for the off-design mission analysis. For this purpose, Missions 2 and 3 were specified in NDARC with fixed sizing data as inputs. The off-mission analysis, not shown, also gave comparable results; the outbound and return cruise power requirements predicted by the UMD sizing methodology were found to be within 9% of the corresponding values obtained from NDARC.

Table 2.1: UMD versus NDARC sizing comparison for sizing mission

Attributes	UMD	NDARC	% Deviation
Payload (lb)	6,245	6,245	–
Empty Weight (lb)	20,212	19,901	-1.6
GTOW (lb)	33,641	34,414	2.3
Mass of Fuel (lb)	6,983	7,588	8.0
Cruise Power to Destination (hp)	3,275	3,429	4.5
Cruise Power on Return (hp)	2,049	2,098	2.3

2.2 Vehicle Sizing Considerations

Before trade studies were conducted to determine the optimal set of blade parameters, an analysis was conducted using the UMD sizing methodology to determine the most demanding mission profile. The RFP, however, only indirectly specifies a payload for each mission. Excluding the three crew members that are required for all missions, Mission 2 (aid distribution) specifies a payload of 2 tons in the form of food, medical care, etc., and Mission 3 (search and rescue) requires the accommodation of 6 victims. The mission with the highest vehicle MGTOW and power requirements determined the vehicle sizing.

Table 2.2 shows the variation of MGTOW, installed power, fuel required, and useful load for each of the three missions. Mission 2 was the mission that set the most demanding flight requirements and would, therefore, qualify as the primary sizing mission. However, in no mission scenario is the requirement of a 6 ton useful load, as specified in the RFP, necessary.

Table 2.2: Sizing without consideration of the 6 ton useful load requirement

	MGTOW (kg)	Installed power (kW)	Payload (kg)	Fuel weight (kg)	Useful load (kg)
Mission 1	8,054	3,537	472	1,701	2,231
Mission 2	12,008	4,641	2,472	1,903	4,451
Mission 3	6,588	3,016	472	960	1,483

To meet the useful load criterion of 6 tons that was mandated by the RFP, the following methodology was adopted to determine the vehicle sizing:

1. One of the three RFP missions was selected as the potential sizing mission.
2. The aircraft was sized with a payload such that the net useful load was at least 6 tons. Care was taken to ensure the potential payload obtained was greater than or equal to that specified in the RFP.
3. Parameters such as the vehicle empty weight, diameter of the proprotor, wing specifications, and size/capacity of the fuel tanks were determined based on the calculated payload.
4. The "sized" aircraft was used to perform the other missions. The extra fuel (fuel tank capacity less the fuel required for the mission) and extra payload (excess payload that can be carried for the mission if the fuel tank is completely filled) were obtained.
5. The potential useful load was now defined as the fuel required for the mission + payload + extra fuel + extra payload.
6. The sizing mission was obtained by repeating the above steps such that the potential useful load was up to 6 tons for all the missions, while also satisfying all of the other requirements of the RFP.

Table 2.3: Sizing with the 6 ton useful load requirement

	MGTOW (kg)	Installed power (kW)	Useful load Mission 1 (kg)	Useful load Mission 2 (kg)	Useful load Mission 3 (kg)
Mission 1	15,260	6,891	6,000	6,020	7,800
Mission 2	14,741	5,647	6,139	6,000	8,114
Mission 3	14,986	6,631	3,957	4,157	6,000

Table 2.3 shows the variation in MGTOW, installed power, and the potential useful load of each mission if the aircraft was sized to satisfy the requirements of a particular mission. The potential useful load is the sum of useful load, extra fuel, and extra payload, which must add up to be a minimum of 6 tons. If the aircraft is sized to either Mission 1 or Mission 2, it satisfies the 6 ton useful load requirement of all missions. However, Mission 1 requires a higher installed power at MSL, which results in Mission 1 having the most demanding sizing requirements. The higher power requirement of Mission 1 is because of the higher required cruise speed of 240 kts compared to only 180 kts for Mission 2. When the aircraft is being sized to meet the requirements of Mission 3, the potential useful load requirement of 6 tons is not met for either Mission 1 or Mission 2. This outcome is reflected in the requirements of Mission 3, which has a load/unload segment that consumes less fuel as compared to Mission 1 and 2, which both contain a relatively long loiter segment. This smaller fuel tank capacity when the vehicle is sized to the requirements of Mission 3 is not sufficient to satisfy the useful load criterion in Missions 1 and 2. Hence, the primary sizing mission is the reconnaissance mission, i.e., Mission 1.

It is clear at this point that if the *HeliX* were to only perform the RFP specified missions, the current design would be grossly oversized. However, the RFP requirement that the useful load be at least 6 tons was interpreted as meaning the vehicle will be used for other missions that may have this requirement. The net result is a more capable aircraft that meets all of the requirements defined in the RFP.

2.3 Trade Studies

The final configuration of the *HeliX* was chosen based on an extensive parametric study to meet the requirements of Mission 1. Notice that in all the studies, the payload was sized (using the methodology outlined in Section 2.2) such

that the net useful load was a minimum of 6 tons. The primary design variables were the disk loading in hover, blade aspect ratio, number of proprotor blades, and the blade tip speed in hover. These parameters were varied to better understand their independent effects on the sizing of the aircraft.

Because the *HeliX* is primarily a search and rescue (SAR) vehicle, it is important that the vehicle produce a low proprotor-induced downwash, which requires a relatively light disk loading in hover. To achieve a low disk loading, a proprotor would generally need to have a large diameter, but such a design does not generally lead to good propulsive efficiency in forward flight. Sufficient stall margin in the proprotor design is also required for maneuvers, and especially for operations in hot-and-high conditions.

A better optimized vehicle performance between the two flight regimes was obtained by using a variable diameter rotor (VDR). For the *HeliX*, the as-designed values of the proprotor parameters are a tradeoff between the required stall margin, safe autorotational characteristics, proprotor-induced downwash, brownout concerns, hovering efficiency, and other constraints that are imposed by choice of a VDR system, such as weight, complexity, and cost.

2.3.1 Selection of Hover Disk Loading

In a SAR effort, high downwash velocities can make the operating environment below the vehicle challenging and hazardous for ground personnel. Traditional tiltrotor concepts have relatively high disk loadings, typically varying from 88–117 kg m^{-2} (18–24 lb ft^{-2}), because the proprotor is sized more to maximize propulsive efficiency. Hence, for a good hovering efficiency and safe near-ground flight operations, a tiltrotor ideally requires a low disk loading, if this can be obtained without significantly compromising the propulsive efficiency.

Figure 2.3(a) shows the variation of vehicle MGTOW for different disk loadings at a constant tip speed, blade aspect ratio, and blade number. Figure 2.3(b) shows the variation of proprotor diameter against disk loading for the same conditions mentioned previously. Although a lower disk loading is preferable, lowering the disk loading leads to an increase in proprotor diameter and also an increase in vehicle MGTOW. A larger diameter proprotor is also beneficial from an autorotational standpoint, mainly because the rotor will have a higher stored rotational kinetic energy. The benefits of a large rotor, however, must be weighed against forward flight efficiency and the various other practical aspects of designing a vehicle with large proprotors. As a compromise between good hover and forward flight performance as well as operational safety, a disk loading of 61 kg m^{-2} (12.5 lb ft^{-2}) at MGTOW was selected.

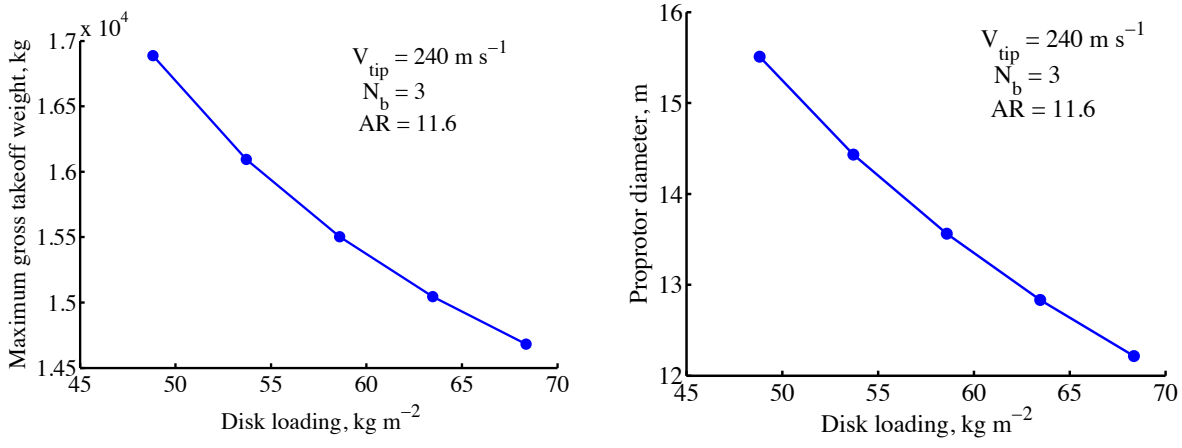

(a) MGTOW versus disk loading

(b) Proprotor diameter versus disk loading

Figure 2.3: Effect of disk loading on: a) maximum takeoff weight b) proprotor diameter

2.3.2 Selection of Blade Aspect Ratio

The blade aspect ratio is related to the solidity of the rotor system. A higher blade aspect ratio will result in a lower solidity when the number of blades are held constant, which will result in a lower blade loading coefficient, and, as a byproduct, a rotor with lower vibrations and reduced noise. However, selecting a large aspect ratio defines a blade with a long radius that can limit propulsive efficiency in cruising flight. A lower aspect ratio blade for a given disk loading, tip speed, and thrust coefficient (C_T), will result in a higher blade loading coefficient (C_T/σ, where σ is the proprotor solidity). However, decreasing solidity is undesirable because the corresponding increase in C_T/σ reduces the stall margin of the proprotor, which must always be retained for maneuverability and gust response, and especially because of the requirement to operate at 6,000 m, ISA+15°. Figures 2.4(a) and 2.4(b) show that an increased aspect ratio is beneficial in reducing the vehicle MGTOW and installed power. Based on considerations set by the disk loading and C_T/σ for a fixed tip speed and number of blades, a blade aspect ratio of 11.6 was selected.

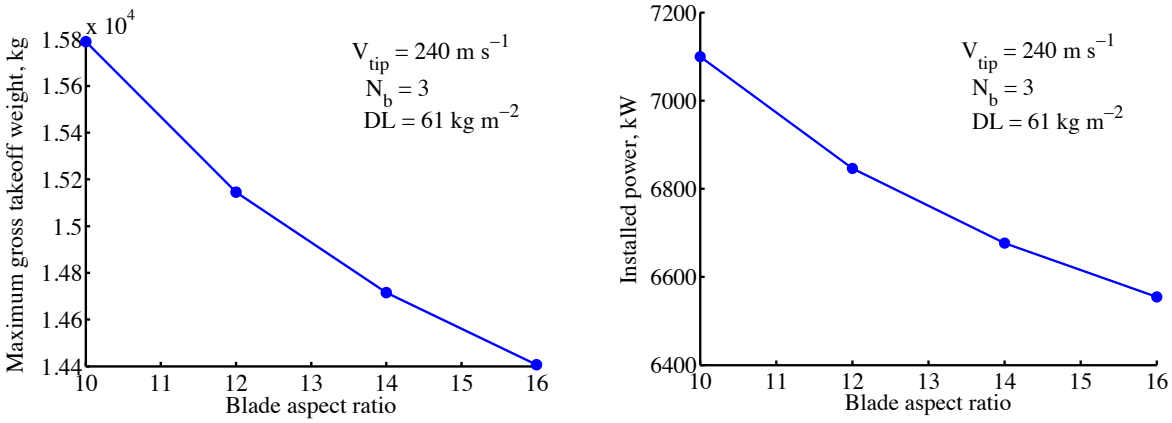

(a) MGTOW versus blade aspect ratio

(b) Installed power versus blade aspect ratio

Figure 2.4: Effect of blade aspect ratio on: a) maximum takeoff weight b) installed power

2.3.3 Selection of the Number of Blades

The number of blades used on the proprotor affect the centrifugal force experienced by each blade as centrifugal force decreases with an increase in the number of blades. Because the *HeliX* is a VDTR concept, a lower centrifugal force helps in the retraction of the blades, explained in Section 6.4. The symmetric arrangement of an even number of blades could be potentially exploited in the design of the retraction mechanism, however, with a higher number of blades the hub would become more complex and heavier. The increase in vehicle MGTOW versus the number of blades shown in Fig. 2.5(a) is because of the reasons previously mentioned.

The decrease in centrifugal force on each blade between a 3- and 4-bladed proprotor design, as shown in Fig. 2.5(b), did not justify the increase in vehicle weight and complexity of the hub design. Acoustic studies performed in Section 16 showed that a 3-bladed rotor falls within the constraints of noise requirements set by the ICAO [4]. A 3-bladed rotor design is also consistent with previous tiltrotors such as the XV-15, V-22, and BA-609.

2.3.4 Selection of Hover Tip Speed

Tip speed has a primary influence on the value of C_T/σ. As the tip speed increases, C_T/σ decreases, as shown in Fig. 2.6(a), thereby providing a better stall margin. Additionally, increasing the tip speed in hover also increases the

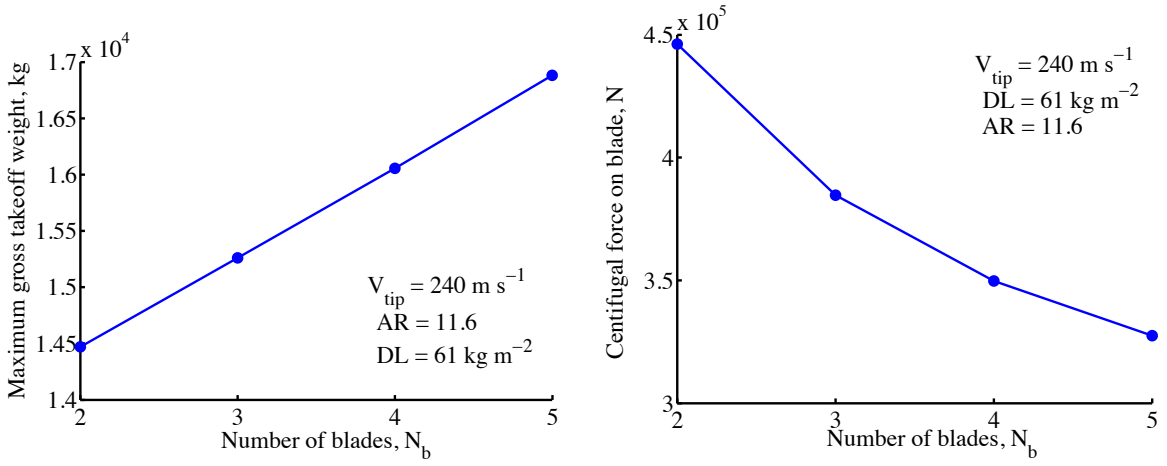

(a) MGTOW versus number of blades

(b) Blade experienced centrifugal force versus number of blades

Figure 2.5: Effect of number of blades per proprotor versus: a) maximum takeoff weight b) centrifugal force on each blade

rotational kinetic energy of the rotor system, which gives improved autorotational transition and landing performance. However, a higher tip speed results in higher profile power losses leading to a lower power loading. This latter effect is reflected in the increase in installed power for increasing hover tip speed, as shown in Fig. 2.6(b). A higher tip speed also increases rotor noise.

The *HeliX* can afford to operate at relatively high tip speeds in hover because the VDR concept lowers the tip speed in forward flight, thereby maintaining cruise efficiency. This issue is discussed in detail in Section 5.5.1. Considerations of flow compressibility do not play as much of a role in the selection of hover tip speed because the speed of sound is higher at the ISA+15°C condition that was specified in the RFP.

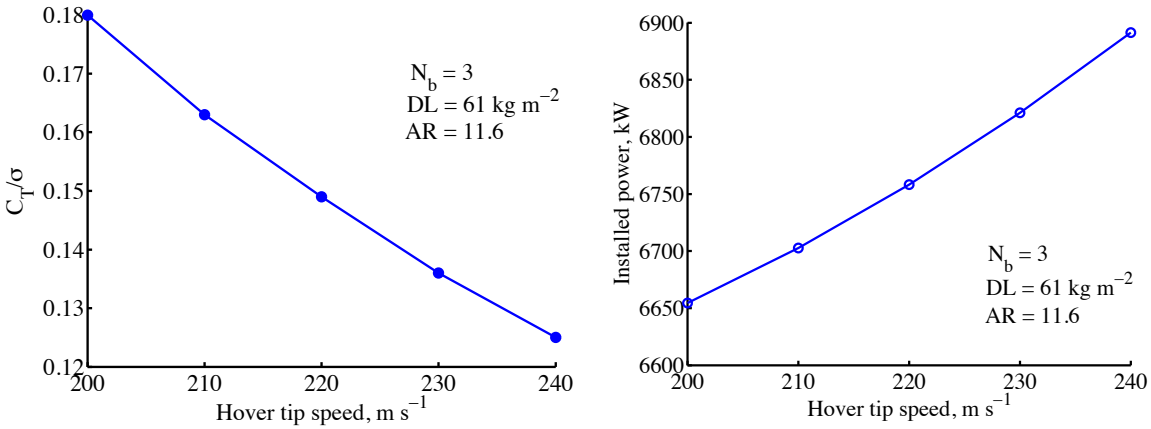

(a) Blade loading coefficient versus hover tip speed

(b) Installed power versus hover tip speed

Figure 2.6: Effect of hover tip speed on: a) C_T/σ b) installed power

2.3.5 Selection of Blade Loading Coefficient

By designing for a lower C_T/σ, the *HeliX* has the benefit of a higher stall margin, which can help in maneuverability, gust response, and flight operations at higher density altitudes. Parametric variations of blade aspect ratio and disk loading for a given hover tip speed and number of blades are shown in Fig. 2.7. A C_T/σ of 0.1254, corresponding to a disk loading of 61 kg m^{-2} (12.5 lb ft^{-2}) with a blade aspect ratio of 11.57, was selected. These values ensure that there is a sufficient rotor stall margin in hover at an altitude of 2,526 m, ISA+20°C, much higher than the 1,500 m, ISA+15°C required by the RFP.

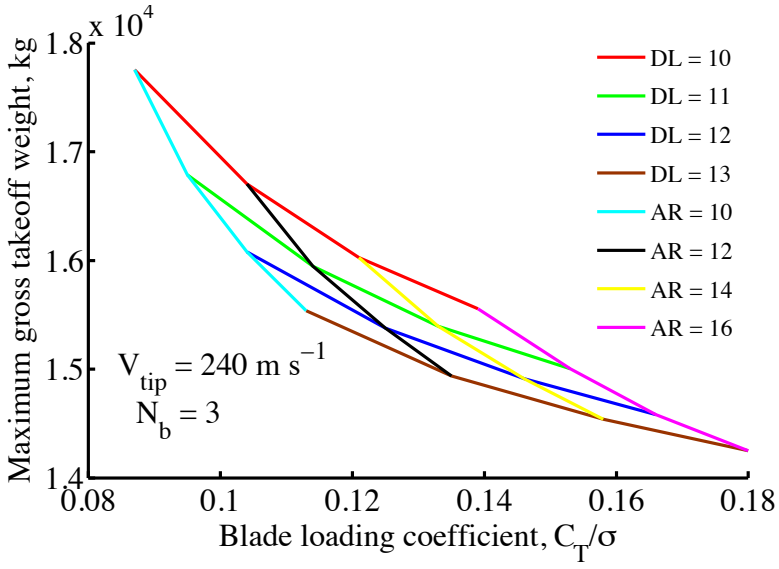

Figure 2.7: Variation of MGTOW and C_T/σ for various *AR* and *DL*. $N_b = 3$, $V_{tip} = 240\ m\ s^{-1}$

2.4 Selection of Wing Parameters

Because the *HeliX* is a tiltrotor, the main wing generates all of the lift when the aircraft is operating in airplane mode. The aspect ratio of a wing affects the induced drag and so the fuel consumption. The low aspect ratio wing, typical of those used on previous tiltrotor platforms, results in relatively higher induced drag, which yields higher fuel consumption. The *HeliX* has outboard wing extensions so that the benefit of a high aspect ratio wing is realized in airplane mode, while simultaneously minimizing the vehicle download penalty in hover; the details of this novel design are explained in Section 8.6.

The main wing span is sized based on the clearance required between the two rotors and the fuselage width, so that if the blades were to fully extend in airplane mode (e.g., because of a failure of the blade retraction mechanism), there is sufficient clearance between the fuselage and the proprotor. Once the aspect ratio and the wing span are known, the wing chord can then be determined.

The nacelles located at the wing tips contain the proprotors and the drive gearboxes. This unit, along with the wing extensions, add to the wing weight. The root chord of the wing must be sized to carry the bending loads in hover and forward flight. Higher aspect ratio wings, though beneficial from an aerodynamic standpoint of having both a lower induced drag, incur higher root bending loads and generally result in heavier wings. Design trade studies were initially performed by assuming a rectangular wing planform.

Table 2.4: Proprotor parameters

Number of blades	Equivalent solidity	Blade loading C_T/σ	Blade tip speed (ms^{-1})	Diameter (m)	Blade chord (m)
3	0.0825	0.125	240	13.2	0.63

Table 2.5: Wing parameters

Tip-to-tip wing span (m)	Wing chord (m)	Wing area (m^2)	Total wing aspect ratio	Outboard extension wing area (m^2)
16.1	2.7	43.5	6.0	6.68

2.5 High-Lift Devices and Download Control

The flaperons on the *HeliX*, shown in Fig. 2.8, have a chord equivalent to 25% the wing chord and span 5.8 m (19 ft) along each wing. Combining the flaps and the ailerons into a single device reduces the mechanical complexity, weight, and cost. The flaperons are used in airplane mode like a conventional fixed-wing aircraft. The symmetric use of these flaperons also helps to generate a higher lift coefficient, as well as slowing the aircraft down by acting as airbrakes. In addition, the flaperons have the capability to be lowered to as much as 80° (see Fig. 3.2) to reduce the vertical download on the aircraft in hover, as discussed in Section 3.2.

2.6 Empennage Configuration and Sizing

The horizontal and vertical tail, along with the elevator and the rudder, provide the lateral and longitudinal stability for the aircraft in pitch and yaw, respectively. Aside from aerodynamic considerations, the design of the empennage included considerations of an aircraft that could be loaded through an aft cargo door, where high structural rigidity has to be provided in the tail assembly.

For a conventional T-tail, Fig. 2.9(a) , the load path from the vertical tail to either side of the aft-loading ramp requires additional structural reinforcement, which adds to the aircraft empty weight. Although a twin tail configuration, Fig. 2.9(c), potentially reduces the required structure, the lateral position of the vertical tails from the aircraft longitudinal axis places the tails directly in the wake of the proprotor, which can be a source of buffeting. A V-tail configuration,

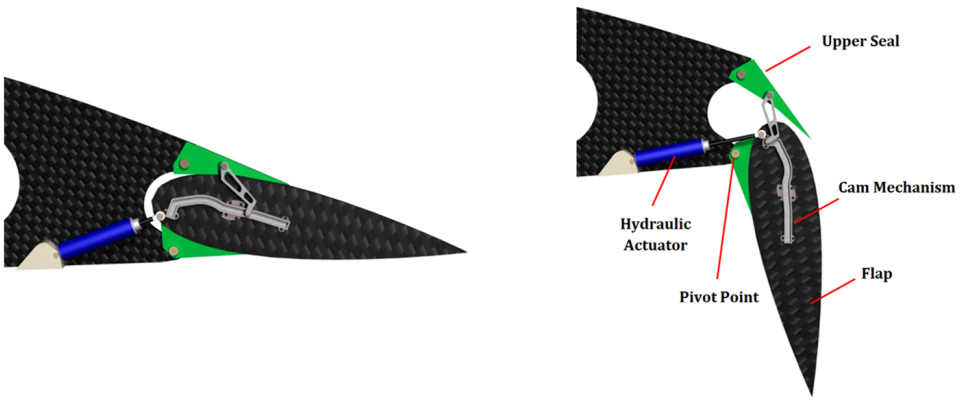

Figure 2.8: Flaperon and associated mechanism

Fig. 2.9(b), is located closer to the longitudinal axis of the aircraft compared to the twin tail, but its choice as a potential empennage would result in the complex mixing of the pitch and yaw controls, especially in transition flight. The V-tail would also need additional structural rigidity if an aft cargo door was used.

For the *HeliX*, an innovative Π-tail was chosen. This particular design combines the advantages of a twin-tail and a T-tail, and was designed to help reduce the structural weight of an aft-loading ramp. As a result, this design makes the aircraft more structurally efficient. The Π-tail also minimizes the aerodynamic pitch-yaw coupling prevalent with a V-tail, especially in transition flight.

(a) Example of a T-Tail

(b) Example of a V-Tail

(c) Example of an H-Tail

Figure 2.9: Examples of different empennage configurations

Table 2.6: Empennage parameters

Surface	Horizontal tail	Vertical tail	Elevator	Rudder
Area (m^2)	16.29	5.02	2.98	1.21
Span (m)	5.98	2.00	5.15	2.00
Mean chord (m)	2.72	1.25	0.58	0.60
Aspect ratio	2.21	1.59	8.88	3.33
Taper ratio	4:3	1:1	1:1	1:1
Sweep (degrees)	3.2	50.5	–	–

The empennage size was calculated using horizontal and vertical tail volume coefficients based on historical data for airplanes in the same weight class as the *HeliX* [5]. A horizontal tail volume coefficient of 0.9 and a vertical tail volume coefficient of 0.075 were chosen. Historical data was used to size the taper ratio and sweep of the tail sections. The vertical tail has a symmetric airfoil of sufficient thickness-to-chord ratio to allow for sufficient stiffening of the horizontal tail under dynamic loading and provides the necessary internal volume for the airframe. The airfoils selected for the vertical and horizontal tail were NACA 0015 and NACA 64A015, respectively. A summary of the empennage parameters is shown in Table 2.6.

2.7 Engine Sizing

The RFP does not specify any particular engine that needs to be integrated into the aircraft, so a "rubber" engine model was used. In each segment of the sizing mission an equivalent MSL static power was computed, based on the power required. This MSL static power is based on standard pressure and temperature lapse rates of a turboshaft engine. The maximum value of the uninstalled MSL power determined is the total power that is installed in the vehicle. The design point for the sizing mission was the cruise segment at 6,000 m, ISA+15°C.

Figure 2.10 shows the takeoff power ratio as a function of pressure altitude for three different ambient temperature conditions. To achieve the power required at cruise conditions, the installed power at MSL ISA must be more than

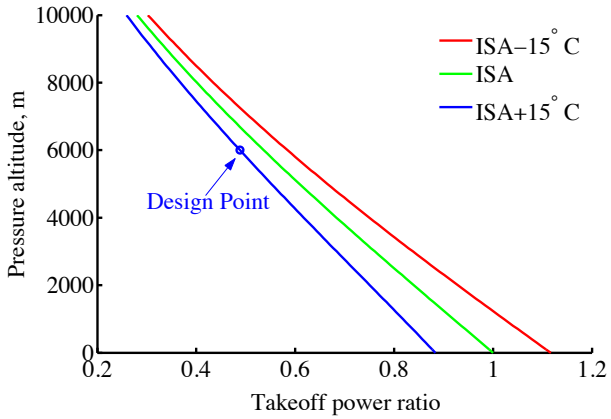

Figure 2.10: Available engine power with varying altitude and temperature

double the power required at 6,000 m, ISA+15°C. The power available at MSL also translates to a large amount of excess power that can be used for other missions. The engine model was derived from a modification to the engine model given in the 2007 AHS RFP and includes the effects of possible improvements from advanced technologies. It is referred to as the UMD Model 2013. The 2007 AHS RFP engine was based on advanced technologies projected to be available in 2020. Figure 2.11(a) shows the variation of specific fuel consumption (SFC) against engine power output for existing engines, the 2007 AHS RFP model, and the UMD Model 2013. The UMD Model 2013 is the most conservative of all the models (Fig. 2.11(b)). A conservative prediction of SFC results in a higher fuel flow rate, so the actual empty weight of the *HeliX* should come in lower than predicted. The engine dimensions were calculated using the relations given in the 2007 AHS RFP.

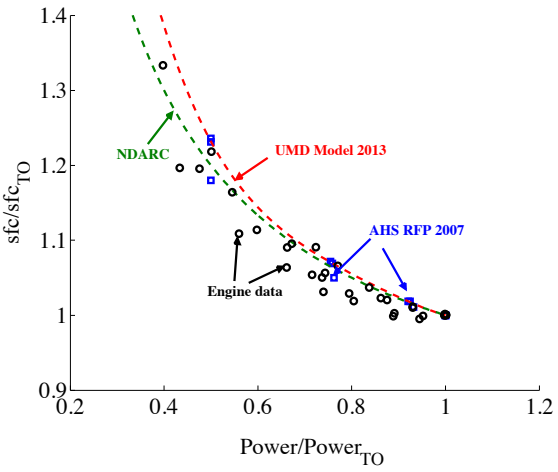

(a) SFC ratio versus power ratio for turboshaft engines

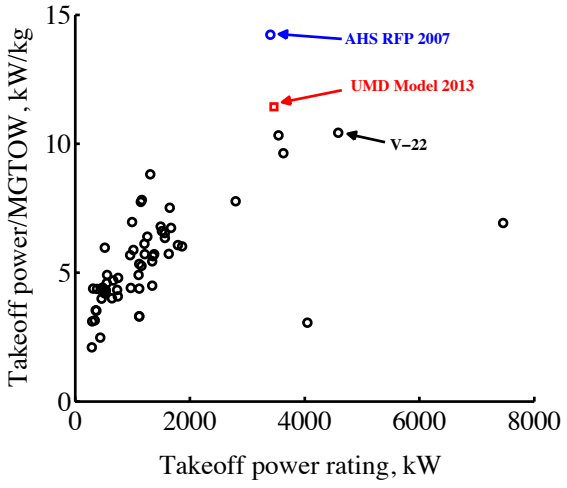

(b) Turboshaft engine power-to-weight versus takeoff power for existing turboshaft engines. Data compiled from *Jane's All The World's Aircraft*

Figure 2.11: Comparison of various engine models to historical trends

3 Performance Analysis

Performance calculations were carried out for hover and forward flight conditions with the vehicle at MGTOW and for each of the three missions in the RFP. The *HeliX* is designed to be an efficient and effective SAR platform, having excellent hovering performance and high cruise efficiencies that yield low fuel consumption. The key in achieving these goals was the use of a variable diameter proprotor, which is discussed in Section 5. The retraction of the proprotor blades in cruise flight reduces the profile losses of the proprotors and improves their propulsive efficiency. The highly streamlined shape of the fuselage aids in reducing the drag. The *HeliX* also has outboard wing extensions that increase the aspect ratio of the wing in cruise and significantly reduces the induced drag. The *HeliX* is also designed to hover at MGTOW at 1,500 m, ISA+15°C, which corresponds to a density altitude of 2,022 m (6,635 ft).

3.1 Drag Estimation

The aircraft drag can be decomposed into three components: profile, parasitic, and induced. The parasitic drag was determined by summing the drag of each individual component and accounting for interference effects. Using a methodology outlined by Raymer [6], the parasitic drag of the fuselage, nacelles, and hub are estimated based on the skin friction coefficient, wetted area (see Fig. 3.1), form factor, and interference effects. A fully turbulent boundary layer was assumed over the entire aircraft and the skin friction coefficients were estimated at cruise conditions (6000 m, ISA+15°C) at 315 kts (TAS). The profile drag of the wing, outboard wing extensions (OWEs; see Section 8.6), horizontal, and vertical tail were determined based on the methodology of Roskam [5]. The wetted area of the components were obtained from the CAD drawings.

Based on historical data from Harris [7], a drag area of 1.65 m^2 (17.72 ft^2) was used during initial sizing [1]. Table 3.1 shows the actual drag breakdown of *HeliX*'s fuselage. The highly streamlined nature of the fuselage, designed for high speed flight, has relatively low drag. The relatively thick wing, designed for torsional stiffness and high whirl flutter speeds, accounts for 45% of the total drag. As recommended by Prouty [8], a 20% increment was added to the calculated drag area to account for component interference effects and so obtains a more practical estimate of the total drag. This increment also accounts for the drag of miscellaneous components such as the pitot probe, antennas, door handles, and hinges. The total parasitic drag area of the *HeliX* was estimated 1.36 m^2 (17.55 ft^2). This is the value used in the performance analysis.

Table 3.1: Drag breakdown

	Drag area (m^2)	% of total
Fuselage	0.347	21.28
Wing	0.736	45.11
Horizontal tail	0.135	8.31
Vertical tail	0.042	5.03
Nacelle	0.042	2.60
Spinner	0.016	1.00
Total	1.359	
+ additional 20%	1.631	

3.2 Vehicle Download

The combined thrust produced by the rotors in hover must exceed the total weight of the vehicle because of the download created by the proprotor wake as it impinges on the wing and the fuselage. A download penalty always requires higher power requirements in hover and low speed flight. For the *HeliX*, the download is alleviated by the deflection of the flaperons to their maximum limit, as done with conventional tiltrotors. Furthermore, the outboard wing extensions are down in hover to minimize the download penalty. Tests performed by Keys [9] quantified the vertical download on wings of different aspect ratios with varying angles of flap deflection. Based on these results and proprotor downwash estimates, the optimum values of flap chord and deflection were determined. The flap chord

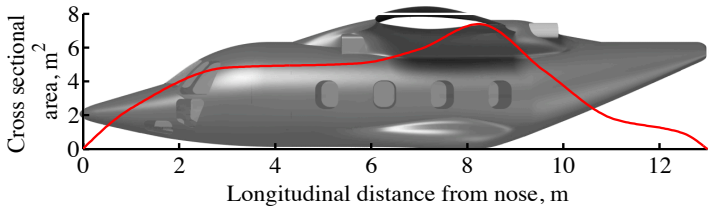

Figure 3.1: Cross-sectional area versus longitudinal fuselage location

was sized to satisfy the high-lift requirements in forward flight (see Section 8.1.1). Figure 3.2 shows the variation of download factor against flap deflection angle for different flap chord lengths. As mentioned in Section 2.5, the flap chord was chosen to be 25% of the wing chord and the maximum flap deflection to be 80°, which reduces the hover download factor to a nominal 9.8%.

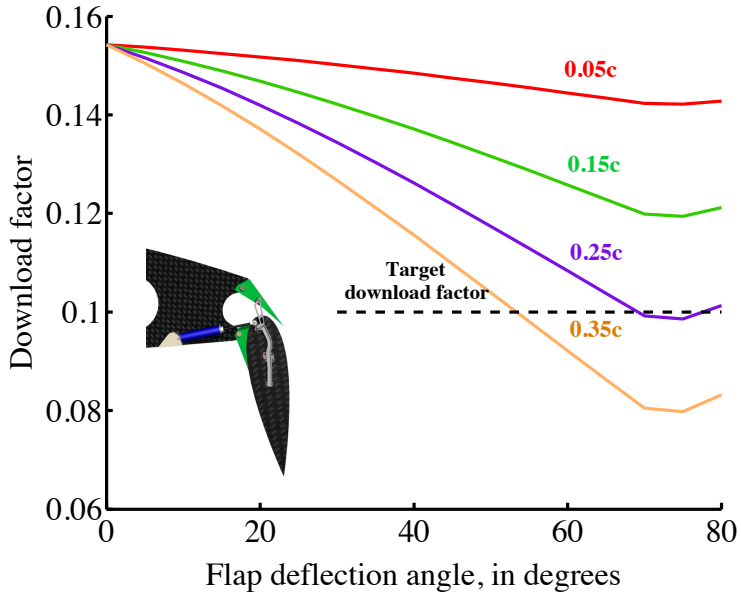

Figure 3.2: Hover download factor versus flap deflection for different flap chords

3.3 Hover Performance

The hover design point for the vehicle is at 1,500 m, ISA+15°C (2,022 m or 6,600 ft density altitude) at MGTOW. Because the primary design point is the cruise condition at 6,000 m, ISA+15°C (see Section 3.4), the available power in HOGE conditions is much greater than that required. Figure 3.3 shows the variation of available engine power and HOGE power required at varying pressure altitudes for different "hot" conditions. At the HOGE design point, the required power is 4,072 kW (5,461 hp) versus the available transmission limited 4,474 kW (6,000 hp). Notice that the transmission limit does not constrain the hover performance at any altitude or temperature condition, allowing for the design of a lightweight transmission. At MGTOW, the vehicle can hover at a pressure altitude of 3,637 m (11,932 ft) under ISA conditions or at 2,526 m (8,287 ft) at ISA+20°C. As shown in Fig. 3.4, for the reduced TOW of Mission 3, the *HeliX* can hover at an altitude of 6,466 m (21,214 ft). This hot-and-high performance capability allows the *HeliX* to excel in mountainous terrain, and increases the safety of flight for emergency medical and insertion missions at high altitudes.

Figure 3.5 shows the historical data trend of useful load versus maximum attainable pressure altitude for various helicopters. Notice that while the *HeliX* is designed for efficient cruise, its hover capability is not compromised and it is placed on the edge of "worldwide capability" of conventional helicopters.

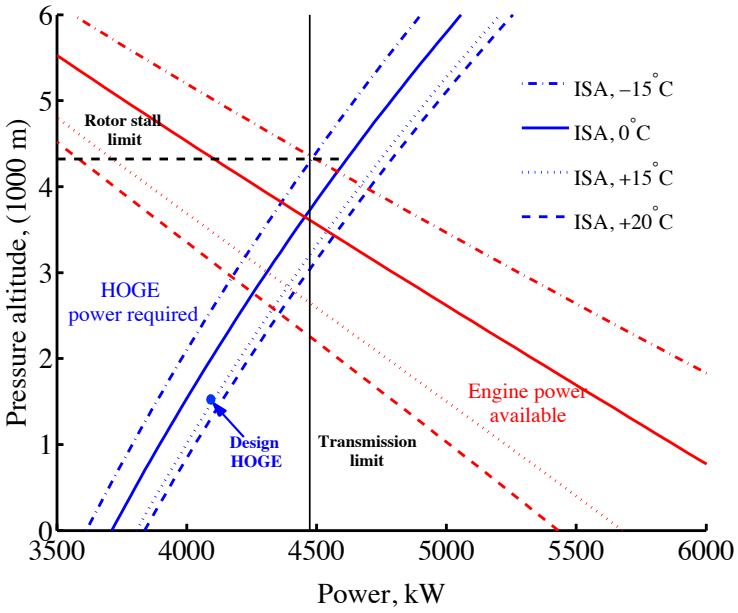

Figure 3.3: Achievable pressure altitude versus power, illustrating HOGE power required and available, for variation in temperature at MGTOW

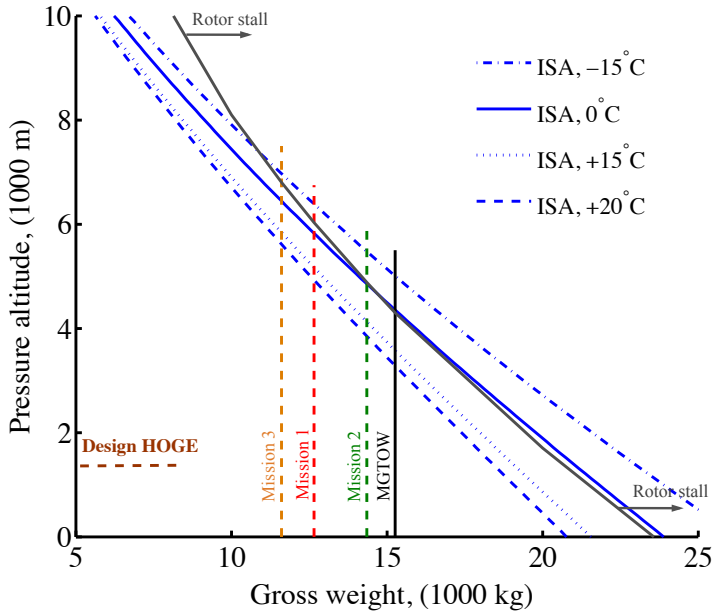

Figure 3.4: Pressure altitude versus gross weight (Weight-Altitude-Temperature curves)

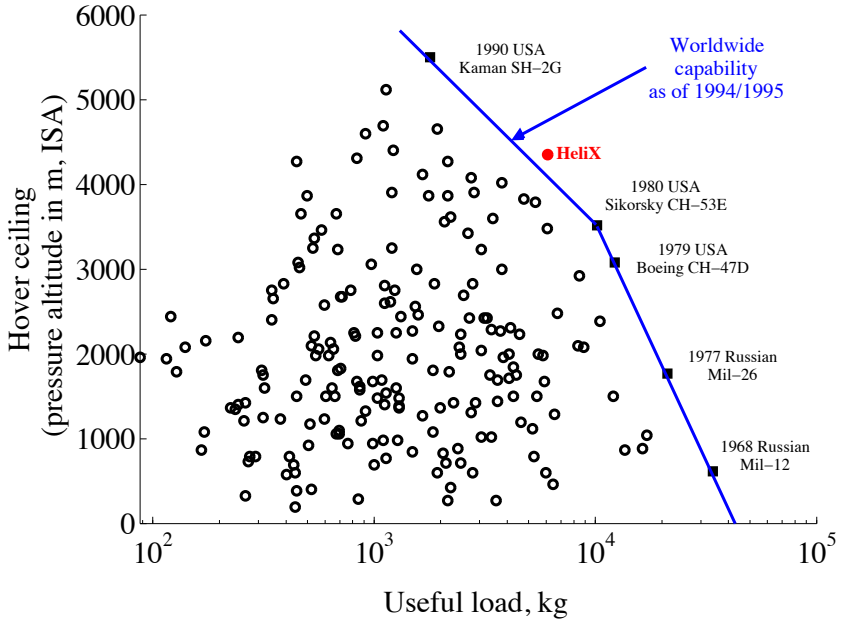

Figure 3.5: Historical trend of hover ceiling versus useful load

3.4 Forward Flight Performance

The engine of the the *HeliX* is sized to provide the necessary power required for cruise flight. In each of the missions specified in the RFP, the cruise altitude is 6,000 m, ISA+15°C (density altitude of 6522 m / 21,373 ft) and the maximum cruise speed to be attained is 240 kts. This specified operating condition places very stringent requirements on aircraft performance and the amount of installed power. Figure 2.10 shows the variation of engine power available as a function of density altitude. At the design point, the ratio of power available to MSL power is 0.48, implying that nearly double the power required to cruise at 6,000 m, ISA+15°C needs to be installed compared to that required at MSL.

The forward flight performance was estimated for the vehicle when at MGTOW and for each of the mission weights at their respective cruise conditions. The proprotor blade retraction in cruise allows for considerably higher propulsive efficiencies to be achieved, as shown later in Fig. 5.1. The deployment of the outboard wing extensions increases the effective wing aspect ratio and the aircraft L/D ratio; as shown in Section 5, the maximum L/D increases from 8.5 to 10.8. The increase in L/D is more significant at lower airspeeds because the wing extensions help to significantly reduce the induced power requirements, which is a higher fraction of the total power required at these airspeeds.

Figure 3.7 shows the forward flight performance of the *HeliX* at the RFP cruise altitude of 6,000 m, ISA+15°C. If the outboard wing extensions are not deployed, then the maximum forward flight speed reduces slightly to 264 kts. With the outboard wing extensions, the aircraft can reach a maximum level flight airspeed of 283 kts.

Figure 3.8 shows the forward flight performance of each mission at the mission TOW. Because the aircraft has been designed with a 6 ton useful load capacity, it operates at a much lighter TOW for each of the three missions. This outcome is reflected in the lower required power and higher maximum cruise speed that are now attainable. Consequently, the maximum cruise speed that can be achieved by the *HeliX* in Mission 3 (SAR) is 317 kts. At this speed, victims can be returned to an operational base that is 600 km away nearly within the "golden hour." The RFP also states that the aircraft should demonstrate an average rate of climb of 612 m min^{-1} from the HOGE altitude of 1,500 m, ISA+15°C to the cruise altitude of 6,000 m, ISA+15°C. Figure 3.9 shows the variation of maximum rate of climb plotted against density altitude. Rate of climb is determined by the excess power available at a given weight, flight

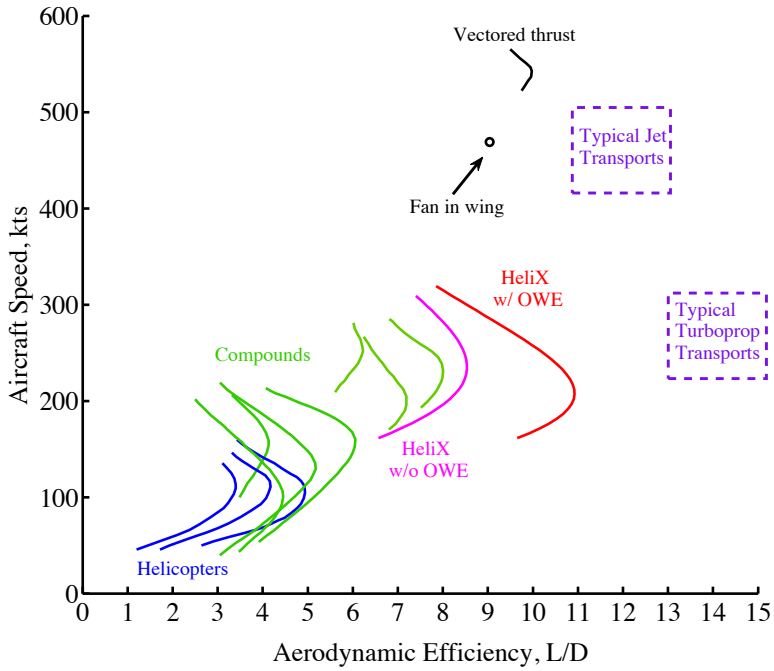

Figure 3.6: Aircraft speed versus L/D for *HeliX* compared to other VTOL aircraft

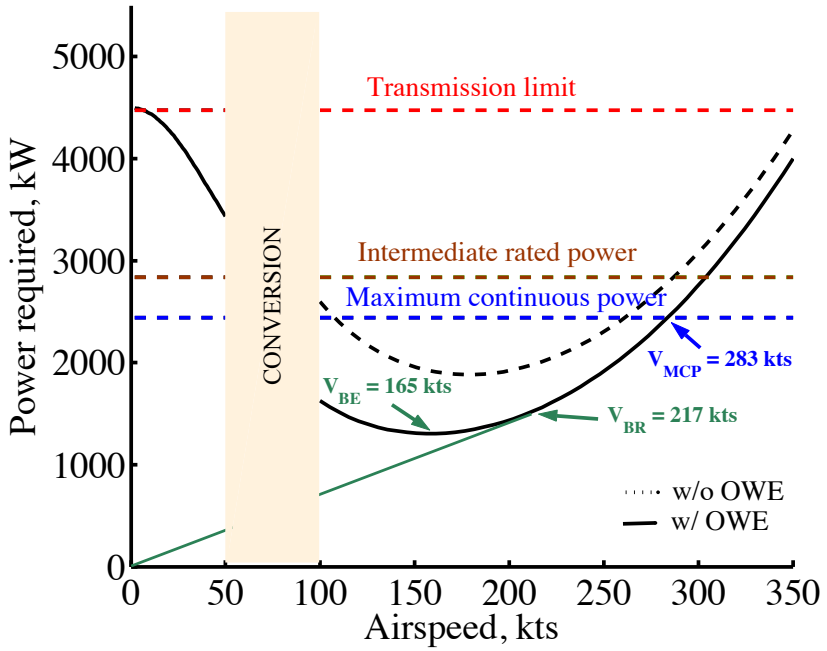

Figure 3.7: Power required versus airspeed, forward flight performance for MGTOW at 6,000 m, ISA+15°

speed, and density altitude. The maximum rate of climb shown in Fig. 3.9, therefore, corresponds to the airspeed for minimum power or for best endurance, V_{BE}. The average climb rate for the MGTOW vehicle is 734 m min^{-1} (2,408 ft min^{-1}), which easily surpasses the requirements of the RFP.

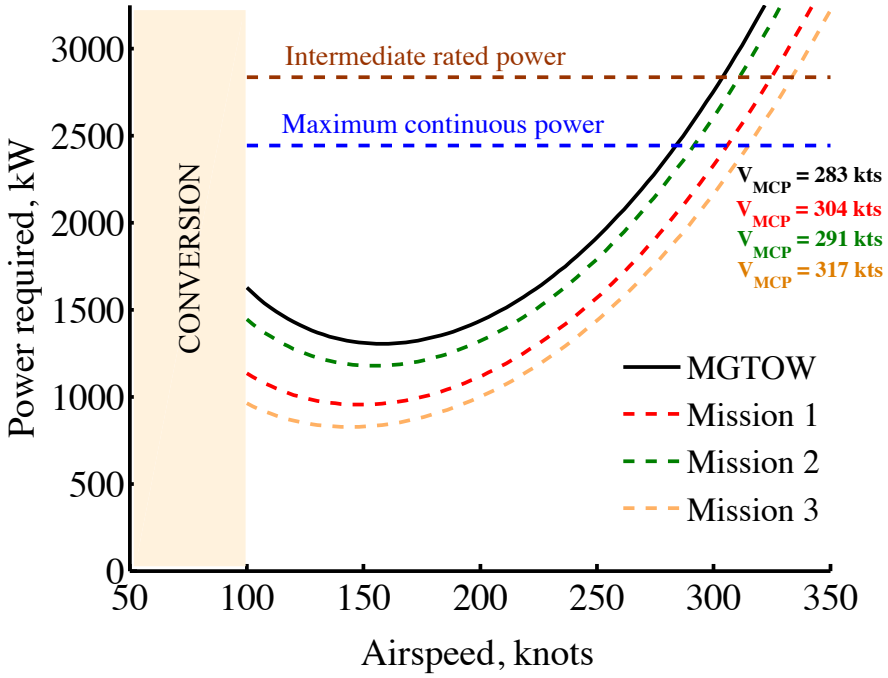

Figure 3.8: Power required versus airspeed for Missions 1,2, and 3 at 6,000 m, ISA+15°

3.5 Range and Endurance

The RFP requires the vehicle to travel a maximum distance of 1,800 km. After maintaining a 30 minute fuel reserve, the achievable range of the *HeliX* at 6,000 m, ISA+15°C is actually 3,373 km (1,821 nm). Using the reserves, the range increases to 3,649 km (1,970 nm); see Fig. 3.10(a). The increase in the maximum range over that required by the RFP is because the operational airspeeds mentioned in the RFP are off-design conditions, which results in a higher fuel flow rate. Figure 3.10(b) shows that the maximum endurance of the *HeliX* at MGTOW with 2,832 kg of payload (maximum capacity) is 9.52 hours.

3.6 Autorotational Capability

As a SAR platform that can potentially operate in remote locations, it is important that the vehicle has good single engine inoperative and autorotational capabilities. Such capabilities depend on the rotor disk area, stored kinetic energy in the rotor system (i.e., blade mass, radius of gyration, angular velocity), and the vehicle gross weight. Figure 3.11 shows the autorotative index, AI, of various helicopters and tiltrotors versus their disk loadings. There exist various ways of quantifying the autorotational capability of a rotorcraft. The Sikorsky AI, i.e., $AI = (I_R\ \Omega^2)/(2\ W\ DL)$, is the ratio between the kinetic energy of the rotor $(I_R\ \Omega^2)$, the weight (W), and disk loading (DL) of the helicopter. The *HeliX* employs a relatively high hover tip speed which increases the stored rotational kinetic energy in the rotor system. This high kinetic energy, coupled with the low disk loading in hover, results in an AI that is comparable to most multi-engine helicopters of similar MGTOW that are currently in service. Therefore the *HeliX* will be able to perform safe autorotational landings.

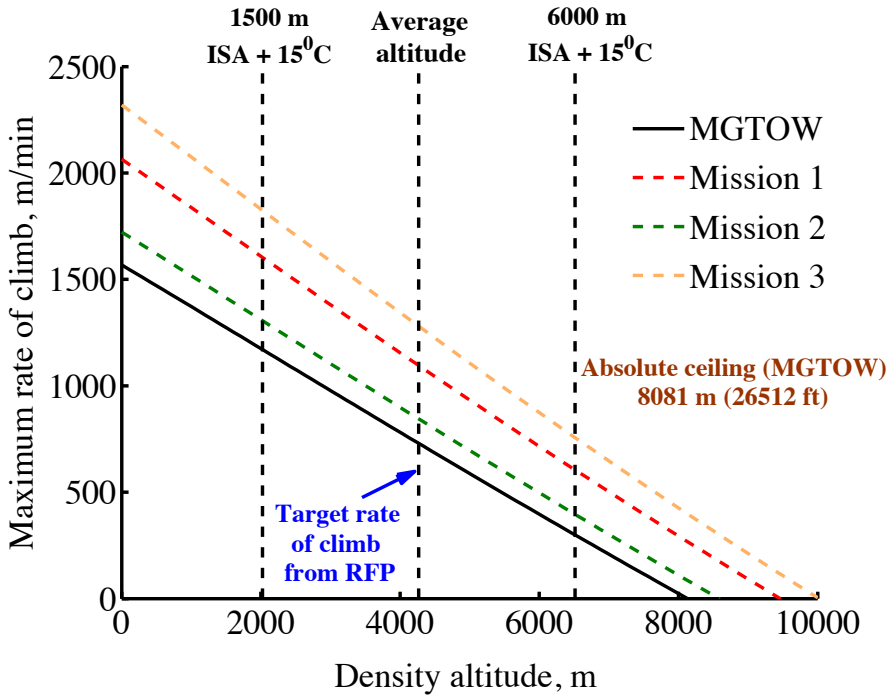

Figure 3.9: Maximum rate of climb versus density altitude

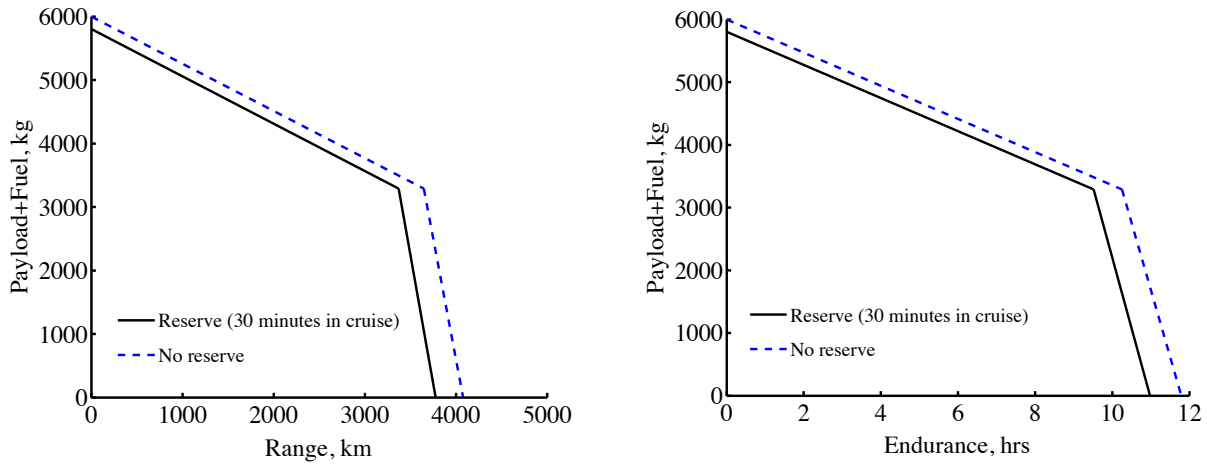

(a) Range (b) Endurance

Figure 3.10: Effect of payload and fuel on range and endurance

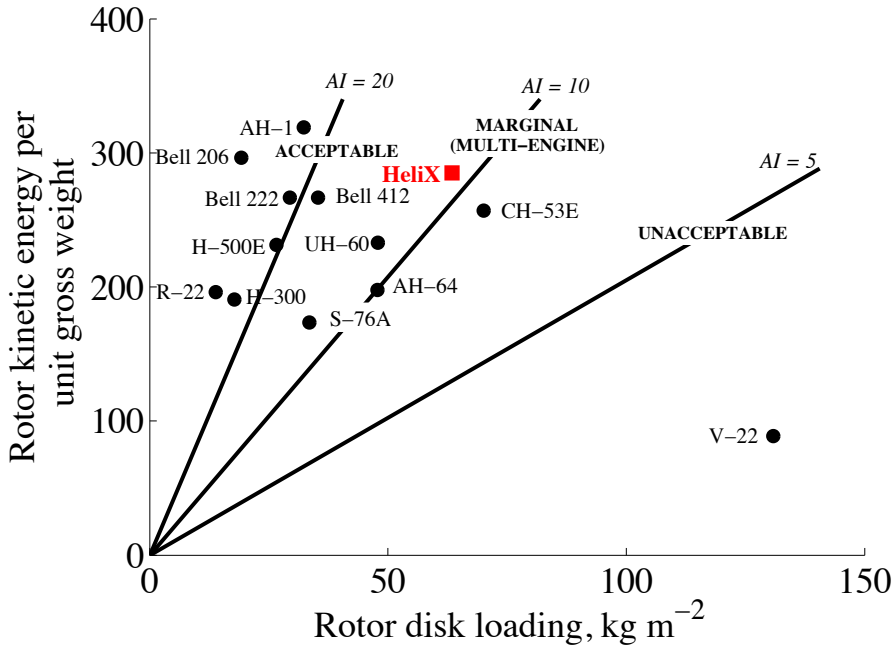

Figure 3.11: Comparison of autorotative index for various rotorcraft

4 Performance Index

A metric for performance used to compare different proposals was defined by the RFP. This Performance Index consists of the sum of five vehicle metrics:

1. PI_{weight} = 15,000 kg/MGTOW
2. PI_{range} = (Mission 1 range)/1,800 km + (Mission 2 range)/1,400 km + (Mission 3 range)/1210 km
3. PI_{speed} = (Maximum speed in kts)/240
4. PI_{DOC} = (1.25 * Black Hawk DOC)/DOC
5. PI_{DMC} = (1.25 * Black Hawk DMC)/DMC

While determining the value of PI_{weight}, based on the information in Section 2.2, and the values of PI_{DOC} and PI_{DMC}, based on information in Section 17, are both fairly straightforward, the range and speed indices require further discussion. Based on the RFP requirements, the *HeliX* was sized to perform the missions with the assumption that the operational base was 600 km away, so the mission specific TOWs are based on the need to have only enough fuel onboard to perform the mission with reserves. However, the 6 ton useful load requirement that was also mandated in the RFP required the aircraft to be designed around a correspondingly larger fuel tank. Therefore, to calculate PI_{range}, the aircraft was loaded with the mission appropriate payloads and the fuel tanks were considered to be full.

The *HeliX* was designed with some special features, as discussed later, that play a role in the capable flight speeds. It was not specified in the RFP whether the maximum speed was to be obtained at any specific mission TOW or MGTOW. Therefore, to be conservative, the maximum speed at MGTOW without deployment of the OWEs (Section 8.6) was used. It should be noted that both the OWE and the vehicle weight play a significant role in determining this value and a better PI_{speed} is possible.

Table 4.1: Performance Index for *HeliX*

PI Category	*HeliX* Value	PI Value
PI_{weight}	15,260 kg	0.98
PI_{range}	3372.7 km, 3616.0 km, 3461.1 km	7.52
PI_{speed}	264 kts	1.10
PI_{DOC}	5499*	0.87
PI_{DMC}	2823*	0.69
Total PI		11.16

* Value in millions of $ per flight hour over 20 years

5 Proprotor Design

The *HeliX* VDR system presents a unique set of aerodynamic and structural design challenges. Aerodynamically, an optimal combination of parameters, such as blade twist and taper and rotor solidity, must provide desired performance in hover and forward flight, despite the dissimilar design drivers between these flight conditions. Beyond the aerodynamic challenges, the VDR must also perform the extension/retraction while maintaining a high level of reliability, structural efficiency, and dynamic stability over the operational range of RPMs. This section presents the systematic aerodynamic methodology and structural design of the VDR system.

5.1 Design Goals

One of the key challenges associated with tiltrotor design is the need for the proprotor to operate efficiently both as a rotor and propeller while in helicopter and airplane flight modes, respectively. The figure of merit, described as *FM* in Eq. 1, was computed during development of the proprotor as one measure of the hovering efficiency. The propulsive efficiency, denoted as η_P in Eq. 2, was also computed to help evaluate the forward flight efficiency.

$$FM = \frac{P_{Ideal}}{P_{Actual}} = \frac{C_T^{3/2}/\sqrt{2}}{C_P} \tag{1}$$

$$\eta_P = \frac{C_T \mu}{C_P} \tag{2}$$

Modern propeller aircraft have propulsive efficiencies in range of $\eta_P = 0.80$–0.90 [10]. Setting an η_P target of 0.85 at the design point of 240 kts at 6,000 m, ISA+15°C emphasized the need for fuel conservation at higher airspeeds and over relatively long distances. A target of *FM*=0.75 at 1,500 m ISA+15°C was chosen to ensure the hovering thrust efficiency remained comparable to modern helicopters. These values drove the final design of the proprotor, which is summarized in Table 5.1.

Table 5.1: Final blade configuration and efficiency results at design point

Inboard Twist Rate	Outboard Twist Rate	Total Twist (Hover)	Total Twist (Cruise)
$-5.81°/\text{m}$	$-4.56°/\text{m}$	$-31°$	$-19°$

Taper Ratio	Solidity	η_P	*FM*
0.45	0.0825	0.85	0.71

5.2 Proprotor Methodology

A well-validated method based on blade element momentum theory configured specifically for proprotor design [11] was used to help determine an optimal proprotor configuration. Selecting a proprotor configuration requires careful evaluation of the performance and efficiency because of variations in operating conditions, vehicle weights and dimensions, and blade properties. Also, slight modifications in vehicle or blade characteristics are often coupled in their effects on performance or efficiency, such that the design inevitably becomes an iterative process of judicious adjustments. Vehicle performance analysis before the proprotor design provided initial inputs for vehicle weight, rotor RPM, and rotor radius. In helicopter mode, an assigned wing download penalty, f_v, of 10% was used, which is consistent with proprotor placement and the vehicle wing design discussed in Section 2.

The sectional drag coefficient for the non-lifting cuff section, or torque tube, that houses the retraction mechanism was estimated to be 0.1, and varying this value did not show significant effects on proprotor performance to suggest any

aggressive shape or structural modifications was needed. A vehicle parasitic drag area, f_x, of 1.64 m^2 (17.6 ft^2) was initially used. The spinner cutout was 15% of the blade radius operating in helicopter, or extended mode ($0.15R_E$), or 22.5% of the blade radius in cruise, or retracted mode ($0.225R_R$). Increasing the vehicle L/D ratio from about 8.5 to 10 did not increase the propulsive efficiency at the cruise design point. As L/D was increased for the same advance ratio, the C_T required was lowered but the corresponding C_P also dropped, resulting in a very slight loss in propulsive efficiency.

5.3 Proprotor Configuration Selection

The steps used in the proprotor design were as follows:

1. Proprotor solidity, vehicle weight, rotor radius, and rotor RPM were prescribed according to outcomes from the performance analysis.
2. Blade twist and taper configurations were evaluated using a parametric study at the hover design point for a given solidity. A best-case combination for a blade designed for hover was evaluated in forward flight so as to understand the propulsive efficiency limitations in cruise flight in airplane mode.
3. Blade twist and taper combinations were evaluated from a parametric study with the retracted blade solidity (i.e., a higher solidity) at the design point in forward flight.
4. A proprotor configuration that maximized FM and η_P was selected for further study. Thrust, speed, and altitude sweeps were undertaken for both hover and forward flight to evaluate the overall performance and efficiency of the proprotor.
5. If a configuration yielded undesirable aerodynamic characteristics or unsatisfactory performance or efficiency in high-thrust or high-speed flight operations, the process was restarted at Step 1.
6. The process was repeated iteratively until a final proprotor configuration was reached that met all of the specified requirements.

Selecting a proprotor that will achieve a high hovering efficiency requires that the solidity be minimized as much as possible, while leaving sufficient stall margin for roll stability and control, operations for precision flight (such as instrument approaches or landings on ships), and good overall maneuverability. In fact, the handling qualities for a tiltrotor is a design issue in that takeoff weight could become limited by a reduction of control capability from occurrence of blade stall.

The VDTR concept has been shown to demonstrate its effectiveness for a wide range of operating conditions in both helicopter and airplane modes. Figure 5.1 shows the substantial benefit in propulsive efficiency as a result of reducing blade radius in cruise flight at the design point. The peak and broad effective range of η_P is highly desirable for fuel conservation. Additionally, a baseline blade with constant diameter at equivalent thrust weighted solidity was also considered. This blade achieved the target value of FM, but had a propulsive efficiency that was initially 12% lower than the target.

5.4 Proprotor Parametric Studies

For a given solidity, the VDTR proprotor was modified to examine a variety of twist rates, taper ratios, and operating conditions.

5.4.1 Twist

The blade twist that was selected was bi-linear with the change in twist rate at $0.86R_E$. The location of the bi-linear twist was limited by the structural requirements of housing the torque tube because it is sheathed in the outboard

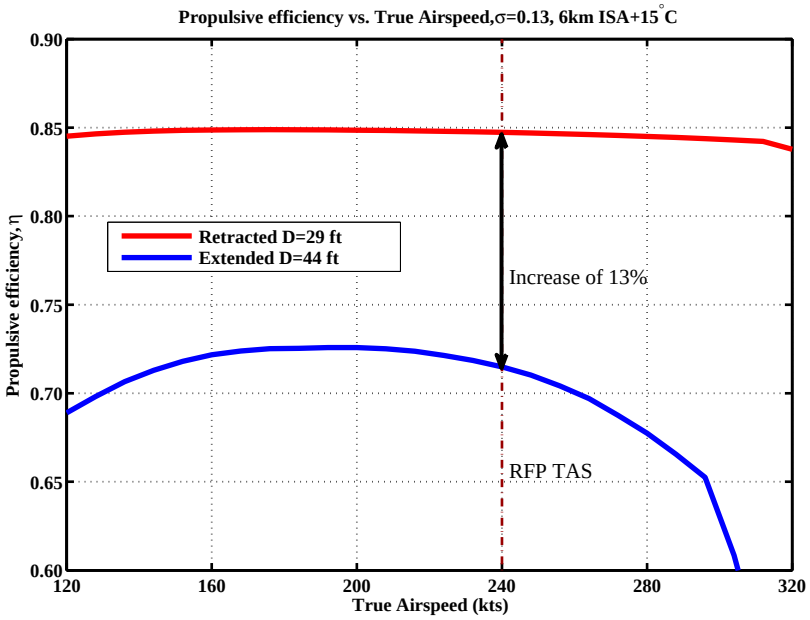

Figure 5.1: Propulsive efficiency versus airspeed for extended versus retracted mode at design point

section in the retracted mode.

The inboard and outboard blade twist rates were varied independently to examine their effects on the proprotor design. The final stages of the design involved generating a matrix of blade twist configurations and evaluating the resulting FM and η_P values. Blade twist was varied from -9.84 to $-3.28°$ per meter (-3.0 to $-1.0°$ per foot) after determining that this range produced optimal hover thrust and forward flight efficiencies, as shown in Fig. 5.2. Notice the steep decline in the value of FM, on the left, compared to the steady decline in η_P, on the right; this outcome indicates that the design may relinquish much more hover thrust efficiency for small gains in propulsive efficiency. Propulsive efficiency benefits most from using high blade twist rates so that the local flow environment allows the airfoil section to operate at more efficient angles of attack. However, less blade twist was desired in hover to avoid inboard blade stall near the root, which became an issue at high thrust and led to compromised stall margins. The values of FM began to decrease when the vehicle was loaded to 110% of the MGTOW because of inboard blade stall, so blade twist rates were decreased to avoid this situation but without resulting in a significant reduction in η_P.

5.4.2 Blade Taper

Blade taper variations were investigated at a constant thrust weighted solidity, with tip to root taper ratios being varied from 1.0 to 0.4. Increasing the taper ratio resulted in a mild increase in η_P, but more benefited hovering FM by decreasing the C_l values inboard on the blades such that these sections could operate closer to their best sectional C_l/C_d ratios.

5.4.3 Rotor Solidity

The vehicle sizing used rotor solidity as an input such that the blade radius, rotor RPM, and MGTOW changed each time solidity was varied. Therefore, varying solidity revealed a more comprehensive understanding of the proprotor aerodynamics because a variety of performance and efficiency trends emerged. Note that the solidity increases from 0.0825 to 0.129 when the blade is retracted.

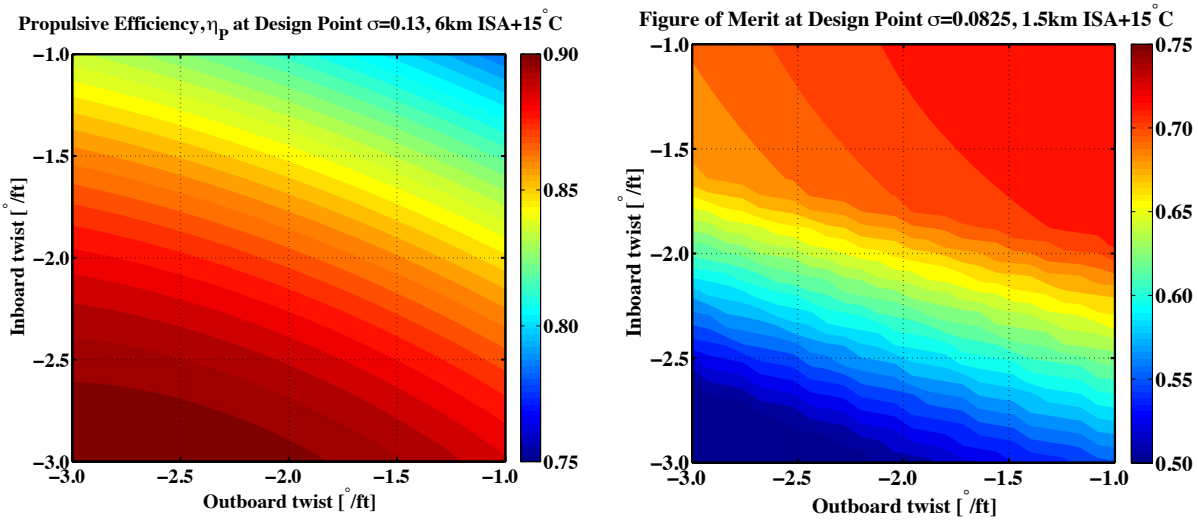

Figure 5.2: Inboard twist rate versus outboard twist rate to illustrate effect on FM and η_P

An initial baseline solidity of 0.08 was evaluated, but the proprotor did not have sufficient stall margin for an assumed C_T/σ stall limit of 0.16. A solidity of 0.09 showed promising performance in both helicopter and airplane modes and gave better stall margins. Solidities between 0.09 and 0.08 were then evaluated to determine if a suitable stall margin could be obtained in hover while the values of η_P and FM could benefit from the decreased solidity. A solidity in hover of 0.0825 was the best choice because of the higher maximum value of FM of 0.71 and η_P of 0.85, while still retaining sufficient stall margins.

5.5 Blade Design to Maximize Efficiency

5.5.1 Benefits of Blade Retraction

When operating in airplane mode the rotor RPM is reduced to 90% of its value in helicopter mode so as to help reduce the helical tip speed of the proprotor. This adjustment, paired with the retraction of the blade, reduces the tip speed by 40%, i.e., from 240 m s^{-1} to 144 m s^{-1}. Reduction in the tip speed of the proprotor allows for the avoidance of compressibility drag rise that rapidly decreases propulsive efficiency and also contributes to proprotor noise.

5.5.2 Airfoil Selection and Design

The blade was designed with an airfoil series based on the GOE-632 and VR-7 airfoils. While the original airfoils provided a good maximum lift coefficient, or $C_{l_{max}}$, and adequate internal space for the structure, positive camber was required to lower the zero-lift angle of attack. The blade section outboard of $0.86R_E$ was designed with a taper ratio of 0.45 and a reduced thickness-to-chord ratio of 12% to minimize profile drag, delay the onset of drag rise from compressibility, and also improve the spanwise lift distribution.

The helical tip Mach number remains below 0.6 in cruise at the design point because of the retraction mechanism and RPM reduction, avoiding the need for creative tip shapes to reduce drag rise from compressibility effects. Models of tip sweep effects showed no propulsive efficiency benefit as forward flight speed increased beyond the maximum airspeed, and there were no significant noise-reduction benefits either, as shown in Section 16.5. Therefore, there was no need for tip sweep to be included in the design of this proprotor.

5.6 Proprotor Blade Structural Design

The proprotor blade, shown in Fig. 5.3, consists of two primary structural members: an inner, non-lifting elliptical segment (torque tube) and an outer, lifting blade segment. During extension/retraction modes of operation, the outer blade segment telescopes over the inner elliptical section, permitting a change in the overall diameter of the proprotor.

The internal structure of the blade assembly was designed with adequate flap bending (EI_y), lead-lag bending (EI_z), torsion bending (GJ), and axial (EA) stiffnesses to sustain the centrifugal/compressive buckling loads, steady and oscillatory flap, lead-lag, and torsional moments and shear stresses resulting from aerodynamic and inertial forces. The design variables considered included: torque tube section dimensions, spar section dimensions and chordwise position, spar and skin thickness, and leading-edge mass. An iterative procedure using the comprehensive flight dynamics code HeliUM [12], developed at the University of Maryland, was used to analyze the sectional properties and blade natural frequencies.

5.6.1 Torque Tube

As shown in Fig. 5.3, the torque tube spans from $0.15R_E$ to $0.53R_E$. The torque tube consists of an elliptical cross section with a hollow center for the passage of straps for the extension/retraction mechanism. The center of the torque tube is aligned with the quarter chord of the outer-blade section. Furthermore, the torque tube has a linear twist rate of -5.81° m^{-1}, which is equivalent to the twist rate of the inboard section of the outer blade segment. The equal twist rates permit the outer blade segment to telescope over the torque tube during retraction/extension.

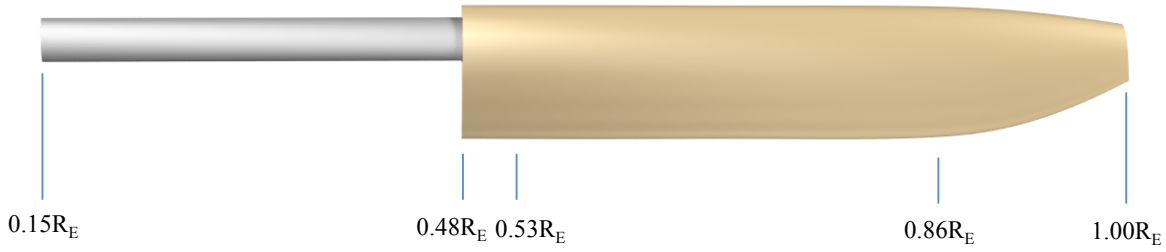

Figure 5.3: Proprotor blade in the extended position (helicopter mode)

A cross-sectional view of the proprotor blade is shown in Fig. 5.4. It can be seen that the *HeliX* blade utilizes a unique angular offset (ϕ) between the torque tube and outer blade segment [13]. As the outer-blade segment telescopes over the torque tube during retraction, the angular offset provides a stepwise increase in the mean pitch angle. The offset value implemented on the blade was $\phi = 10^\circ$; larger offset values were limited by structural interference between the torque tube and outer blade segment. This simple, passive method augments the large pitch collective setting required in forward flight and helps reduce the loads and deflections required from swashplate actuation.

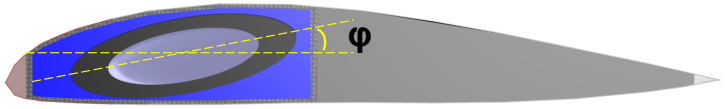

Figure 5.4: Torque tube angular offset

5.6.2 Outer Blade Segment

The outer blade segment spans from $0.48R_E$ to the blade tip. An exploded view of the outer-blade segment is shown in Fig. 5.5. The main structural elements include: airfoil skin, D-spar, core filling, trailing-edge block, a filler material in the D-spar, leading-edge mass, de-icing layer and erosion shield.

The primary load carrying member of the outer blade is the spar. The D-spar design was chosen as it offers a simple closed-section structure with high torsional rigidity. The spar extends from a chordwise position of $0.02c$ to $0.42c$ from the leading edge. The blade employs a negative elastic flap bending-torsion coupling (flap up-pitch down) through the composite lay-up in the D-spar. Previous studies [14] have shown that the use of pitch-flap structural coupling can increase the whirl flutter stability margins for a tiltrotor.

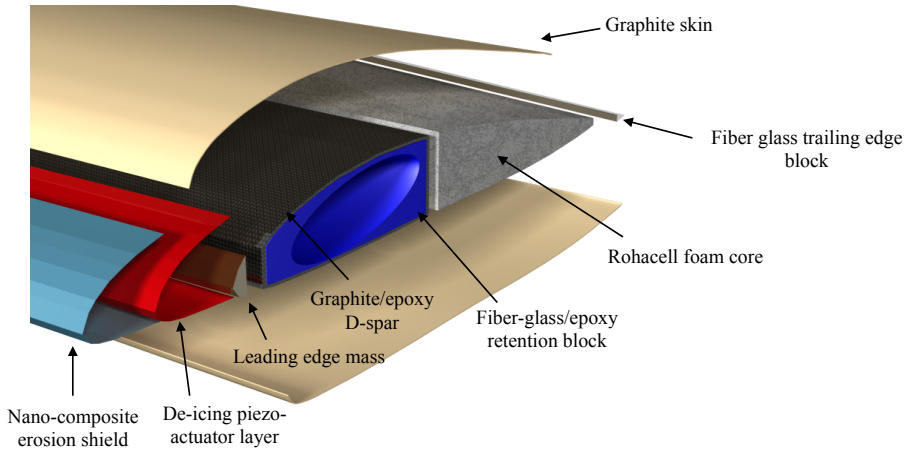

Figure 5.5: Exploded view of outer segment of proprotor blade

The D-spar includes a restraint surface at a spanwise location of $0.86R_E$ formed by an increased thickness of the internal wall of the spar [15]. During blade retraction/extension, the restraint surface provides a load path for centrifugal forces from the outer blade segment to an attachment block and subsequently to the hub. The details of this mechanism will be discussed in Section 6.4. The attachment block was designed to maximize the contact area with the restraint surface.

The center of gravity location of the outer blade segment was placed at $0.23c$ from the leading edge using a stainless steel ballast weight in the nose of the blade. This places the CG at $0.02c$ ahead of the elastic axis ($0.25c$) and ensures sufficient pitch-flap-flutter stability margin even with slight increases in weight in the aft section of the blade that may, for example, result from moisture absorption by the foam core material.

The *HeliX* blade utilizes a nano-composite erosion protection shield and a non-thermal-based de-icing system, which together require lower maintenance and power consumption. For enhanced erosion protection, polyurethane protective tape 8542HS manufactured by 3M was chosen because of its low weight, structural conformity and ease of repair [16]. This tape is made from an abrasion resistant polyurethane elastomer that resists erosion, puncture, tearing, and abrasion, as well as ultraviolet light damage. The added flexibility enables twisting and flexing that is not possible with metal protective sheaths (i.e., titanium, steel or nickel).

The de-icing system used on the blade consists of a series of actuators (0.002 m thick, PZT-4) along the leading edge between the blade skin and erosion shield. These actuators produce ultrasonic frequency distortion of the blade surface to shear off any accumulated ice; the ice detaches from the blade from centrifugal and aerodynamic forces. Other de-icing methods considered include electro-thermal-based methods and pneumatic deformation methods. Electro-thermal-based methods were not chosen because of their high power consumption (3.875×10^4 W m^{-2}) compared to

the high frequency skin distortion method that was chosen here (1.86 x 10^3 W m^{-2}) [17]. Pneumatic methods were not chosen because they utilize thin inflatable bladders along the blade leading edge and require pressurized air lines in the rotating frame, which can pose a significant design challenge.

5.7 Material Selection

Fiber-reinforced composite materials were chosen for the *HeliX* blade because of their superior specific strength, excellent fatigue characteristics and ability to conform to complex geometries. The torque tube is made of IM-7/977-3 graphite/epoxy. Graphite provides higher specific stiffness and ultimate strength as compared to other materials, such as glass fiber, as well as provides high bending and torsional stiffness and minimize weight. The inner and outer surfaces of the torque tube are coated with Stanyl 46 polyamide, which allows the outer blade and strap to slide along the torque tube with minimal frictional losses [18].

The blade skin consists of four balanced [$\pm 45°$] plies of S-2 glass/epoxy for high torsional stiffness. The D-spar is made of unidirectional [0°] plies of IM-7 graphite/epoxy with inner and outer torsion wraps made of woven [$\pm 45°$] graphite/epoxy fabric. Layers of unidirectional [20°] plies are used to introduce appropriate elastic flap bending-torsion coupling. The layup of the D-spar is [$+45_2/0_8/-20_6/-45_2$].

Rohacell 75 foam was chosen as the core material for preserving the aerodynamic contour of the blade. In the initial design process, Nomex honeycomb was chosen because of its superior bonding properties and low moisture absorption. However, the lower cost and ease of machining makes Rohacell foam an attractive option compared to honeycomb. Lastly, the trailing edge block is made of fiberglass reinforced epoxy.

5.8 Blade Manufacturing

The torque tube is manufactured using a silicone mandrel and a closed-die molding assembly, which define the internal and external geometries of the torque tube, respectively. The entire molding assembly is placed in an autoclave for curing the composite lay-up under heat and pressure.

The spar of the outer blade segment is manufactured separately using a solid mandrel assembly, which defines the internal geometry of the spar including its restraining surface. The lay-up is vacuum bagged and the assembly is cured in an autoclave. Next, remaining structural elements including the core material, trailing edge block, and leading edge mass are placed alongside the D-spar, and the entire assembly is wrapped with graphite/epoxy cloth to tightly contain the structure. The assembly is placed in a second mold for curing, which creates a small step along the leading edge. The erosion protection tape and de-icing layer are implemented in this step to complete the outer blade assembly.

5.9 Proprotor Dynamic Analysis

The spanwise distributions of blade mass, flap stiffness, lag stiffness and torsional stiffness are given in Fig. 5.6. The rotor has a $0.15R_E$ root cut-out. The torque tube spans from $0.15R_E$ to $0.53R_E$ and the outer blade segment spans from $0.48R_E$ to $1.0R_E$. The overlap region between the torque tube and outer blade segment between radial locations of $0.48R_E$ and $0.53R_E$, leads to increased blade stiffness and mass properties in this region. Furthermore, the increased internal wall thickness of the D-spar of the outer blade and the presence of the strap attachment block lead to increased blade stiffness and mass between radial locations $0.84R_E$ and $0.88R_E$. The outer blade is uniform up to a radial position of $0.86R_E$ and then tapers by a factor of 0.45 to the tip.

The spanwise blade properties were tailored through an iterative process to ensure that the flapwise, lagwise and torsional modal frequencies are properly placed so that they do not intersect the per-rev frequencies of the rotor. The spanwise distributions of stiffness, mass and inertia properties were implemented into the structural dynamics module of the comprehensive structural dynamics code HeliUM to calculate the vibratory modes. Blade parameters including

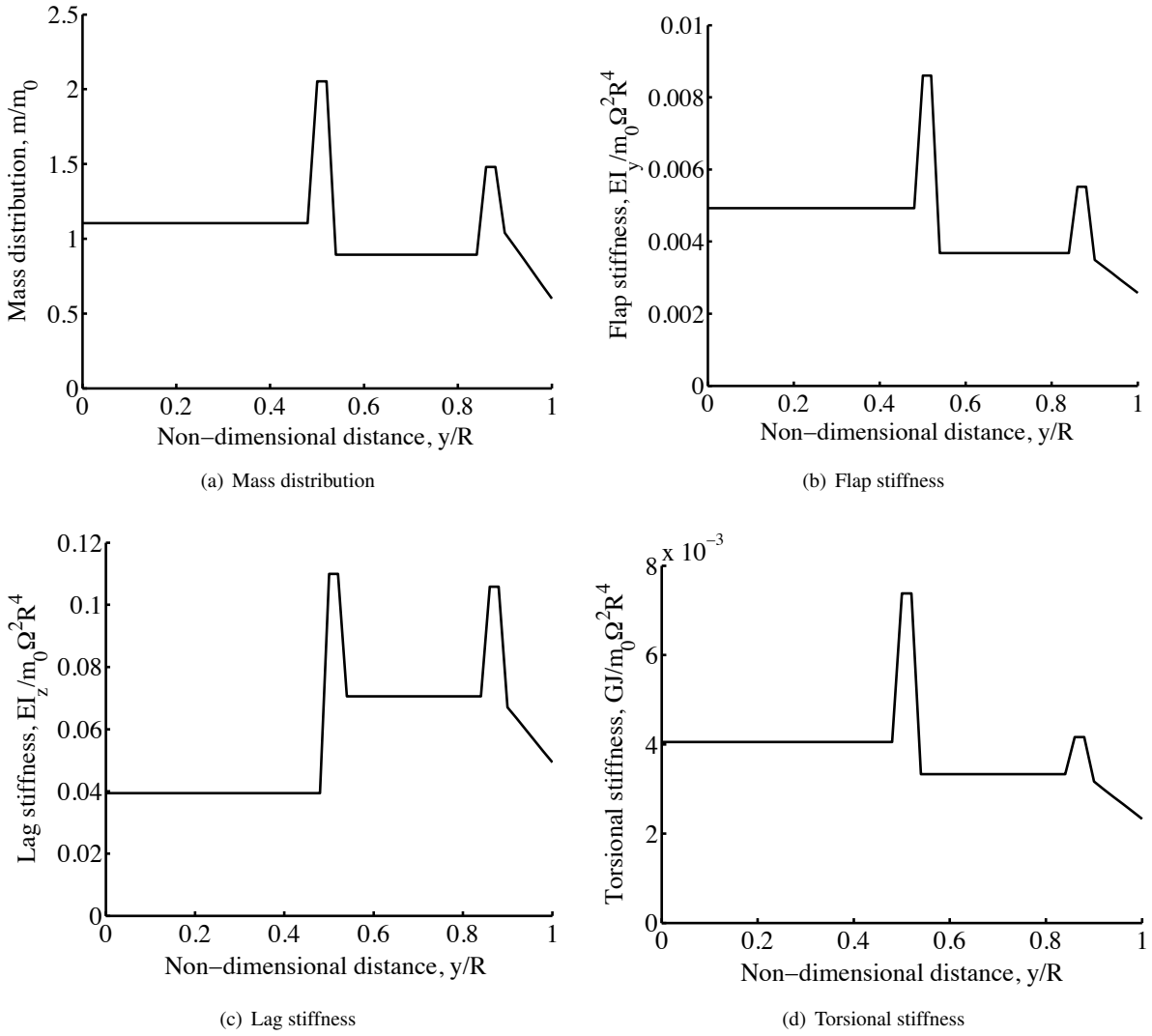

(a) Mass distribution

(b) Flap stiffness

(c) Lag stiffness

(d) Torsional stiffness

Figure 5.6: Sectional properties along the blade

torque tube thickness and width, D-spar flange thickness, airfoil skin thickness, and trailing edge block size were varied accordingly until the desired blade structural frequencies were achieved at the operational RPM.

Figure 5.7 shows the fanplot for the *HeliX*'s rotor system. The plot indicates that the modal frequencies are adequately spaced from the per-rev lines at the operating RPM in helicopter mode. The rotor is stiff in-plane, alleviating concerns about ground and air resonance, with a first lag frequency of 1.47/rev. The first flap frequency is 1.14/rev. In forward flight, the rotor must be modeled in the gimbal-lock mode and the flap, lag, and torsion frequencies must be kept sufficiently away from the bending and torsion modes of the wing to ensure whirl-flutter stability. This will be discussed further in Section 8.3.

5.10 Proprotor Design Summary

Using a well-validated proprotor BEMT methodology, parametric studies and judicious adjustments of blade characteristics converged on a design with propulsive efficiency of 0.85 and figure of merit of 0.71, at each respective

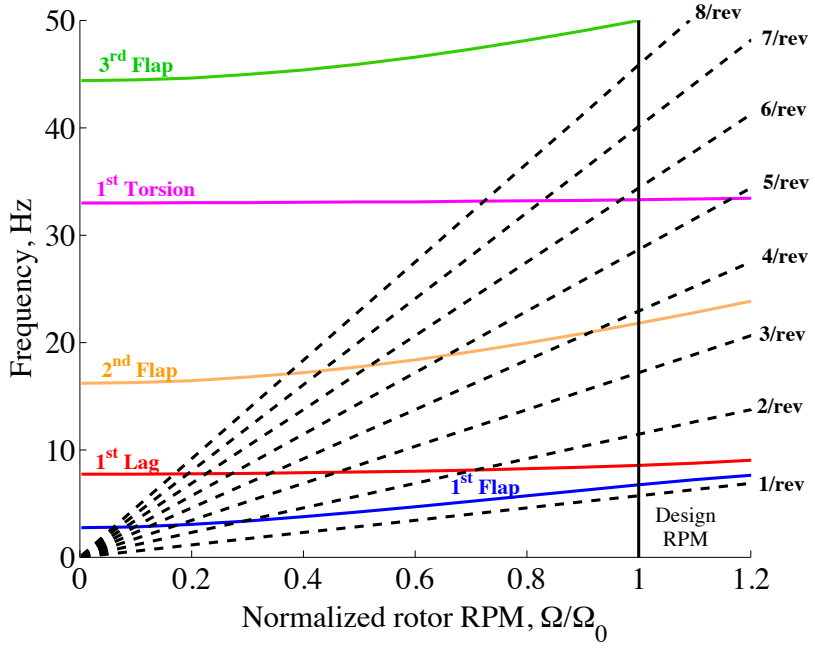

Figure 5.7: Fan plot showing blade structural modes as a function of RPM in hover

design point. This VDR system achieves aerodynamic efficiencies significantly higher than other configurations for the desired range of flight conditions. Furthermore, the blade spanwise structural stiffness and mass distribution were determined through an iterative process to ensure the proper dynamic stability margins were met at the design RPM.

A

A

B

B

Blade cut-away view

D-spar

Strap end

Titanium bolts

Restraint surface

Strap attachment

Retention block B

Retention block A

Blade lock pins

Guide rails

Spar

D-spar (cut-away shown)

Extended

Retracted

A-A

B-B

6 Hub Design

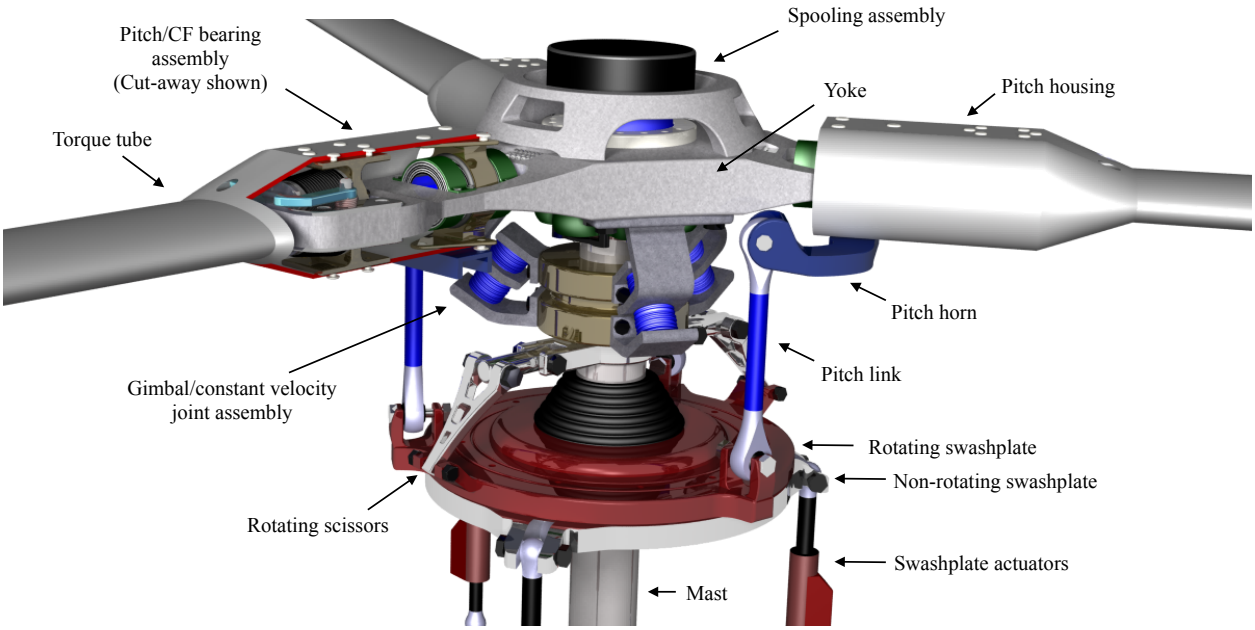

Figure 6.1: Proprotor hub

6.1 Proprotor Yoke

The proprotor yoke, shown in Fig. 6.1, transmits the torque, in-plane loads, and thrust loads between the rotor mast and the blade assemblies. The yoke is stiff in-plane, and each of its three arms consists of an elastically tailored flexure region that acts as a virtual coning hinge. The flexure separates two apertures in the yoke arm, which house the inboard and outboard bearing assemblies. The center of the yoke is hollow to accommodate the extension/retraction spooling assembly. The yoke is fabricated from filament wound unidirectional glass fibers that are reinforced with epoxy. The maximum thickness of the yoke occurs at its center; the yoke arm decreases in thickness up to the flexure region and then increases in thickness at the blade attachment region.

6.2 Bearing Assembly

The bearing assembly is shown in the foldout. The inboard bearing assembly consists of a unique interconnection between three radial elastomeric bearings and one spherical elastomeric bearing, all of which share the torsional motions and blade shear reactions between the pitch housing and yoke arm [19]. The three radial bearings are parallel to each other and are connected at the center by a hollow shaft. The inner radial bearing is enclosed by a spherical bearing, which in turn is connected to the pitch housing using a clamp. Therefore, a torsional moment imparted by the pitch housing is first transferred to the spherical bearing, then to the inner radial bearing, and finally to the two outer radial bearings through the connecting shaft. The sharing of torsional loads between the bearings allows for the large pitch range required between hover and forward flight modes, while also minimizing the diametric size of the assembly.

The outboard pitch bearing is a large conical elastomeric bearing. The radially outboard side of the bearing is attached to the yoke arm, and the inboard side is attached to the pitch housing through a clamp. The conical bearing is always under compression and reacts to the centrifugal loads and flap and lag shear forces between the blades and the yoke.

6.3 Constant Velocity Joint and Hub Springs

As shown in the hub foldout, the gimbaled hub of the *HeliX* consists of a constant velocity (CV) joint, also referred to as a homo-kinetic drive system, and outer elastomeric gimbaled bearings, which act as flapping springs. The CV joint and hub springs were designed specifically to accommodate the strap spooling assembly.

The elastomeric CV joint allows for a smooth, efficient transfer of torque from the rotor mast to the yoke without inducing vibrations. If a constant velocity joint is not utilized, the misalignment between the yoke and the mast would result in angular velocity variations in the rotor system, which in turn would induce vibration at twice the rotational frequency (2/rev) and velocity in the torque transferred to the yoke/rotor. The *HeliX* utilizes a constant velocity joint [20] which employs six elastomeric bearing assemblies. Three of the elastomeric bearing assemblies are connected to the yoke through U-shape posts, and the remaining three assemblies are connected to splined sections of the mast through two triangular plates. The six bearing assemblies are identical in geometry. Each assembly consists of an inner cylindrical elastomeric bearing and an outer spherical elastomeric bearing, which are separated by rigid metal plates. The cylindrical bearings allow for axial deformations and the spherical bearings allow for angular deformations. Together, these deformations permit the gimbal degree of freedom between the yoke and mast and allow the mast to rotate the yoke at constant angular velocity.

The outer elastomeric bearings connect the rotor mast to the yoke and act as hub springs. The deformation in compression of the hub elastomeric bearings limits the angular misalignment between the yoke and mast and allows for the transfer of the thrust loads.

6.4 Extension/Retraction Mechanism

Several methods of blade extension/retraction were considered in the initial design process [21–24]. The four mechanisms for extension/retraction considered were: a lead-screw/jack screw, steel cables, centrifugal force actuated springs and high-strength fiber straps/belts. In addition, three types of VDR actuation methods were considered: a shaft concentric with the main rotor shaft using differential gears, a hydraulically actuated system and an electric motor with a high gear reduction. The advantages and disadvantages of each of these systems are given in Tables 6.1 and 6.2. Multiple combinations of the extension/retraction mechanisms and actuation types were evaluated. Ultimately, a high-strength fiber strap system, in combination with an electric motor with a high gear reduction, was chosen for the VDR system of the *HeliX*. This latter system offers relatively reduced weight and power requirements, while minimizing the overall mechanical complexity.

Table 6.1: Mechanisms for blade extension/retraction

Mechanism	Advantages	Disadvantages
Lead-screw/Jackscrew	Precise extensioin/retraction of blade	Large heat dissipation/high thread wear/large size
Steel cables	Small size/high tensile strength	Low fatigue tolerance/low strength-to-weight
Centrifugal force actuated spring	Passive mechanism (no actuation required)	Rotor RPM dependent/unequal individual blade extension/retraction
High-strength fiber straps/belts	High strength-to-weight/multiple load paths/high fatigue tolerance	Ultraviolet light damage

The VDR system of the *HeliX* consists of a high-speed, low torque electric motor, high gear reduction harmonic drive system, spool drum, Kevlar fiber straps, three load transferring structural members, and a blade lock system. In the remainder of this section, the various elements of the VDR system will be discussed in detail.

Table 6.2: Actuation types for blade extension/retraction

Actuation Type	Advantages	Disadvantages
Concentric shaft with differential gears	Coupled to rotor drive shaft	Mechanical complexity/high weight
Hydraulic system	Large actuation forces	Complexity (rotating frame)
Electric motor with gear reduction	Lower power requirement/lightweight feedback control	Potential motor size

6.4.1 Variable Diameter Rotor System Operation

The electric motor operates in the inertial frame of the hub and is housed on top of the proprotor yoke. The motor is connected to a spool drum located at the center of the yoke. A high gear reduction is achieved between the motor and the spools through a harmonic drive system (HDS) [25]. The HDS, shown in the foldout, provides a unique way to achieve a high gear ratio, while allowing for a compact and lightweight design. The HDS system consists of a rigid ring gear, a flexspline, and an elliptical wave generator. The flexible gear conforms to the elliptical wave generator as it rotates, and engages different sections of the rigid circular ring gear to provide a high gear ratio of 1:300.

The spool drum houses three high-strength Kevlar straps for each of the three blades. One end of the Kevlar strap is attached to a spool driven by the motor, and the other end is rigidly attached to the outer blade segment at a radial location of $0.86R_E$. During extension/retraction of the rotor, the motor drives the spooling assembly to retract the Kevlar straps, in turn permitting the three outer blade segments to telescope over their respective torque tubes. A series of structural members are integrated into the proprotor blade to transmit the centrifugal loads of the outer blade segment to the rotor hub during its various modes of operation. Lastly, a blade lock system is used to fix the position of the outer blade segment in the retracted mode.

6.4.2 Strap and Motor Sizing

During extension/retraction of the proprotor blades, the Kevlar strap must transmit the high centrifugal loads of the outer blade segment to the rotor hub. The dimensions of the Kevlar strap were sized based on calculations of the centrifugal force of the outer blade, with the rotor operating in the extended position (R_E). The spanwise location of the center of mass of the outer blade was calculated based on the blade mass distribution given in Fig. 5.6(a). A high load factor was applied to ensure safety and reliability of the retraction mechanism. The final calculations of the centrifugal loads were used in conjunction with the ultimate strength of Kevlar to determine the strap thickness and width dimensions; see Table 6.3. The blades extend radially as a result of their centrifugal forces and uniform

Table 6.3: Kevlar strap sizing parameters

Extended rotor radius, R_E	6.59 m
Rotational speed, Ω	348 RPM (36.44 rad s^{-1})
Outer blade mass	57.83 kg
Outer blade center of mass	$0.67R_E$
Outer blade centrifugal force	3.39 x 10^5 N
Safety factor	4.5
Tensile strength (Kevlar 49)	3,600 MPa
Kevlar strap thickness	44.45 mm (1.75 in)
Kevlar strap width	9.53 mm (0.38 in)

extension of all three blades is ensured by the single spool design. To retract the blades, however, a large torque must be applied over a relatively short time interval to counteract the centrifugal forces. High-torque motors generally weigh significantly greater than low-torque motors and, therefore, may not be suitable for the *HeliX*. A low-torque motor can

provide the same power transfer as a larger motor, but needs to operate at a higher operating speed and therefore requires a large gear reduction. The harmonic drive system discussed previously (Section 6.4.1) is used to provide a gear reduction of 1:300. An analysis was conducted to determine the electric motor requirements based on the maximum torque required to retract the blades and total actuation time. The compromise between decreased actuation time and increased motor torque requirements led to the selection of an actuation time of 25 s. The corresponding motor operating speed and power requirements were determined and the motor weight was estimated based on existing designs [26]. These values are presented in Table 6.4.

Table 6.4: Extension/Retraction motor sizing parameters

Retraction time, Δt	25 s
Spool speed, Ω_{spool}	6 RPM (0.63 rad s^{-1})
Harmonic drive gear ratio	1:300
Motor operating speed, Ω_{motor}	1,800 RPM
Motor torque required	157.91 N m
Motor power required	29.77 kW (40 hp)
Motor weight	125–150 kg

6.4.3 Load Transfer Mechanism

A cut-away view of the blade showing the VDR assembly is given in Fig. 6.2. The key advantage of this design is that it allows the Kevlar strap to be completely off-loaded when the rotor operates in the extended (hover) and retracted (forward flight) modes, shown in Fig. 6.3, thereby improving the overall operational safety and reliability. The VDR

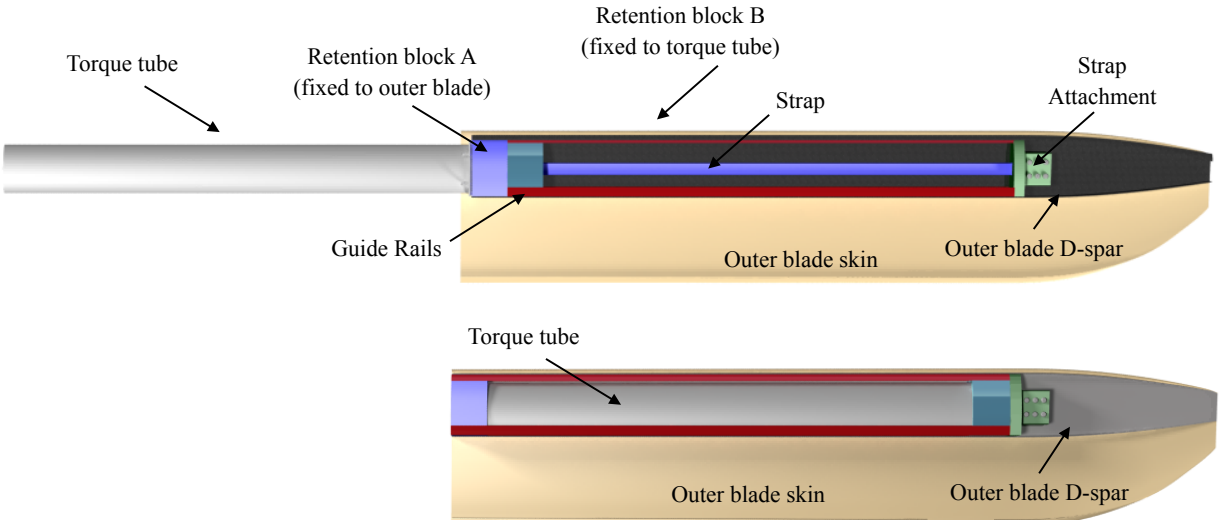

Figure 6.2: Extended and retracted blade positions

assembly consists of two retention blocks (denoted blocks A and B), one strap attachment block, and a blade locking system. The two retention blocks allow the outer blade segment to telescope over the torque tube. Retention block A is rigidly attached to the root end of the outer blade and retention block B is attached to the tip end of the torque tube. A set of guide rails in the D-spar allow retention block B to travel inside the outer blade. Once the blade reaches its extended position, retention block B comes into contact with retention block A, preventing the outer blade from telescoping outward. The centrifugal forces of the outer blade segment are transmitted through the retention blocks

and to the torque tube, completely off-loading the Kevlar strap.

When the blade is retracted, a locking system is used to fix the position of the outer blade [27]. The locking system consists of two spring-loaded engagement hooks and two lock pins. The engagement hooks are attached to the yoke arm and are enclosed inside the pitch housing. The lock pins are attached to the D-spar of the outer blade and are enclosed by a small overlap of the blade skin. Two apertures in the pitch housing allow the lock pins to travel inside the housing and engage with the hooks, locking the outer blade in place. The centrifugal forces of the outer blade are transmitted directly to the yoke arm through the lock mechanism. To ensure system integrity and safety, the Kevlar

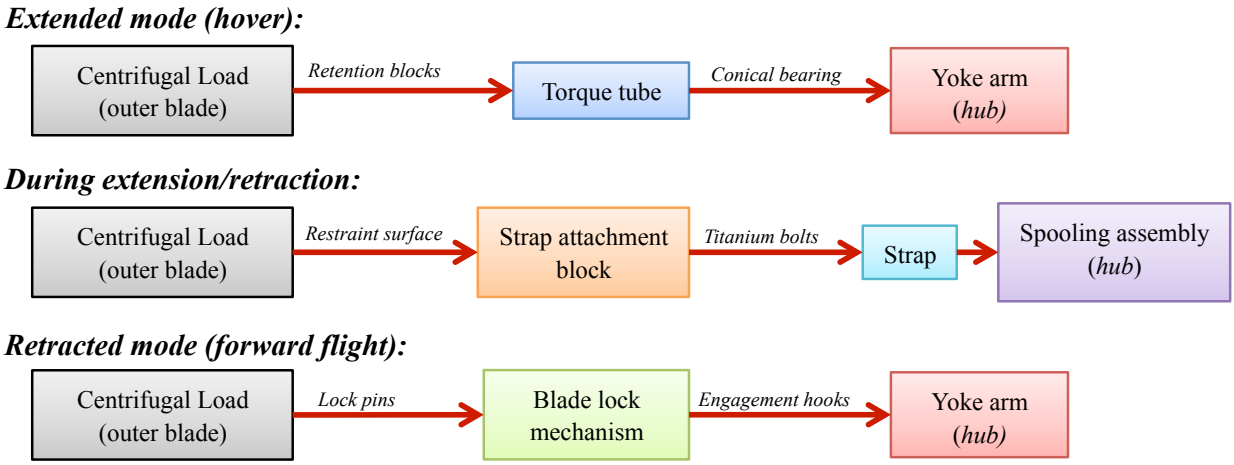

Figure 6.3: Load paths during various modes of operation

straps are only loaded during the extension/retraction of the blade. The end of the strap is reinforced with epoxy resin to make it rigid, and is secured to a fiber-glass/epoxy block with titanium bolts. The strap end has increased thickness (25.4 mm) and width (127 mm) to better distribute the loads. An increased thickness of the D-spar at $0.86R_E$ forms a restraint surface. The strap attachment block is in contact with this restraint surface and is fastened to the sides of the spar to prevent chordwise movement. During extension/retraction, the centrifugal loads of the outer blade segment are transferred through this restraint surface. Therefore, the part of the outer blade radially inboard of the attachment location ($0.86R_E$) is placed under compression and the part radially outboard of this location is under tension.

BEARING ASSEMBLY

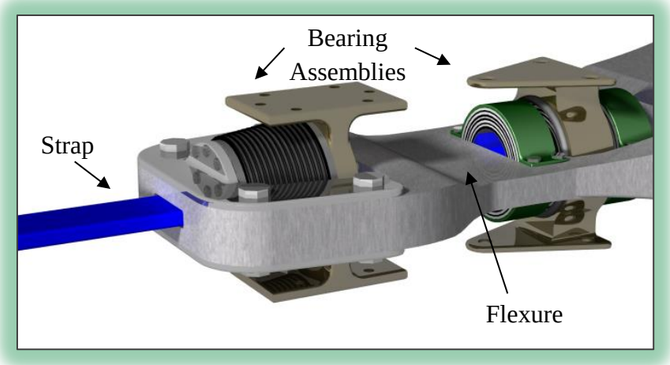

BEARING ASSEMBLY (EXPLODED VIEW)

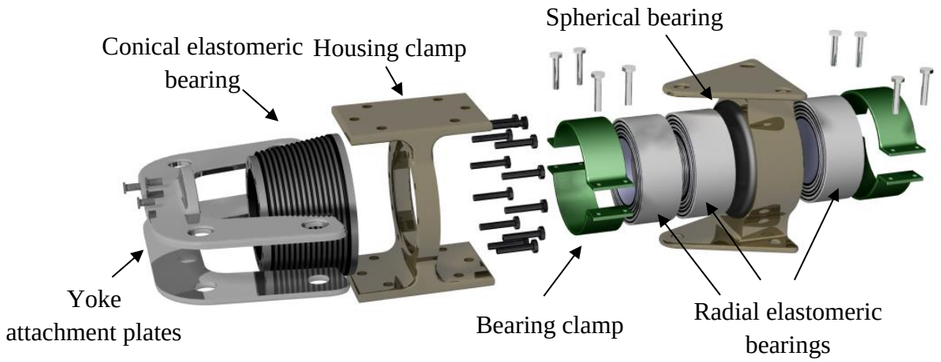

SPOOLING ASSEMBLY

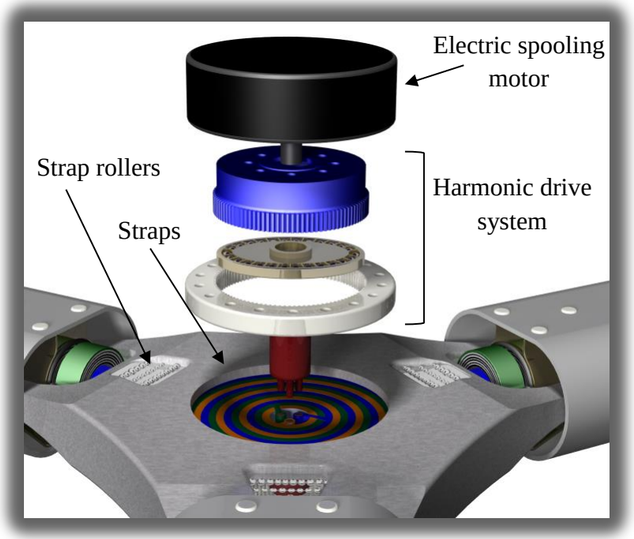

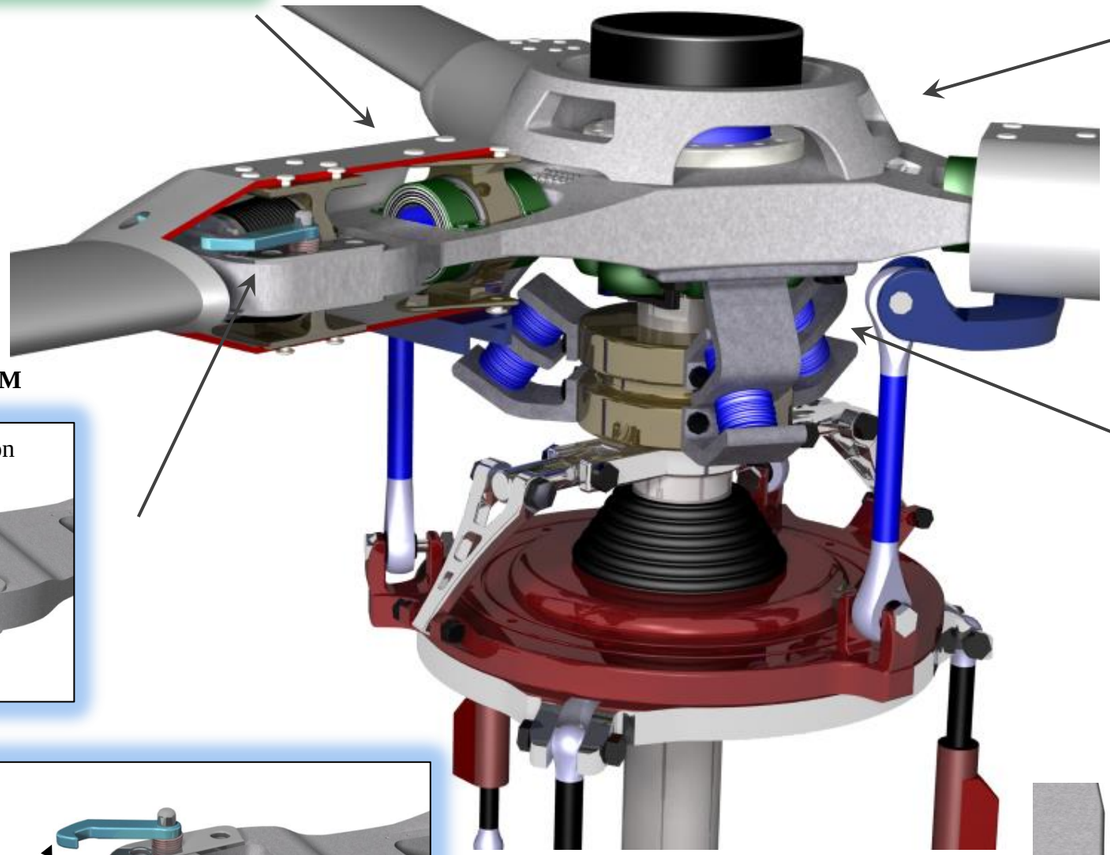

BLADE LOCKING MECHANISM

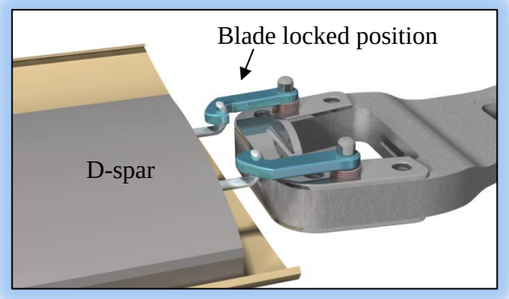

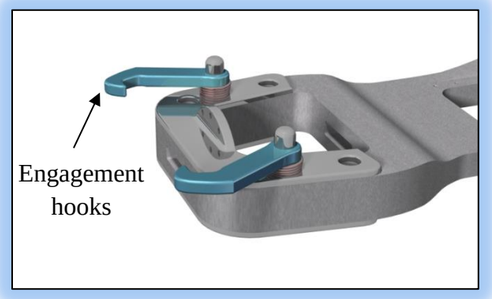

GIMBAL AND CV JOINT ASSEMBLY

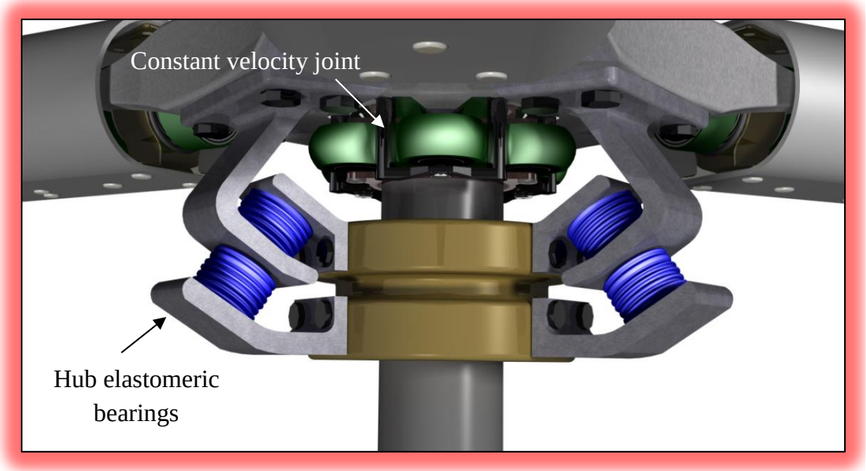

CONSTANT VELOCITY JOINT (EXPLODED SIDE VIEW)

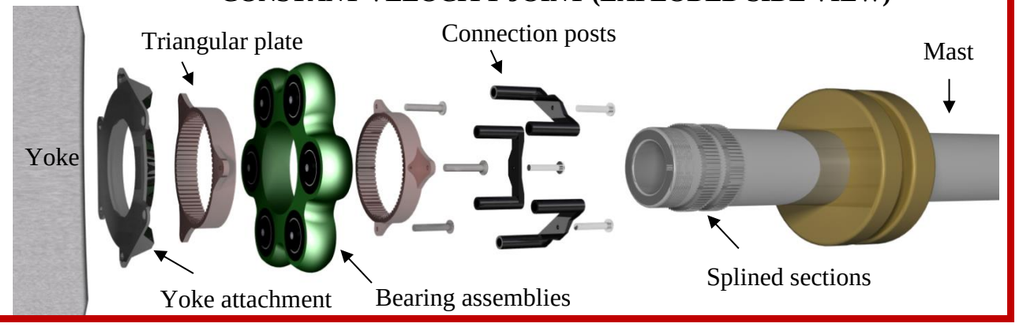

7 Transmission

This section covers the design and optimization of *HeliX*'s transmission. Given requirements from the customer, engineering characteristics were formulated to determine the specifications needed to design the proper transmission layout.

7.1 Engine Selection

As mentioned in Section 2.7, no particular engine was specified in the RFP, so various engine types were examined, including electric, turboshaft, and reciprocating/piston diesel engine. Trade studies were performed to determine the best engine for the *HeliX*. These trades included performance, development time, cost, maintainability, durability, reliability, size, weight, and placement.

An electric engine was discarded after calculating that to provide even 15 minutes of power, approximately 4,800 power cells would be needed, weighing around 7,185 kg (15,840 lbs) total [28, 29]. Until there are significant advancements in batteries and fuel cell technology, an electric engine would not be suitable for this aircraft size. A hybrid power system [30] was also considered, but the low TRL value and lack of proven capability in aircraft made it unsuitable for a vehicle where reliability is crucial.

The turboshaft engine was selected for a number of reasons, including its much higher power-to-weight ratio. Turboshafts also have higher time-between-overhaul requirements; they generally need to be serviced every 1,000 hrs or so, whereas piston engines must be serviced more frequently. There is a lower maintenance cost associated with turboshafts and the use of jet fuel. Turboshaft engines also have the advantage that they are able to start at lower ambient temperatures and can provide full power without a long warm-up period, which makes them ideal in this case.

In the process of determining the best layout for the *HeliX*, the use of two or three engines was considered. Although not typical for an aircraft of this size and weight, the three engine configuration was considered, primarily because of safety considerations. Because this vehicle was designed to act as an effective SAR platform, a third engine would allow the vehicle to perform and land safely in the event of a one-engine out situation. Additionally, if three engines were installed, it could be possible to shut one down during cruise to save fuel and achieve longer ranges and higher endurances. However, to be able to achieve the required speeds with only two engines in the cruise phases of the three missions, at least 20% more total power had to be installed, substantially increasing the vehicle weight. It should be noted that this is not recognized as a typical practice and would require FAA approval. A preliminary layout of the three engine configuration is shown in Fig. 1(a). Other three engine layouts were considered but suffered from issues including transmission complexity and housing concerns. Table 7.1 summarizes the trades in the number of engines. In the end, it was decided that a twin engine configuration was optimal for the *HeliX* and the missions it must perform.

Table 7.1: Three engine design advantages and disadvantages

Advantages	Disadvantages
– Increased operational safety	– Increased operational and maintenance cost
– Lower fuel flow rates in cruise leading to increased endurance	– Complex gearing and associated failure rates
– Twin engine cruise capability leading to better ranges	– 2.2% empty weight penalty if one engine turned off
– Capable of uncompromised performance in OEI condition	– More engines need to be housed leading to potential increase in flat plate area
– Military applications benefit from excess power	– 20% increase in SL installed power beyond that required for missions
	Higher acquisition cost penalty

7.2 Transmission Design

A variety of transmission layouts were studied, starting with the configuration used on the V-22. The engine placement inside the proprotor nacelles moves weight away from the center of gravity and requires additional structural stiffness in the wing [31, 32]. Another major concern with this is in the case of a one engine failure scenario; having a long shaft with a moment exerted on one end and a resistance on the other end means a thicker shaft is required to carry the load. A variation to this layout was made to enhance engine placement for optimal transmission design and improve the safety of the aircraft. As shown in Fig. 7.1(b), the *HeliX* has both of its engines placed on the fuselage and inboard of the wings. This decision reduces the weight of the wing, decreases vehicle drag, and protects the engines when the the aircraft may operate in a hostile environment. The efficiency of the transmission system ranges between 96–98%, because of the optimal gear selections. It should be noted that the inboard engine placement has other design issues, including higher noise levels in the cabin, as discussed in Section 16.1 After the overall layout of the transmission

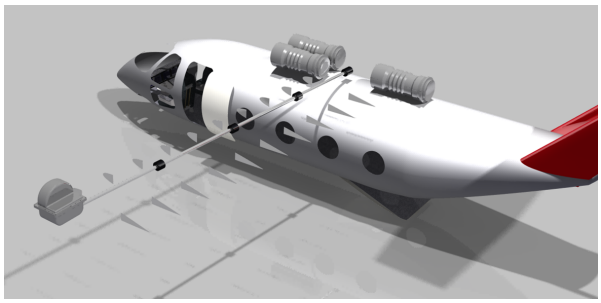

(a) Preliminary three engine design consideration

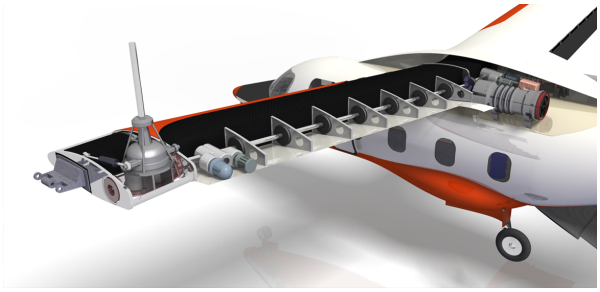

(b) Current two engine design

Figure 7.1: Comparison of two transmission configuration options

Table 7.2: Factors affecting split-torque versus planetary gear system decision

Planetary	Split-Torque
High efficiency	Weight reduction
Flexible gear ratios	Lower energy losses
Compact and high torque transmission	Increased safety/reliability with separate drive paths
	Fewer gears and bearings, i.e., less complex

was decided, the main gearboxes to reduce the RPM from the engines to the proprotors were taken into consideration. Two ways for reducing the RPM are by using a planetary or split-torque setup, and their trades are summarized in Table 7.2. The proprotor gearboxes were originally sized with a split-torque design. However, after the large bull gear was sized to be over 0.46 m (18 in), which would be difficult to manufacture, a hybrid design using both a split-torque and planetary system was employed. Not only did this design decision reduce the overall size of the bull gear, but it also reduced the weight of each main gearbox by 54.4 kg (120 lbs). A comparison of these two designs is shown in Fig. 7.2 and Table 7.3. An additional advantage to the hybrid design is the fact that the ring gear of the planetary gearbox can be incorporated into the casing of the main gearbox, reducing its overall size and weight.

Table 7.3: Comparison of split-torque and hybrid transmission designs

	Split-Torque Transmission	Hybrid Transmission
Total Gear Weights	346 kg (763 lb)	292 kg (643 lbs)
Largest Gear	Bull Gear at 0.46 m (18.1 in)	Planetary Ring at 0.45 m (17.9 in)

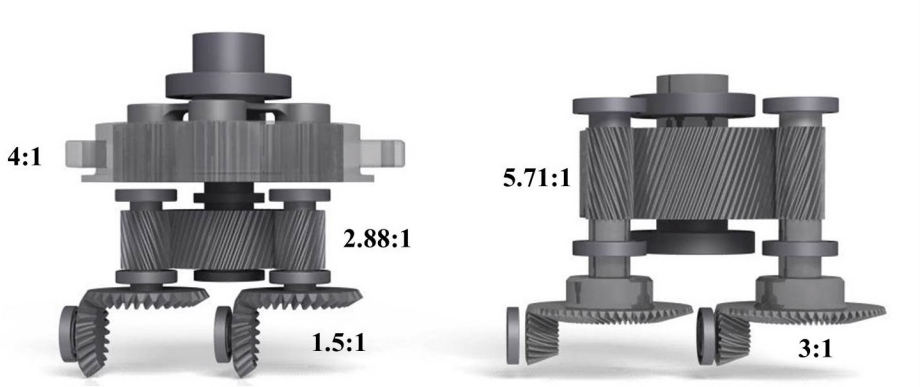

Figure 7.2: Three-stage planetary-split-torque hybrid vs. two-stage split-torque design

7.3 Transmission Organization

A sprag clutch was placed between the engines and the drive shaft so that the engines can drive the system but the proprotors cannot drive the engines. This is important because in the event that an engine malfunctions, this clutch will allow for autorotation. By flame-plating the housing bore with tungsten carbide, wear problems associated with overrunning were alleviated. Also, a high oil flow rate is ensured by pressurized lubrication during overrunning.

The transmission shafting is hollow with a high diameter to thickness ratio. This design reduces the weight of the shaft, while ensuring that the shaft is still be able to handle torsion, axial tension, and bending loads. Because of the vibratory nature of the shaft while rotating at high RPM, a margin of safety of 2 was used between the three stresses acting on the drive shafts.

A central Auxiliary Power Unit (APU) is located between the two engines, Fig. 7.3, and is used to start a generator and hydraulic pump for the central systems. After the engines start, there are two other sets of generator and hydraulic pump units located out at the nacelles to run the units located around the corresponding gearboxes [33–35]. These also provide triple redundancy. The APU will automatically switch off and decouple from the drive system once the engines reach 70% of their normal running RPM.

The bearings placed in the transmission are designed for 3,000 hour overhaul intervals [6]. These bearings are made from M-50 type steel to obtain maximum reliability. Bearings along the interconnecting shaft through the wings are able to handle deflections that occur during flight because of normal wing bending.

A primary lubrication system connected to the two main gear boxes in the nacelles are used to cool the gears, which generate some heat from friction. The placement of oil jets within the gearbox is optimized such that the flow of oil enhances the performance of the gears. In the event there is a loss of lubrication during flight, the gears are designed to run dry for up to 30 minutes. The lubrication system is designed to operate in either the forward flight position or hover position. A vane type lubrication pump is installed to provide a better flow of oil through the gear case. Low pressure screens are located at the pump inlet with 40-micron filters in between the cooler and the pump, which ensures no contaminated oil goes through the pump. A chip detector is also located inside the gearbox as part of the HUMS (see Section 14). A vent valve is located on the gearbox to limit any excess pressure.

To ensure an equal torque split between the two input bevel gears on the split-torque transmission stage of the main gearbox, a special shaft was placed between the bevel and spur gears such that it deflects small amounts to account for gear mounting tolerances and to be sure that the torque is split equally [36].

The two main gearboxes are located within each of the nacelles. The main drive shaft running through the wing span

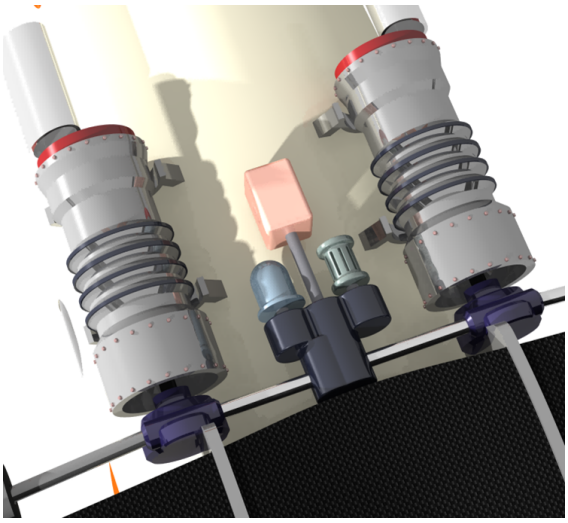

Figure 7.3: Center gearbox configuration

of the aircraft connects to two split-torque transmissions on each side, followed by a planetary system. Within the split-torque transmission there are two stages. The two bevels on the main drive shaft give an initial 1.5:1 gear ratio to reduce the RPM from 6,048 to 4,032. From the first and second compound gear there is a shaft that drives these two gears to the next set of spur gears which then drive the bull gear that has a larger gear ratio of 2.88:1 and brings the speed down from 4,032 to 1,400 RPM. Finally the planetary gear system, through a gear ratio of 4:1, brings the speed down to the operational RPM of 350. A layout of this system is shown in Fig. 7.4.

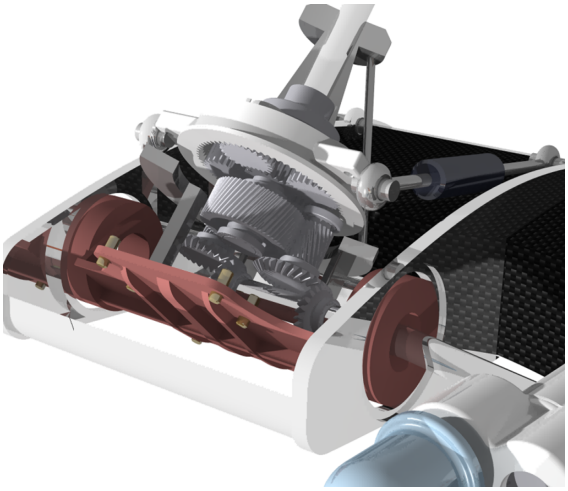

Figure 7.4: View of split-torque planetary hybrid gearbox and associated tilting mechanisms within the nacelle

Gear sizes were determined using AGMA 2001-C 95 and AGMA 2003-B97 standards [37,38]. Also, AGMA 911-A94 and AGMA 908-B89 were used for helicopter-specific designs. The dimensions of the gears were formulated using the compressive stresses and teeth were designed around the necessary bending strength. An important aspect that was studied was the backlash ratings of the gears and the stresses induced by tooth-on-tooth contact. A safety factor of 1.5 was used. The gears in the main gearboxes are rated to 2,000 hours between overhaul. A surface finish of 8 RMS is used on the gears to improve performance. Helical gears were used to reduce the backlash and create a more precise transmission system. Using the helical gears introduces an axial load to the shaft, but this was addressed by careful

placement of thrust bearings. Gear specifications are given in Table 7.4.

Table 7.4: Gear specifications

Stage Type	Gear Type	No. of Teeth	Gear Ratio	RPM	Pitch Diameter (in)	Diametrical Pitch (in^{-1})	Face Width (in)	Pressure Angle (degree)	Helix Angle (degree)	No. of Gears	Weight (lbs)
1 Split Torque	Bevel	20	1.5:1	6048	5.83	3.5	1.24	20	20	4	8.4
		30		4032	8.98					4	19
2 Split Torque	Spur	20	2.88:1	4032	3.12	6.5	4.1			4	11
		58		1400	8.98					2	94
3 Planetary	Sun	24	4:01	1400	5.59	4.5	2.79		0	2	22
	Planet	24		N/A	4.47					8	22
	Ring	72		350	17.87					2	349

7.4 Gear Manufacturing

The gears will be made with a slightly modified standard gear process. This additional process, outlined in Fig. 7.5, is designed based on the material selection of Ferrium C-64. The process, which involves vacuum carburizing, adds extra strength to the gears, thereby reducing their size and weight. This process aids in the reduction time spent post grinding, allows the gears to handle higher temperatures, and ensures that the gear retains more uniform case depth between flanks and roots.

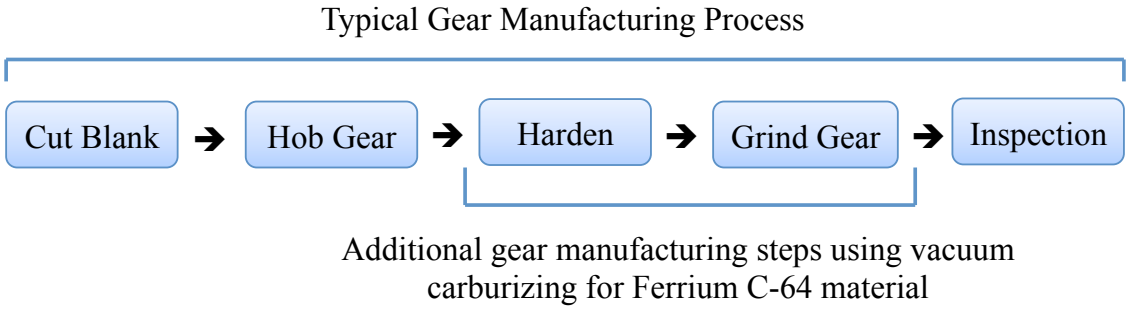

Figure 7.5: Modified manufacturing process for gears made of Ferrium C-64

7.5 Gearbox Casing

The gearbox casing is to be manufactured from aluminum through die casting because of its large size. Although magnesium is about 30% lighter than aluminum, it has a much lower strength and is susceptible to corrosion especially in saltwater environments. Magnesium also has a higher thermal expansion rating, which would affect the overall alignment of the transmission as it is heated or cooled. After each gearbox casing is finished, it should be laser scanned and compared to the CAD model to ensure the required tolerances are met. A cone shaped mast housing alleviates the lift from the rotors being placed directly on the gearbox casing and transmission; the connection points transfer the lift to the torque box in the wing. The final main gearbox casing is shown in Fig. 7.6.

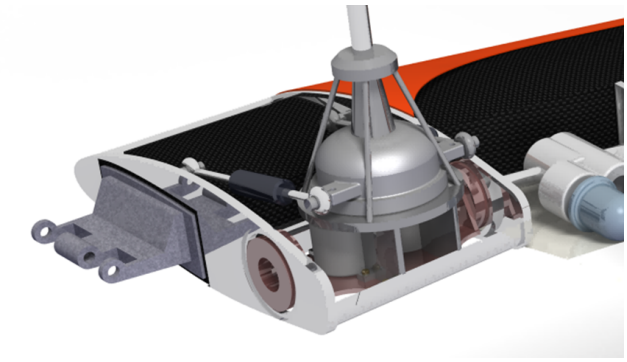

Figure 7.6: View of three-stage nacelle-gearbox casing

7.6 Transmission Summary

As this section has described, a fully functional transmission design was produced in which all RFP requirements were exceeded in terms of safety, weight reduction, and durability. The inboard twin engine configuration paired with the split-torque hybrid gearbox achieved superior performance characteristics when compared to other configurations. All gear designs followed strict AGMA standards to meet the demanding industry needs.

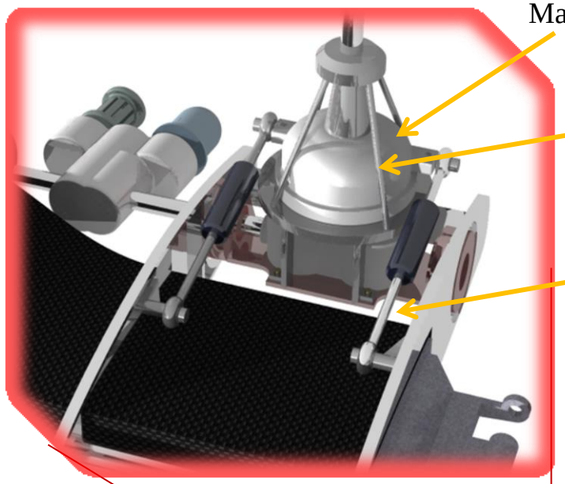

Main Gearbox

Static Mast

Tilting Hydraulic Actuators

Generator

Hydraulic Pump

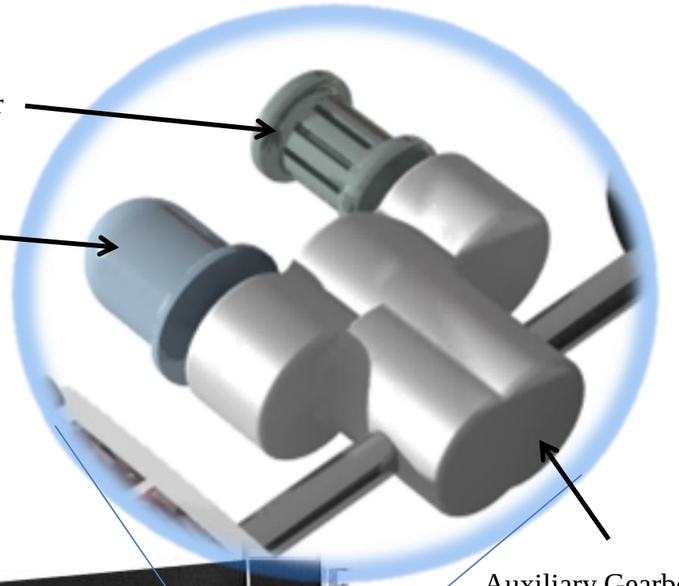

Auxiliary Gearbox (Triple Redundancy)

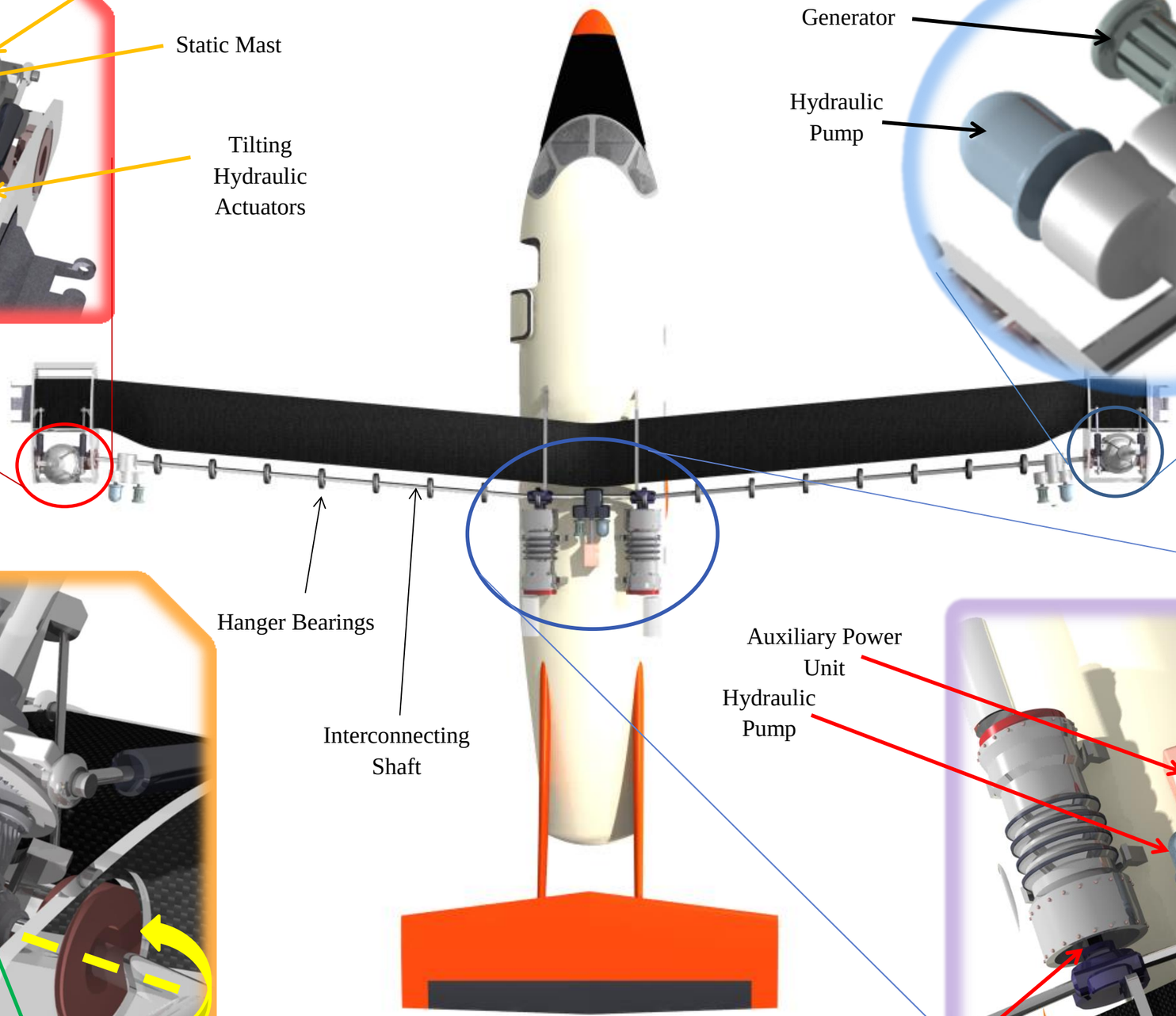

Transmission (Planetary 3rd Stage)

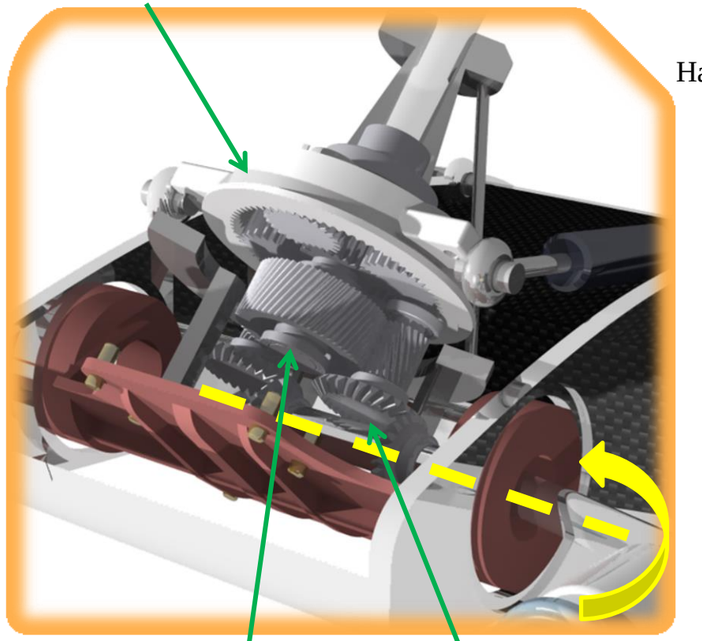

Hanger Bearings

Interconnecting Shaft

Transmission (Split Torque 2nd Stage)

Transmission (Bevel Gear 1st Stage)

Generator

Auxiliary Power Unit

Hydraulic Pump

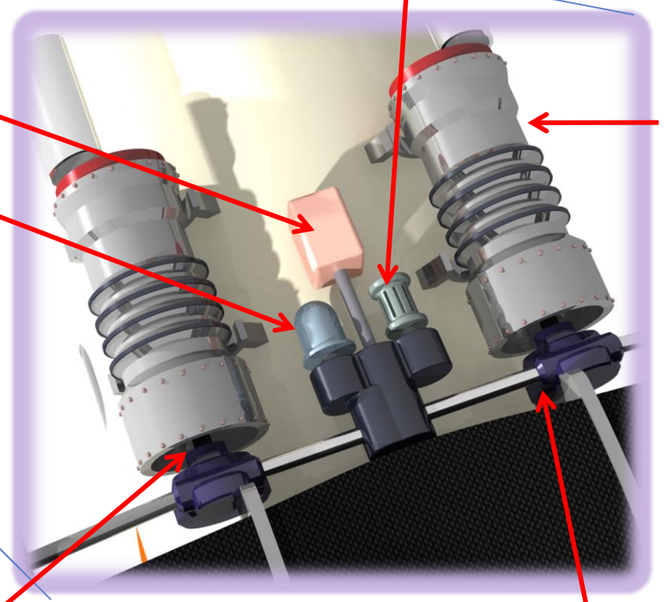

Engine

Sprag Clutch

Nose Gearbox

8 Wing Design

The wing on the *HeliX* provides the lift required in airplane mode. The wing must carry the proprotor and its associated mechanism at the wing tips, as well as the outer wing extension (OWE) and its mechanisms. The aerodynamic design has to embrace all the flight conditions outlined in the RFP and must be able to provide adequate lift with sufficient stall margin in each mission scenario. The structural design has to withstand a 3.5g normal load factor with a factor of safety of 1.5 in accordance with FAR regulations. Additionally, the presence of proprotors and their location outboard on the wing can potentially lead to aeroelastic instabilities in the form of pylon whirl flutter, which has been accounted for in the design of the wing, as discussed in Section 8.3.

8.1 Aerodynamic Design

The aerodynamic design of the wing required trades on various parameters that included: planform area, wing span, wing aspect ratio, airfoil section, wing dihedral, wing sweep, vertical and horizontal position relative to the fuselage, and the use of high lift devices. Some of these parameters (wing aspect ratio, wing span, and wing area) were defined during the initial sizing methodology (Section 2, and others were chosen based on other design considerations. A summary of the wing parameters are given in Table 8.6.

8.1.1 Lift Requirements

The lifting requirements of the wing were outputs from the sizing methodology. The cruise/loiter segments of the three missions vary, as shown in Table 11.1, and are flown at different vehicle weights. For a given wing geometry and operating condition, the wing lift coefficients (C_L) required were determined, as shown in Table 8.2. The design of the wing of the *HeliX* wing is similar to conventional airplane design in forward flight. Table 8.2 shows the C_L

Table 8.1: Cruise speed for each mission segment (kts)

	Mission 1	Mission 2	Mision 3
Onward cruise	240	180	240
Loiter	120	80	N/A
Return cruise	180	140	240

Table 8.2: Lift coefficient requirements of each mission segment

	MGTOW	Mission 1	Mission 2	Mision 3
Onward cruise	0.60	0.46	1.16	0.45
Loiter	1.73*	1.35*	3.61*	NA
Return cruise	1.10	0.87	1.45	0.44

* Rotorcraft operates in hybrid mode

required if all the missions were to be performed in airplane mode for the fully sized aircraft (with the 6 ton useful load capability) and the TOWs for the missions themselves. Because the loiter segments of Missions 1 and 2 are to be at low airspeeds, they must be performed by the *HeliX* in helicopter mode or in hybrid mode where the proprotors are partially tilted forward. The results show that the aircraft is expected to operate efficiently over a wide range of C_L values when in airplane mode. The cruise operating conditions are outlined in Table 8.3.

Table 8.3: Key wing parameters at design cruise point

Altitude	Cruise Speed	Operating C_L	Mach no.	Chord Reynolds no.
6,000 m, ISA+15°C	230 kts[1]	0.61	0.37	1.2×10^7

[1] Corresponds to V_{BR}, see Fig. 3.7

8.1.2 Airfoil Selection

The airfoil selection for the wing was based on: (a) the C_L requirements outlined in Table 8.2, (b) a relatively high section thickness-to-chord (t/c) ratio (15–20%) for torsional stiffness to prevent whirl flutter instabilities (see Section 8.3), and (c) a preferably high sectional C_l also with gradual stall onset, and with a wide drag bucket range around the operating C_l. Because the operating Mach number at cruise altitude (0.37) is sufficiently below the drag divergence Mach number, compressibility effects on the wing were not a consideration.

The three-dimensionality and the finite aspect ratio of the wing reduces the effective lift curve slope, which was accounted for in the two-dimensional C_l required. Other aircraft components, such as the empennage and fuselage, can contribute to the lift, positively or negatively as much as 20%. In the initial design stage, the C_l required was further increased by a factor of 1.05 to account for these effects, arriving at a conservative estimate of 0.71.

Different airfoils were considered, and based on the constraints outlined earlier a NACA 65_3-618 airfoil was chosen as a candidate. The lift and drag polars of the airfoil are shown in Fig. 8.1 along with the values at design point. Notice that the airfoil provides a shallow drag bucket from a C_l of 0.3–1.0 allowing for low wing drag over a wide range of flight conditions.

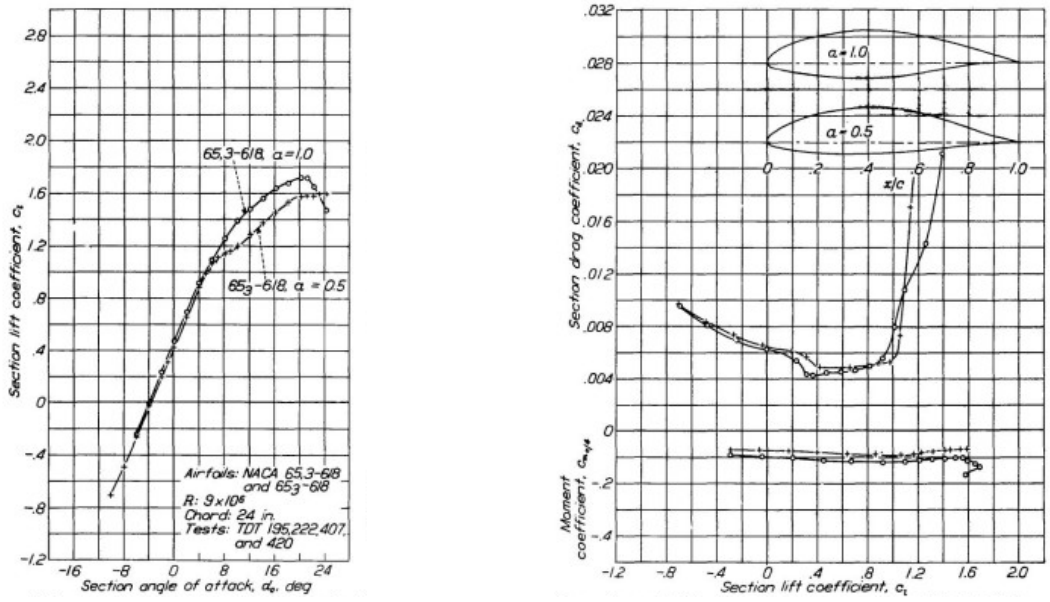

(a) Lift characteristics of the NACA 65_3-618 airfoil

(b) Drag characteristics of the NACA 65_3-618 airfoil

Figure 8.1: Characteristics of the NACA 65_3-618 airfoil

8.1.3 Selection of Other Wing Parameters

The wing incidence angle was set so that during cruising flight, the wing must generate the required lift and produce minimum drag. The fuselage operates at near zero angle of attack, AOA, for the least parasitic drag and also for maximum passenger comfort. Figure 8.1 shows that, based on the design point, the wing incidence needs to be 2.5°.

A high wing configuration was chosen for the *HeliX*. This eases and facilitates the loading and unloading of cargo and patients. It also provides a high mounting point for the proprotors, which further increases the safety during ground operations around the vehicle. Because electrical lines and hydraulics run along the entire wing span, a high wing configuration has the additional benefit that it maximizes the amount of cabin space. The wing dihedral, based in part on the dihedral of past tiltrotors (Table 8.4) increases the lateral stability of the vehicle (C_{l_β}). Traditionally, wing

Table 8.4: Wing dihedral of various tiltrotors

HeliX	V-22	BA-609	XV-15
4.00°	4.30°	3.68°	0.00°

sweep is beneficial in delaying compressibility effects, adjusting the aircraft center of gravity, and improving static lateral stability. In the case of a tiltrotor, forward wing sweep is essential for providing blade flapping clearance for the proprotors because they are mounted to a gimbaled hub; a forward wing sweep of 6° was determined to be adequate. For this same clearance consideration, the wing extensions were also given a backward sweep of 6°. Taper of a wing

Table 8.5: Wing sweep of various tiltrotors

HeliX	V-22	BA-609	XV-15
6.00°	5.43°	7.05°	6.11°

is usually used to give a closer to elliptical lift distribution along the span, which reduces the induced drag of the wing. However, for a tiltrotor the tip of the wing needs to be structurally stiff to house the proprotor mechanism and, in the case of the *HeliX*, also the outboard wing extensions. Furthermore, the downwash of the proprotors increases the dynamic pressure on the outboard sections of the wing, altering the lift distribution. It was decided that a wing without taper was the best compromise between the aerodynamics, structural weight, and stiffness.

Twist rates (geometric or aerodynamic) are generally employed for two reasons: (a) for the avoidance of tip stall before root stall and, (b) for the modification of the lift distribution to a more elliptical one to reduce induced drag. The aerodynamic effect of the proprotors on the outboard sections of the wing, as stated earlier, means that the chord line of the twisted wing tip may not align with the proprotor thrust vector, which adds complexity to the manufacturing process. For these reasons, the main wing was not twisted.

High-lift devices on the wing are employed in the form of flaperons over the trailing 25% of the wing chord. They were sized based on vehicle download considerations in hover, as discussed in Section 3.2. Figure 8.1 shows that the $C_{l_{max}}$ of the airfoil with deployed flaps increases to 2.4. The flaps significantly decrease the stall speed and enables pure airplane operation at relatively low flight speeds. The variation of stall speed for the aircraft as a function of altitude is shown in Fig. 8.2. Table 8.6 gives a summary of the *HeliX*'s wing characteristics.

8.2 Structural Design

The wing of the *HeliX* is mainly comprised of a single torque box, which is manufactured to run the length of the wing span (16.1 m). Figure 8.3(a) shows the torque box with the ribs and internal fuel tank without the skin. The torque box was designed to provide the necessary stiffness to prevent the onset of pylon whirl flutter instabilities, as well as to support all of the anticipated aerodynamic and structural loads during normal flight operations.

Figure 8.3(b) shows that the torque box is composed of front and rear vertical webs located at 10% and 50% of the chord, respectively. The front and rear webs are connected by an upper and lower skin, which create a closed thin-

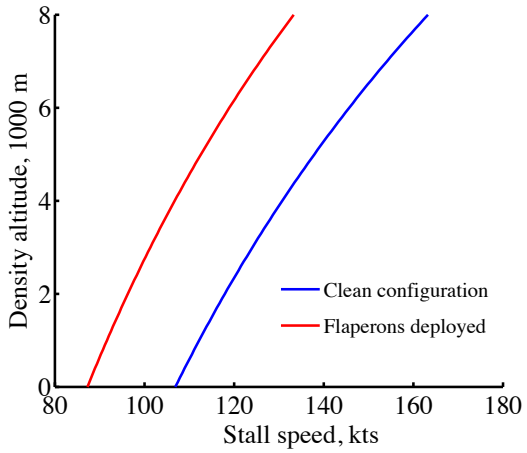

Figure 8.2: Density altitude versus stall speed for a clean wing and for a wing with flaperons deployed

Table 8.6: Summary of key wing aerodynamic parameters

Wing planform area	51.25 m^2 (551.73 ft^2) *
Aspect ratio	8.5*
Wing span	18.43 m (60.486 ft) *
Mean aerodynamic chord	2.69 m (8.83 ft)
Vertical position on fuselage	High-wing
Horizontal position	7.48-7.83 (airplane-helicopter mode)
Airfoil	NACA 65_3-618
Taper ratio	1
Twist angle	0°
Sweep angle	6° forward sweep
Dihedral angle	4°
Wing incidence	2.5°
High lift device	TE flaperons (25% chord) $C_l = 2.4$

* Includes outboard wing extensions

walled section, increasing the torsional stiffness of the torque box. Four spar caps were added to the torque box to increase the stiffness in the beamwise and chordwise directions and minimize the stresses and deflections during loading. Down the length of the upper and lower skin are a series of top-hat stringers which aid in preventing buckling of the skin panels and provide a small amount of additional bending stiffness. Along with withstanding most of the bending and torsion loads along the wing, sizing of the torque box included provisions for housing all of the fuel tanks necessary to complete the missions of the RFP. The ribs within the wing structure are spaced to provide support to the control surfaces and proprotor/nacelle structure, maintain the airfoil profile shape, and have cutouts for the interconnecting transmission shaft, electrical wiring, and hydraulic lines.

8.2.1 Initial Sizing

In conventional fixed-wing aircraft design, the structural components of the wing are sized to meet strength requirements based on the the typical loads that are expected to act on the wing. The estimated wing loads are used to approximate the shear and moment distributions along the wing span. From the shear and moment distributions, the

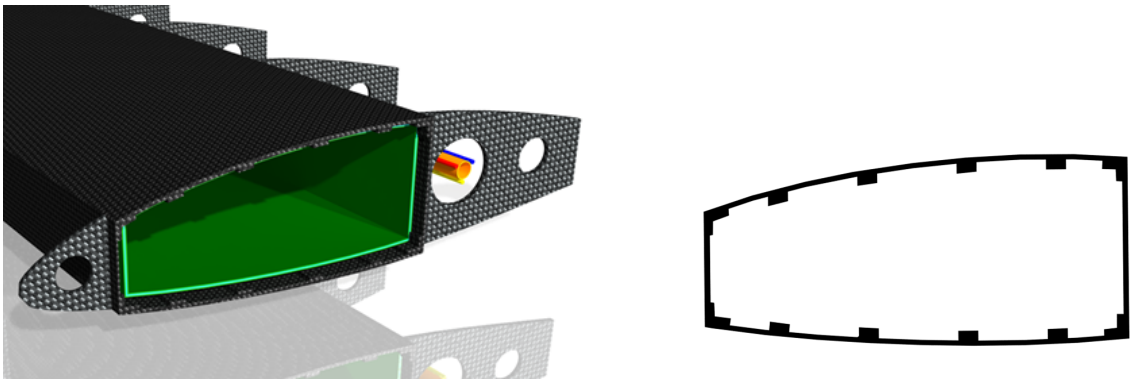

(a) Torque box with ribs and internal fuel tank

(b) 2-Dimensional view of wing torque box

Figure 8.3: Wing torque box design

respective shear and bending stress acting along the wing can be calculated and the torque box is sized to ensure a factor of safety of at least 1.5 for the most critical load case. However, unlike conventional fixed-wing aircraft, the wings of tiltrotors are typically sized to meet stiffness requirements, not strength requirements. The initial sizing of the torque box for the wing is based on providing adequate bending and torsional stiffness to prevent the onset of prop-whirl flutter at the airspeeds the aircraft is intended to operate.

The initial sizing of the torque box was based on a need to provide adequate bending and torsional stiffness to delay the onset of pylon whirl flutter at operational speeds. A methodology proposed by Peyran and Rand [39] was followed to calculate target stiffness values to which the torque box design was sized. After the initial sizing of the torque box to avoid pylon-whirl flutter, an analysis of the wing was conducted based on Euler–Bernoulli beam theory and St. Venant torsion theory.

Distributed loads and point forces were used to represent the aerodynamic forces, proprotor thrust, wing weight, and nacelle/proprotor tip weight at the MGTOW. The maximum tip deflections and bending stresses were determined, and the torque box was resized to ensure that minimum rotor ground clearance and margins of safety under normal flight operations were fully met. To more thoroughly investigate the structural characteristics and stress distributions along the wing, a Finite Element Analysis (FEA) was conducted on the wing, as described in Section 9.2.

8.2.2 Material Selection

From a structural standpoint, an efficient wing is one that is capable of withstanding all the loads it is expected to be subjected to during service while also being as lightweight as possible. When deciding upon the material to be used to manufacture the wing, a trade study was performed to determine the expected weight of the torque box when built out of different materials. Table 8.7 shows the percent difference in the weight of the torque box when using typical materials for aerospace applications. A graphite-epoxy composite material, while more expensive than aluminum, was chosen for the construction of the torque box because it met the high material stiffness requirements of the design while providing a 34% reduction in weight, thereby significantly reducing the empty weight of the aircraft.

The front and rear webs have a spacing of 1.08 m (3.54 ft) and a thickness of approximately 6.5 mm (0.26 in) while the upper and lower sections of skin connecting the front and rear webs have a thickness of 13 mm (0.51 in). The lay-up of the front and rear webs is $[0_6/90_6/\pm45_7]_S$ and the lay-up of the upper and lower torque box skin is $[0_{12}/90_{12}/\pm45_{13}]_S$ assuming a typical ply thickness of 0.127 mm (0.005 in). Unlike the torque box, the skin covering the entire wing is made of E-glass/epoxy. This approach was used because the skin does not require as large a stiffness as the torque box and using E-glass/Epoxy will reduce the overall cost of materials needed to construct the wing. The wing skin has

Table 8.7: Weight comparison of torque box for various materials

Material	Density, kg m^{-3} (lb ft^{-3}	Mass, kg m^{-1}	Percent Reduction
Aluminum	2,700	75.2	N/A
Fiberglass	1,900	71.4	5%
Graphite-Epoxy	1,600	49.7	34%

thickness of 1.3 mm (0.05 in) with a lay-up of unidirectional [0°] plies.

Because the wing is made of composite materials, it is able to be constructed as one long continuous unit from nacelle to nacelle. Prefabricated molds of the wing structure are used to house the reinforced graphite fiber layers along with the preformed assemblies of the stringer and spar cap sections. Mandrels within the mold are used to shape the internal geometry of the torque box and then the entire assembly is vacuum bagged. Unlike conventional curing methods using an autoclave, out-of-autoclave (OOA) techniques such as Vacuum Assisted Resin Transfer Molding (VARTM) reduce the cost and complexity of manufacturing large scale composite parts while maintaining product quality [4]. Given that composite materials are poor conductors of electricity, an aluminum mesh is applied to the outer-most ply of the wing to prevent damage to the structure in the event of a lightning strike. Because the *HeliX* can fly at high altitudes, it is necessary that some form of de-icing be incorporated into the wing. A thermal-based anti-icing system was chosen over alternative de-icing mechanisms to ensure that no ice forms along the wings leading edge.

8.3 Whirl Flutter Analysis

In airplane mode, the *HeliX* is essentially a propeller driven aircraft and as such can potentially experience pylon whirl flutter instabilities. Given that whirl flutter instabilities are more problematic at high forward airspeeds, such as those at which the *HeliX* is intended to operate, it is essential to design the wing so that flutter is not an issue. To perform the flutter analysis, a formulation developed by Johnson [40], further modified by Nixon [41], was used.

In this analysis, the wing of the *HeliX* was represented as a cantilevered beam by using finite elements. Aerodynamic and structural models for both the wing and rotor were used to represent the dynamics of the system. The eigenvalues and eigenvectors were numerically determined, and then used to calculate the damping ratio and frequency of the various modes present in the system. Figure 8.4 shows the change in damping ratio with respect to forward flight speed for the torsion, chord-wise bending, and beam-wise bending modes. These three modes are shown because they are typically the first to become unstable. The chord-wise bending mode is the first mode to become unstable at an airspeed of approximately 430 kts. This maximum flutter airspeed proves that the design of the *HeliX*'s wing provides an adequate margin of safety to ensure that it is flutter-free during all flight operations.

8.3.1 Composite Tailoring

Past research into the topic of prop-whirl flutter has shown that the use of aeroelastic tailoring of the wing, primarily by using bending-torsion coupling, can further increase the whirl flutter boundaries of the aircraft. Figure 8.5 shows the change in damping of the wing modes under the influence of bending-torsion coupling. To incorporate bending-torsion coupling into the wing structure, the lay-up of the graphite-epoxy plys must be adjusted. The uncoupled torque box structure would be made of alternating layers of [±45°] plys with the outer layer plys oriented at [0°/90°]. The front and rear webs are comprised of a 50/50 blend of [±45°], implying that there are an equal number of +45 and -45 plys within that section of the torque box. Following a study by Nixon [42], a 70/30 ratio of [±45°] plys in the upper and lower sections of the torque box generates a favorable aeroelastic tailoring that can increase the whirl flutter onset speed of the design while only slightly influencing the initial structural stiffness. By comparing Fig. 8.4 with Fig. 8.5, it can be seen that composite coupling would further expand the prop-whirl flutter boundary of the *HeliX*. However, the uncoupled design provides a safe whirl flutter boundary while avoiding the added manufacturing complexity and cost of creating an aeroelastically tailored composite.

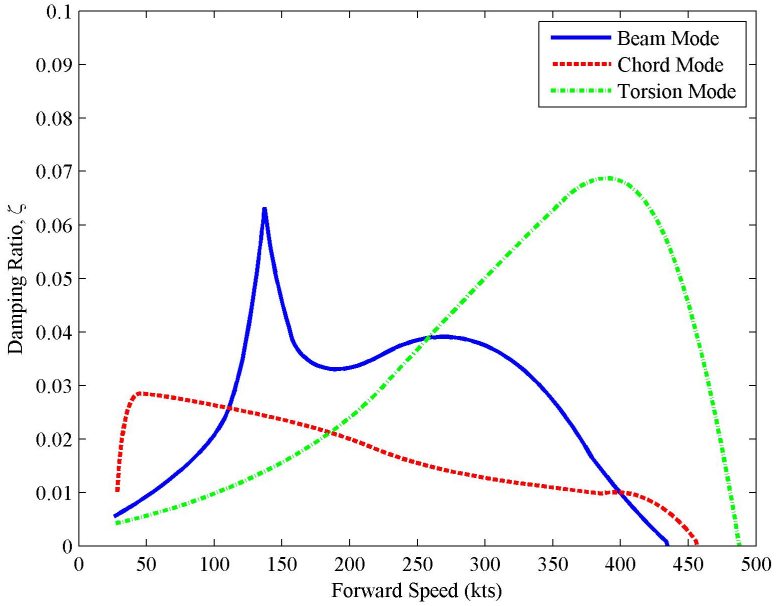

Figure 8.4: Wing damping ratio versus forward airspeed

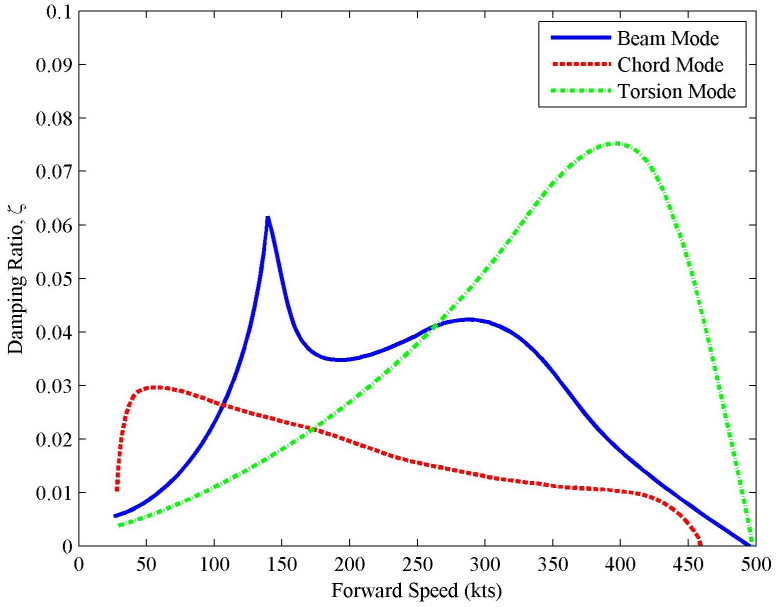

Figure 8.5: Damping ratio versus airspeed for composite coupling whirl flutter analysis

8.3.2 Influence of Blade Retraction

One novel aspect of the *HeliX*'s design is its variable diameter rotor system. While decreasing the rotor diameter in cruise is beneficial from a propulsive efficiency standpoint, it is important to understand its influence on the whirl flutter stability of the wing rotor system in comparison to the extended blade configuration. Figure 8.6 shows the

damping of the wing modes assuming that the blades are fully extended during forward flight. With blades extended, the whirl flutter speed drops from 430 kts in the retracted case to approximately 270 kts. This shows that retracting the blades during forward flight provides a significant increase to the whirl flutter speed of the *HeliX*, enabling the aircraft to safely fly at its high cruise speed. However, if the blade retraction mechanism were to malfunction and the blades were to remain extended during forward flight, Fig. 8.6 shows the aircraft would still be able to operate safely but at a reduced flight speed.

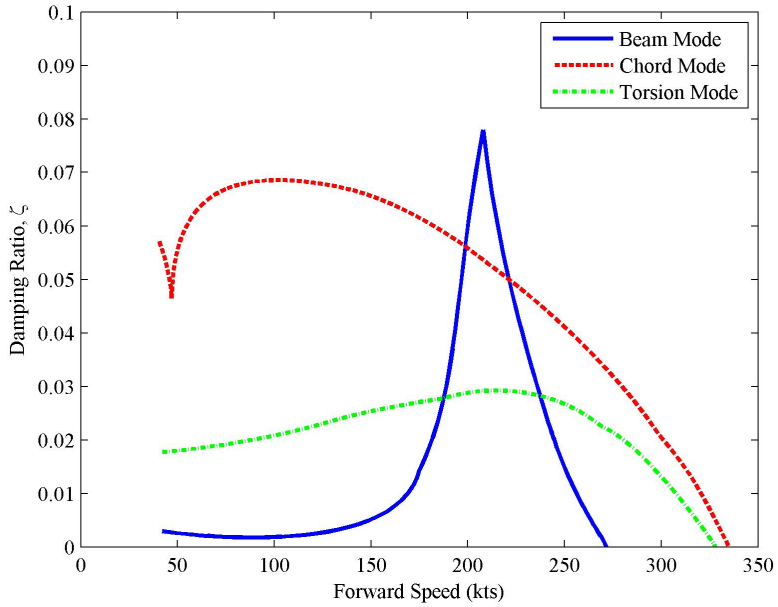

Figure 8.6: Damping ratio versus airspeed for extended rotor whirl flutter analysis

8.4 Nacelle Integration

To create a structurally sound attachment for the proprotor at the wing tips, the composite torque box was designed to continue under the nacelle by using a modified cross-sectional shape. This portion of the wing more closely conforms to the spar size of the wing extension. The aluminum structure allows loads to be transferred from the rotor, through the thrust bearing built into the nose of the gearbox and hinge, to the torque box.

8.5 Nacelle Design

The nacelles were streamlined in order to minimize drag in forward flight. They hinge about the point where they meet the transmission shaft, which is located in the wing at approximately 60% of the blade chord. The external shape is designed to clear the wing spar while still containing the main gearbox and swashplate. Dual hydraulic actuators (doubled to reduce actuator size) are used to tilt the nacelle when transitioning from helicopter mode to forward flight. In forward flight, the nacelles are fixed in position by using a solenoid and locking pins.

8.6 Wing Extensions

The outboard wing extensions (OWE) are a novel concept that provide many advantages to the *HeliX*. As shown in Fig. 3.6, when the OWE are fully deployed they give the vehicle a lift-to-drag ratio of over 10 at intermediate airspeeds, putting the *HeliX* in a class of aircraft all on its own.

The OWE each have an area that is 7.5% of the main wing area, and are 2.5 m (8.2 ft) long so that when they are drooped down they provide adequate ground clearance. To avoid the possibility of proprotor strike in forward flight, the OWE are swept back 10°. The OWE are tapered, which also gives a better spanwise loading efficiency and reduces the induced drag.

8.6.1 Deployment

To improve the autonomy of the vehicle, the OWE are designed to aerodynamically deploy automatically, i.e., the lifting forces on them that are produced when increasing airspeed exceed the weight of the extensions themselves. Although other mechanical methods were considered, it was determined that using aerodynamics alone would keep the weight and complexity of the system to a minimum, as well as limit the maintenance costs.

To avoid an asymmetric deployment, the positions of the OWE are monitored by sensors within a feedback loop and small flight control surfaces are used for control. The control surfaces controlled by an electric servo motor are actively deflected up and down to ensure that the OWE deploy together. Necessary wiring is protected from the elements. In the event of a malfunction, the vehicle has enough control authority to account for any rolling moment that would be produced when one OWE is drooped down and the other fully deployed.

Because the OWE are located out at the wing tips, their weight had to be accounted for in the torque box design. Original design ideas for their deployment included a gearing system, shown in Fig. 8.7(a), to raise the 125 kg wing panels as the nacelles are tilted from helicopter to airplane mode. However, the added weight and complexity of such system, as well as the inefficient use of gears, made this an undesirable design choice.

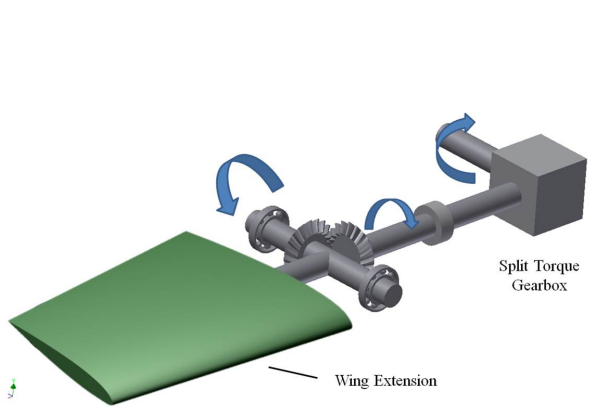

(a) Preliminary OWE deployment concept

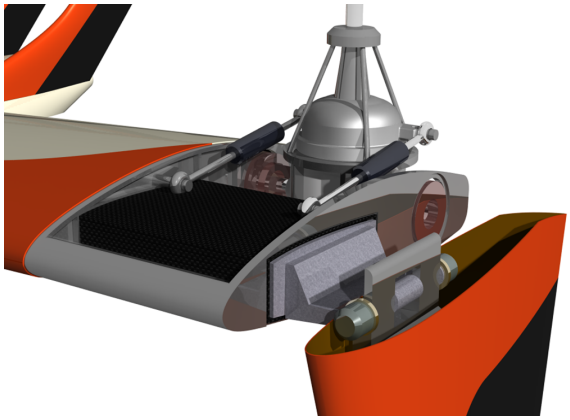

(b) Final aerodynamically deployable OWE configuration. Electrical lines not shown for clarity.

Figure 8.7: Comparison of outboard wing extension deployment methods

9 Finite Element Analyses

As part of the SDC Graduate Student category, a deeper study of the *HeliX* was conducted by using a Finite Element Analysis (FEA) on both a dynamic component (the gears in the main gearbox) and a static component (the wing structure).

A solid mesh type, containing tetrahedra and wedges, was used for both the dynamics and static FEA analyses, with an example shown in Fig. 9.1. A solid mesh was used, in comparison to a shell or layer mesh to gain a better accuracy in the simulation. Though more demanding computations are associated with a solid mesh, the results yield a better estimate of what deformations and stresses the parts will see when their respective forces are applied.

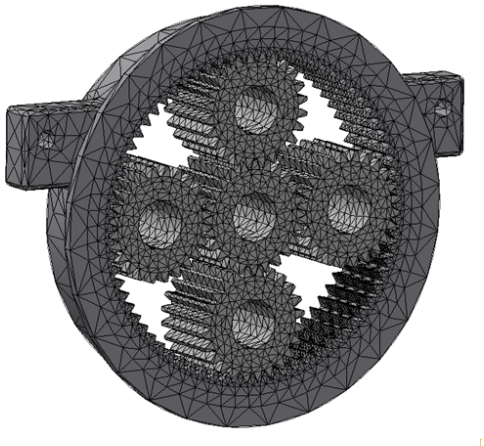

Figure 9.1: FEA mesh of planetary gear stage

9.1 Gear FEA

The dynamic element analysis was performed on the gears within the nacelle to ensure that the gear teeth were appropriately sized because during flight they are in a constant state of high loading. The constraints were that the outer surface of the ring gear was held fixed and the contact loads were applied between the teeth surfaces. Figure 9.2 shows that the displacement is within the allowable backlash limits for this setup. Structural stress, structural displacement, and safety factor analyses were also examined for each component.

A bending fatigue test was performed where the gear was loaded to 140% of the load it is expected to handle to add an extra safety factor to the gears within the transmission system, as per industry standards. The gear material selected was Ferrium C-64 because it is lightweight and has greater durability compared to other materials such as 8620 alloy. This material also offers reduced manufacturing cost and time with better quality control. The material properties consist of a yield strength of 199 ksi and ultimate tensile strength of 229 ksi. Trade studies were conducted to ensure that the gear material choice was suitable. As shown in Fig. 9.3(a) and Fig. 9.3(b), using carbon steel reduces the minimum safety factor to 0.68 whereas using Ferrium C-64 yields a minimum safety factor of 2.63.

A similar FEA was performed on all the crucial transmission gear components, and the results are given in Table 9.1.

9.2 Wing FEA

A static FEA was performed on the wing structure to ensure that it was properly designed to withstand all of the forces and stresses it would endure during operation as well as provide the necessary beam-wise, chord-wise, and torsion stiffness to prevent the onset of prop-whirl flutter. Because both sides of the wing experienced the same static loading, the FEA was only performed on half of the wing with the wing root constrained in a cantilever boundary condition.

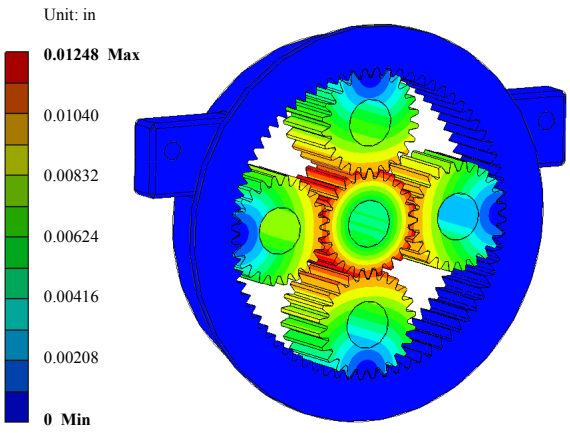

Figure 9.2: Displacements of gears under load

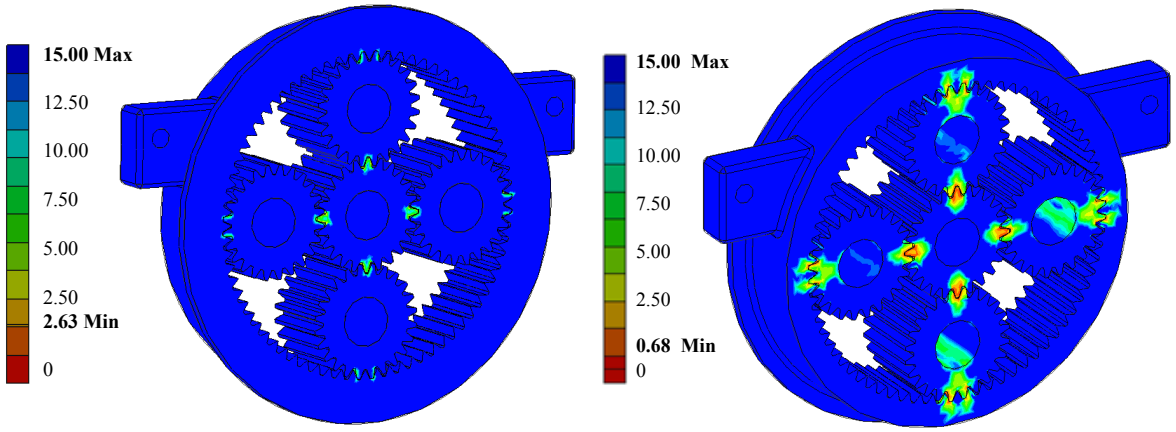

(a) Tooth stress for Ferrium C-64 gear

(b) Tooth stress for carbon steel gear

Figure 9.3: Materials used in the FEA

The stress, displacement, and safety factor were calculated for a range of load factors from -1g to 3.5g in both airplane and helicopter mode. A brief description of the load cases and the results are given in Table 9.2. All of the cases were performed with the assumption that the aircraft was operating at MGTOW.

From Table 9.2, it can be seen that the most critical case is in forward flight at a load factor of 3.5g with no fuel. While the wing would be less likely to experience such a loading situation in practice, per the FAR (CFR) Section 23.337 requirements the wing must be able to withstand a load factor of 3.5g and still maintain a safety factor that is more than 1.5. Under that particular loading condition, the safety factor for the *HeliX* wing is 1.81. Therefore the wing design easily satisfies the FARs.

The second most critical load case is when the wing is in hover with no fuel in the wing tanks. While the *HeliX* would not operate at MGTOW without fuel, the factor of safety obtained in this case gives confidence in the structural design. Figure 9.4 shows the wing bending displacement for the specified load case, while Fig. 9.5 shows the factor of safety along the torque box.

Figure 9.4 shows that even under the hover load case where half of the vehicle lift force is assumed to be applied at the wing tip, the maximum wing displacement is only 121 mm (4.78 inches). Recall from Section 8.3 that the stiffness of

Table 9.1: Nacelle gearbox FEA analysis results

Gear	Transmitted Load kg (lb)	Displacement mm (in)	Allowable Backlash mm (in)	Von Mises Stress (ksi)	Yield Stress (ksi)	Safety Factor
Small Bevel	2615.4 (5766)	0.031 (0.00122)	0.20–0.28 (0.008–0.011)	40.6	199	4.90
Large Bevel	2615.4 (5766)	0.025 (0.001)	0.20–0.28 (0.008–0.011)	36.6	199	5.44
Small Spur	6821.6 (15039)	0.025 (0.001)	0.13–0.25 (0.005–0.010)	43.6	199	4.56
Large Spur	6821.6 (15039)	0.052 (0.002)	0.13–0.25 (0.005–0.010)	31.9	199	6.24
Sun	9143.5 (20158)	0.032 (0.00127)	0.20–0.41 (0.008–0.016)	35.9	199	5.54
Planet	9143.5 (20158)	0.032 (0.00127)	0.20–0.41 (0.008–0.016)	35.9	199	5.54
Ring	9143.5 (20158)	0.024 (0.000939)	0.20–0.41 (0.008–0.016)	44.3	199	4.49

Table 9.2: Wing FEA load cases and results

Case	Load Factor	Von Mises Stress (Mpa)	Displacement, mm (in)	Safety Factor
On ground w/ fuel	0	12.6	−41.0 (−1.6)	5.3
On ground w/o fuel	0	10.03	−35.5 (−1.4)	6.8
Forward flight w/fuel	1	5.74	11.6 (0.5)	9.6
Forward flight w/o fuel	1	8.03	17.0 (0.7)	6.9
Forward flight w/fuel	−1	26.4	93.2 (3.7)	2.2
Forward flight w/o fuel	3.5	56.7	147.7 (5.8)	1.8
Hover w/ fuel	1.1	24.1	115.8 (4.6)	2.3
Hover w/o fuel	1.1	26.3	121.3 (4.8)	2.1

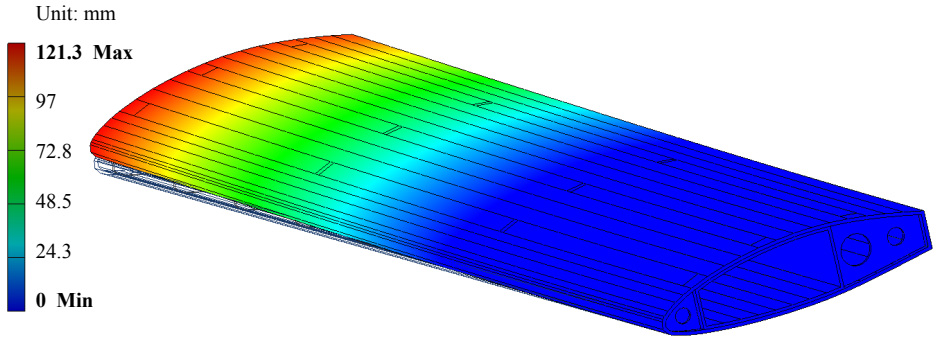

Figure 9.4: Bending displacement along the wing in hover mode without fuel (root on right)

the wing was designed to prevent whirl flutter, which gives a relatively stiff wing in bending. The results in Fig. 9.5 shows the factor of safety along the torque box and how the average stress is distributed along the wing. While the wing skin was included in the analysis, it was omitted from the image to better show the torque box, which carries most of the bending. As expected, the highest stress is concentrated at the wing root, which then decreases towards the tip from the decreasing bending moment.

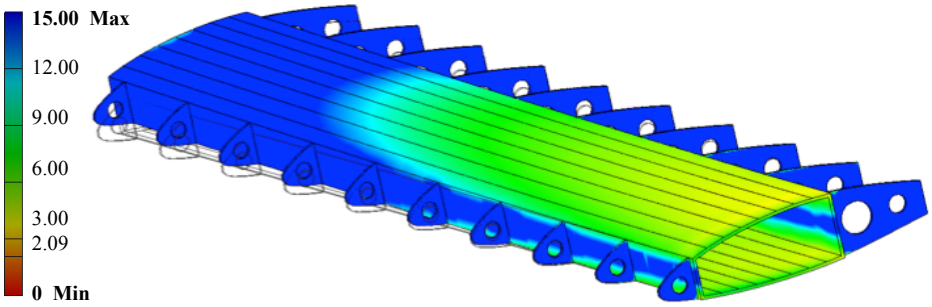

Figure 9.5: Factor of safety along the wing torque box (root on left)

9.3 Conclusions of FEA

As shown in this section, numerous components were validated for their safety as part of the aircraft as a system. The planetary gear system proved safely operational for its selected material to 140% of the typical loading. The wing was shown to perform to industry standards during flight conditions that could be encountered during operation.

10 Airframe Design

The airframe, shown in more detail in the airframe foldout, was designed to maximum space for the cargo and crew while maintaining a low drag shape. Additional design considerations included preparedness for harsh environments and a pressurized cabin at high-altitude flight. Many of the cabin components were designed to create a highly reconfigurable aircraft for multi-mission operations.

10.1 Fuselage Structure

The *HeliX* airframe is a semi-monocoque design with an aluminum-lithium (Al-Li) frame (see Section 10.4) and a load-bearing composite skin. A high-wing design was utilized to give maximum clearance from the rotor blade tips and to ensure personnel safety during ground operations. The wing is swept forward by 5°, providing 14° of clearance for the rotor blades in flapping when the nacelles are oriented in their forward flight position.

The *HeliX* airframe has well-defined load paths from the rotors at the wing tips to the rest of the vehicle. The transmission is mounted to a hinged plate which transfers the loads to the torque box. The torque box passes in front of the hinged plate and an aluminum structure is bolted to the torque box at this point. This design not only provides a strong point for the transfer of loads from the rotor to the torque box, but also allows the torque box to continue into the wing extension.

As discussed in Section 8.2, the torque box is designed as a single composite piece from wingtip to wingtip. This approach increases the structural efficiency of the wing-to-fuselage connection point and reduces the total number of fasteners that are required. The aluminum wing box in the center of the airframe consists of two main structures to create a three point bending condition with the torque box. The torque box is bolted to the wing box with three primary high-strength bolts on each side and constrains the torque box in the longitudinal direction. The wing box is bolted to two primary bulkheads, made of Al-Li, and transfer the loads from the wing box to keel beams in the floor. The Al-Li keel beams are the primary structure used to carry the cargo load, and are integrated into the ramp frame and empennage supports.

The engines are mounted behind the wing and are supported by one of the larger bulkheads. Another large bulkhead is located at the ramp and is intended to take the loads during hoist and winch operations. Detailed images of these structures are shown in the airframe foldout.

10.2 Ramp and Door

Based on the design choice to pressurize the cabin, the number of doors was chosen keeping in mind FAA regulations on passenger safety. A sliding passenger door (see Fig. 10.1(a)) located on the port side behind the cockpit, is used for passengers and crew to enter and exit the vehicle. There is also a large aft-loading ramp (see Fig. 10.1(b)) to allow for the rapid distribution of relief aid and quick, spacious boarding of crew or casualties. As discussed in Section 12.6, the *HeliX* has three emergency exits. The door frames were designed to be crashworthy and do not distort in the event of a crash. They were also designed to be airtight to minimize air leaks when flying at higher altitudes.

An aft-loading ramp was incorporated into the aircraft design to allow for relief distribution in forward flight. To reduce drag without making the ramp too large, a ramp upsweep of 24° was used. The rear ramp consists of two parts: 1) a large, upward-swinging plug door, and 2) a smaller, downward-swinging ramp. The ramp has the ability to swing approximately 110° to clear space during the use of the hoist. Placement of the hoist inside of the vehicle decreases the drag and allows hoisting to take place closer to the center of gravity of the aircraft. It also allows the hoist operator to stand firmly on the aircraft floor instead of on the ramp itself, increasing crew safety.

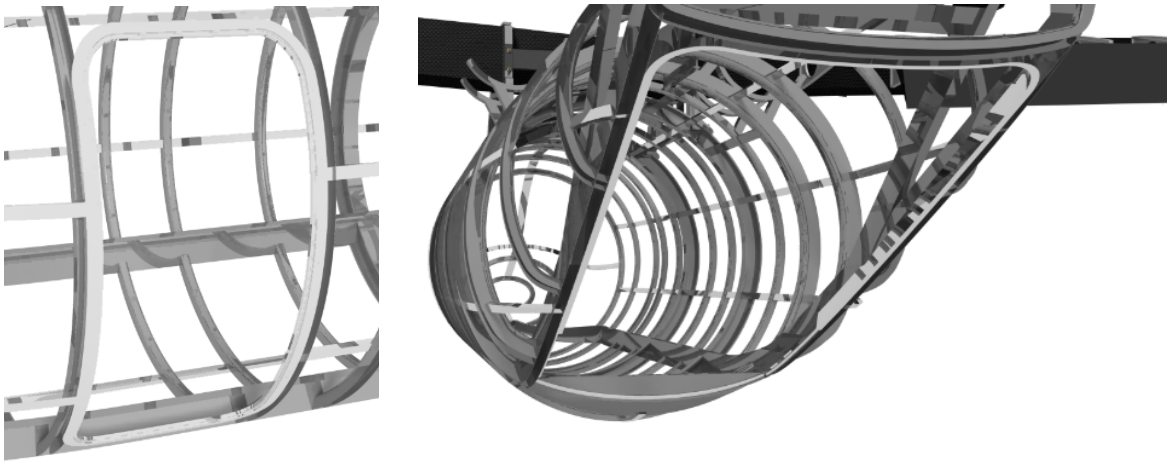

(a) Side, sliding door frame

(b) Aft-loading ramp frame

Figure 10.1: Door frame structural design

10.3 Empennage

The *HeliX* uses an innovative Π-tail, allowing the empennage to structurally integrate with the frame of the rear ramp. The two vertical stabilizers are aligned with the ramp frame and keel beams, and the composite structure of the empennage is bolted to the keel beams. An Al-Li brace at the bottom of the structure helps to transfer the loads. The horizontal stabilizer connects the vertical stabilizers.

10.4 Material Selection

Aluminum-Lithium (Al-Li) was chosen for the construction of the main fuselage because it is lighter than standard aluminum while still having the ability to be manufactured using traditional techniques. Alloy 2099 was chosen for its good corrosion resistance, considering the likelihood of operation in flooded areas or other harsh environments. Additionally, this alloy will have reduced operating costs because of its relatively greater resistance to fatigue than standard aluminum.

HeliX uses a carbon fiber skin for the fuselage, wing fairings, and sponsons. The carbon fiber construction yields high stiffness and fatigue resistance while minimizing the number of fasteners and support structures needed. Because the skin must act as a pressure vessel, [±55°] layers of carbon fiber are used to give twice the strength in the circumferential direction as in the longitudinal direction. A [0°/90°] layer is used as well to give strength for flight maneuvers. The skin is constructed in large panels using prepregs in an autoclave. Out of autoclave (OOA) prepregs were considered, but the traditional method was chosen because the tooling required can be reused to construct for serial production. Using traditional prepregs also reduces the potential for air bubbles and other imperfections in the skin, which could present a serious safety hazard with a pressurized cabin.

The empennage is a composite construction to reduce weight. The two vertical tails and top horizontal stabilizer use Kevlar/carbon/glass, with the top layer being made of Kevlar/epoxy. In addition to reducing weight, the composite structure is resistant to many of the harsh environments in which the aircraft will likely be operating.

10.5 Pressurization

The RFP requires that the aircraft be able to cruise at an altitude of 6,000 m, ISA+15°C. According to the FARS Part 25, no civil aircraft can operate at cabin pressure altitudes above 4,267 m (14,000 ft) unless each occupant is provided

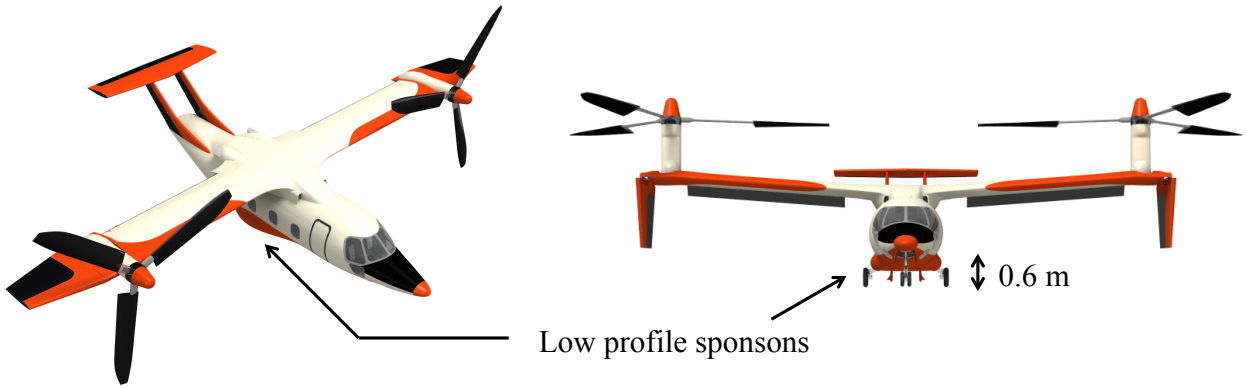

Figure 10.2: Depiction of low profile sponsons and landing gear height

with, and uses, supplemental oxygen. Based on the requirement of Mission 3 to retrieve 6 wounded persons, it was more desirable to pressurize the cabin and increase patient comfort than just simply supply them with supplemental oxygen masks. In the case of any malfunction, oxygen masks are provided. The pressurization of the cabin also ensures airborne contaminants, such as radioactive or biological contaminants, are kept outside of the vehicle.

The aircraft is pressurized using air bled from the turboshaft engines, which is then cooled and filtered before being mixed with the cabin air. The pressure of the cabin is regulated through the use of an outflow valve. The passenger door and rear ramp use rubber seals to limit air leaks. The vehicle is designed to maintain a pressure altitude of 2,440 m (8,000 ft) inside the cabin at any altitude above 2,440 m. Pressurization adds approximately 167.7 kg to the empty weight of the aircraft.

10.6 Landing Gear

The landing gear of the *HeliX* was designed with the expectation that the vehicle will operate in both VTOL and short takeoff (STOL) modes. Like many other aircraft, the *HeliX* has a tricycle type of landing gear configuration, with three points of contact: one at the nose of the vehicle, and a pair farther back below the wings. Two wheels are used for the nose landing gear for redundancy in the case of a puncture, and one wheel is used for each side of the main landing gear.

Because of the relatively high airspeeds at which the *HeliX* will operate, the *HeliX* was designed with retractable landing gear. However, the pressurization requirement puts a restriction on where the landing gear can be stored, i.e., the gear must be located outside of the pressurized cabin. Therefore, the nose landing gear was sized to fit within the nose of the aircraft, and the main landing gear are stored within two low profile sponsons located on either side of the aircraft, shown in Fig. 10.2.

Wheel selection was based on maximum dynamic and static loads, as well as the 7% safety margin defined by the FAR Part 25 provision. The nose wheel, a 17.5x5.75-8 Goodyear tire, is expected to take between 10 to 15% of the total static load, while the main wheels, 25.5x8.0-14, are expected to share the remaining 85 to 90%.

The lateral separation of the main landing gear was based on the lateral stability of the aircraft during takeoff, landing, and taxiing. The overturn angle was designed to be 59.4°. Although the *HeliX* is not an airplane and is not designed to the same landing standards, the landing gear was placed considering the tip back angle, which is generally considered when performing runway takeoffs. For the *HeliX*, this angle was 41.9°.

10.7 Landing Configuration

The landing gear was originally designed to be tall enough for the aircraft to takeoff and land in airplane mode, significantly improving the aircraft's crashworthiness. Unfortunately, because of the large proprotor diameter and the FAR Part 25.925 regulation on the proprotor tip clearance, it was determined that the landing gear would have to be long enough such that the belly of the vehicle was a minimum of 1.0 m (3.4 ft) off the ground. This minimum height does not, however, take into account roll instabilities that could occur during taxi. Because of this possibility, the landing gear of the *HeliX* would have to be substantially longer. Not only would this require added steps for the crew to enter through the side door, but also would impact the speed and ease of patient evacuations. For these reasons, the *HeliX* is unable to land in full airplane mode, but can still land safely in hybrid mode. The landing gear were sized to be 0.6 m from the ground to the vehicle belly, as shown in Fig. 10.2.

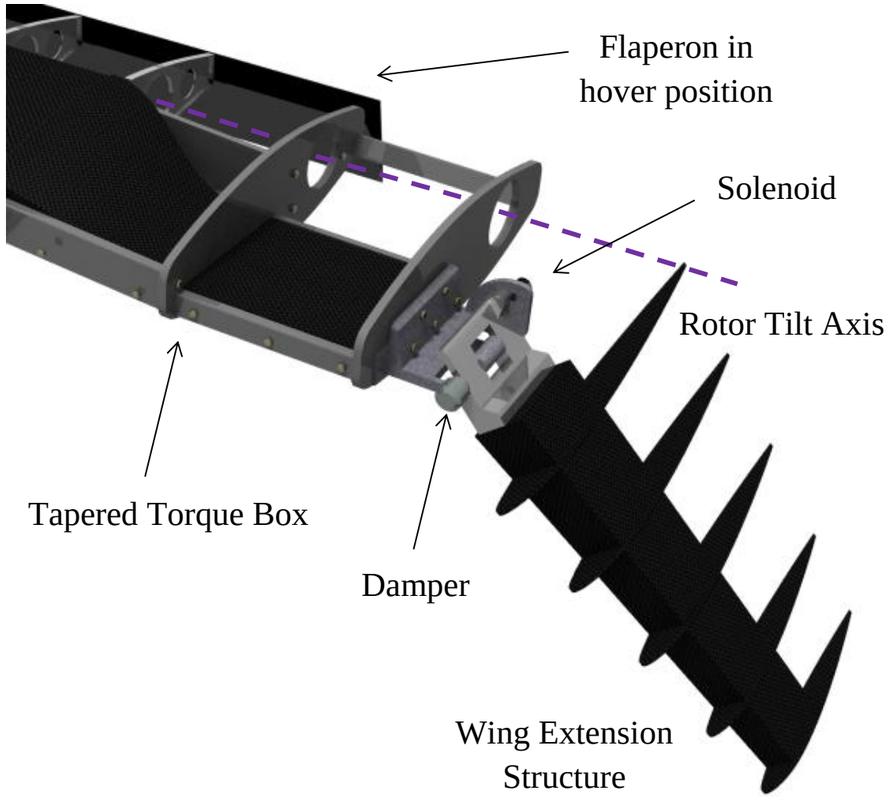
Flaperon in
hover position
Solenoid
Rotor Tilt Axis
Tapered Torque Box
Damper
Wing Extension
Structure

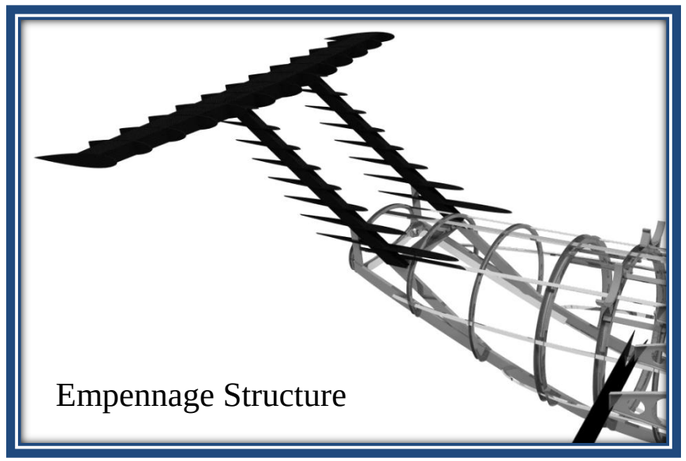
Empennage Structure

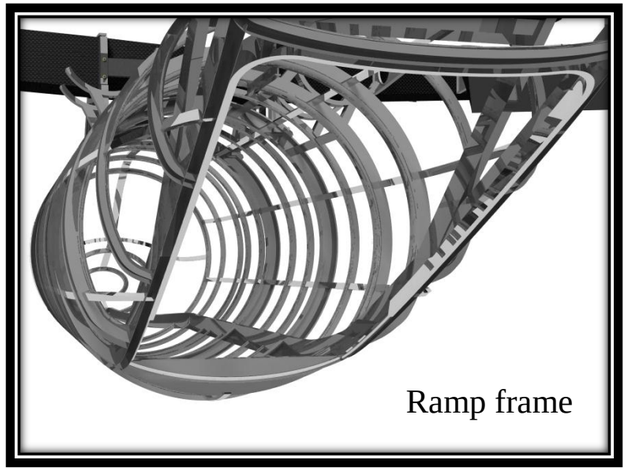
Ramp frame

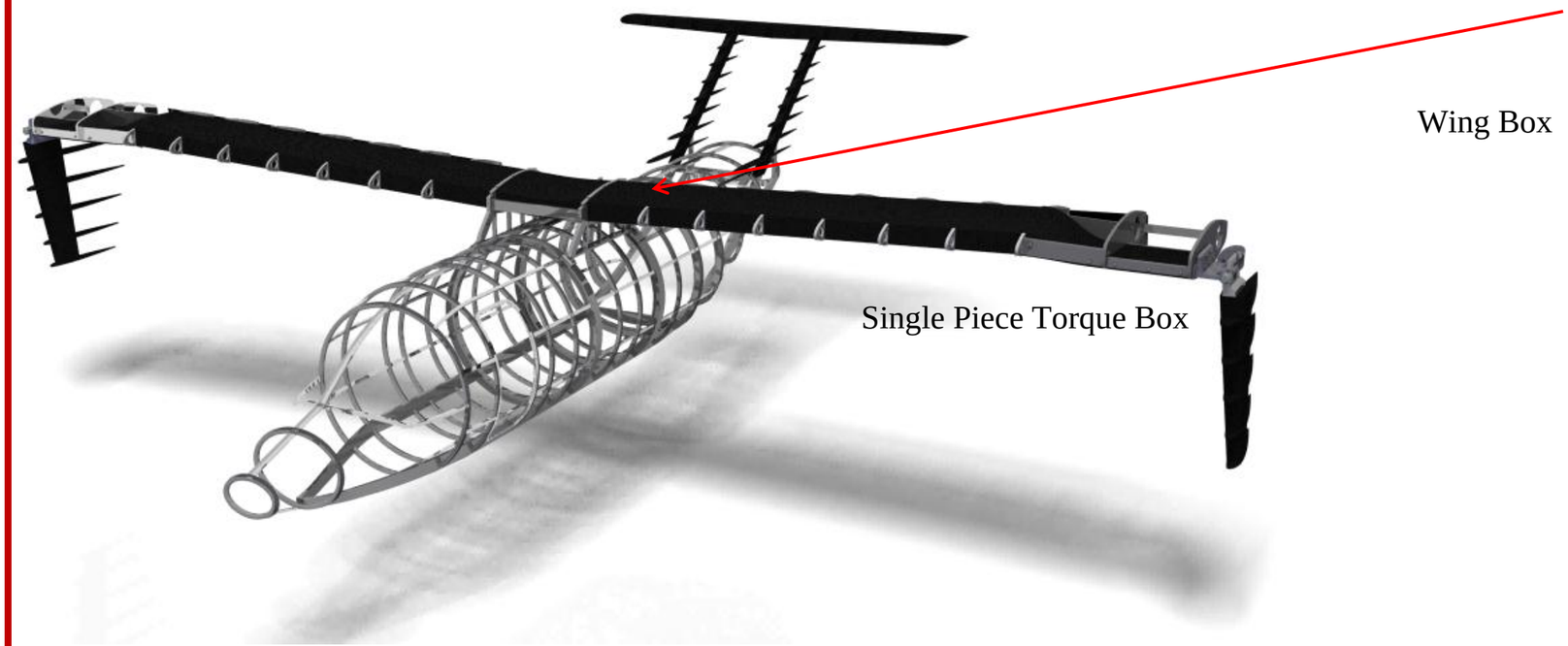
Wing Box
Single Piece Torque Box

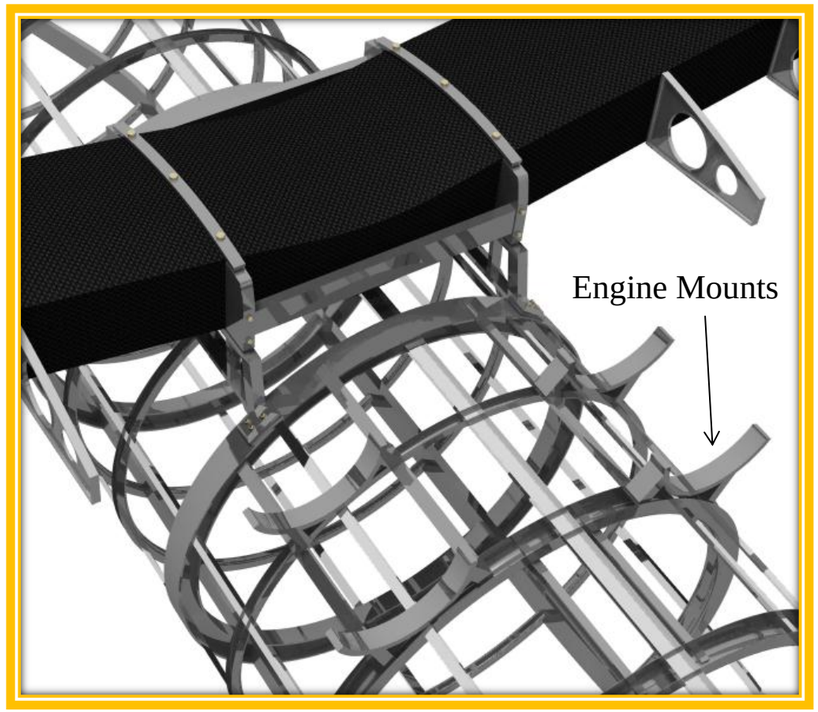
Engine Mounts

11 Weight Estimates

Table 11.1: *HeliX* weight estimates

	Component description	Weight (kg)	% Empty Weight	Helicopter x_{cg} (m)	Helicopter z_{cg} (m)	Airplane x_{cg} (m)	Airplane z_{cg} (m)
1	Wing group	886.9	9.7 %	7.85	3.30	7.85	3.30
	Primary structure	576.8	6.3 %	7.65	3.30	7.65	3.30
	Fairing	42.9	0.5 %	8.73	3.30	8.73	3.30
	Flaperons	160.7	1.8 %	8.45	3.30	8.45	3.30
	Wing fittings	106.4	1.1 %	7.65	3.30	7.65	3.30
2	Rotor group	1378.5	15.0 %	7.95	5.60	5.85	3.40
	Blades	704.3	7.7 %	7.97	5.67	5.85	3.40
	Hub	548.9	6.0 %	7.97	5.47	5.95	3.40
	Spinner	125.3	1.3 %	7.97	5.90	5.45	3.40
3	Empennage group	231.5	2.5 %	14.77	3.67	14.77	3.67
	Horizontal tail	115.7	1.2 %	15.40	4.10	15.40	4.10
	Vertical tail	115.7	1.2 %	14.15	3.25	14.15	3.25
4	Fuselage group	2399.7	26.1 %	7.11	1.25	7.11	1.25
	Primary structure	2096.1	22.8 %	7.15	1.25	7.15	1.25
	Pressurization	167.7	1.8 %	7.15	1.25	7.15	1.25
	Crashworthiness	69.6	1.5 %	6.45	1.25	6.45	1.25
5	Landing gear group	566.6	6.2 %	8.54	0.43	8.54	0.43
6	Engine group	578.4	6.3 %	9.10	2.73	9.10	2.73
7	Air induction group	358.5	3.9 %	8.74	2.61	8.74	2.61
8	Fuel system group	170.7	1.9 %	8.22	3.30	8.22	3.30
9	Drive system group	1133.0	12.4 %	7.66	3.62	7.39	3.55
	Gearbox	930.6	10.2 %	7.65	3.50	7.55	3.50
	Rotor shaft	139.0	1.5 %	7.65	4.50	6.15	3.90
	Drive shaft	25.3	0.3 %	7.65	3.50	8.15	3.50
	Rotor brake	38.0	0.4 %	7.65	3.50	7.65	3.50
10	Flight control system	553.9	6.0 %	8.01	3.14	8.01	3.14
11	Hydraulic group	107.2	1.2 %	7.95	3.07	7.95	3.07
12	De-icing group	7175.6	1.9 %	8.15	3.25	8.15	3.25
13	Common equipment	657.0	7.7 %	5.39	1.99	5.39	1.99
	Empty weight	**9168.3**	**100.0 %**	**7.83**	**2.82**	**7.48**	**2.48**
	2 Pilots + 1 Crew	272.2		4.23	1.27	4.23	1.27
	Payload	2651.8		7.61	1.00	7.61	1.00
	Fuel	3167.4		7.85	3.30	7.85	3.30
	Gross weight	**15260.0**		**7.73**	**2.58**	**7.52**	**2.37**

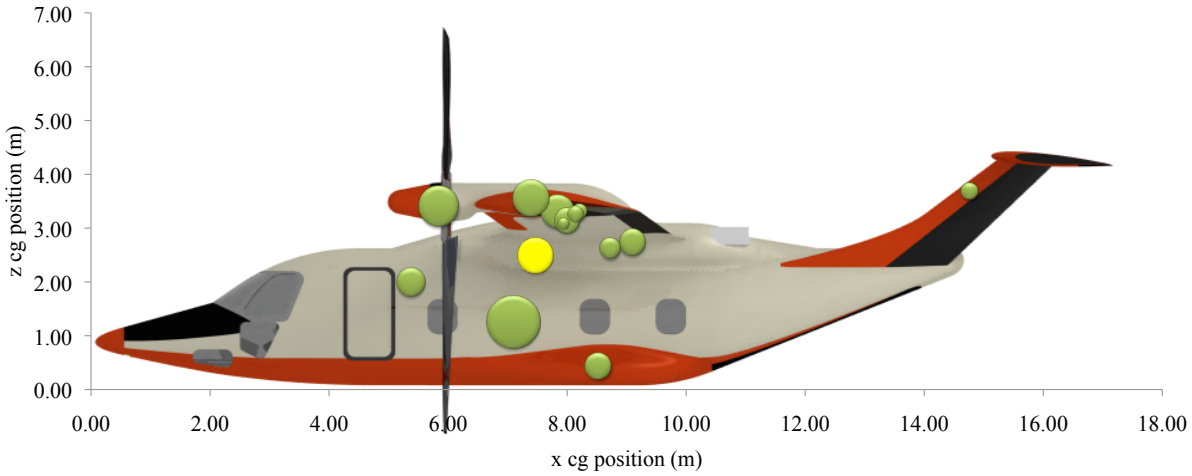

Figure 11.1: Location of longitudinal center of gravity in airplane mode

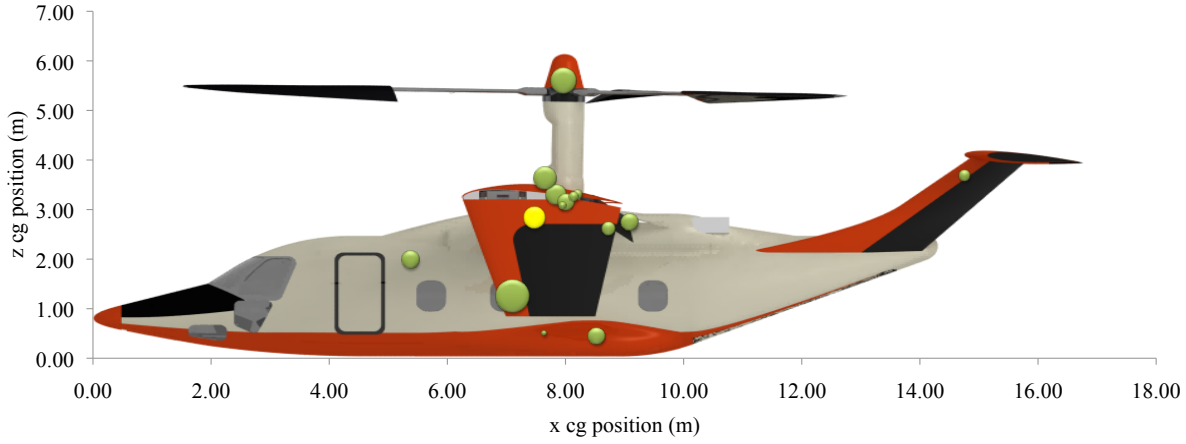

Figure 11.2: Location of longitudinal center of gravity in helicopter mode

12 Crashworthiness

The *HeliX* is designed to safely and successfully operate in a disaster environment, but is also well-prepared for the unlikely event of an emergency landing. The *HeliX* meets or exceeds the FAA Federal Aviation Regulations (FAR) Part 29 Transport Category Rotorcraft airworthiness standards.

12.1 Fuel Tank

There are six fuel tanks in the *HeliX*, with three in each wing; this distribution reduces fuel sloshing in the tanks. The self-sealing fuel tanks have been sized for a 10% total air cushion in the event of a hard landing when fully loaded, but also to provide ullage for a fuel expansion space according to FAR 29.969. They are also able to withstand drop test requirements and load factors according to FAR 29.952.

12.2 Seats and Litters

12.2.1 Crashworthy Seats

Selecting a seat that provides both comfort and safety to the crew and passengers is a high priority for the *HeliX*. Minimal vibrations that are transferred to the seats during flight operations allow for increased comfort and reduced pilot fatigue. A seat that absorbs a sudden deceleration by stroking and protecting the spine of the pilots and crew increases the likelihood of the occupants walking away from a crash with minimal injury, and also allowing them to help assist the wounded in the event of a crash during a rescue operation.

The seats and litters conform to the baseline inertial load requirements outlined in FAR 29.561, 29.625, and 29.785. Beyond these requirements, the latest technologies for comfort and crashworthiness were also used. Energy absorbing technologies were evaluated in Table 12.1 for their ability to be load adjusted and for their weight penalty aboard the aircraft. These technologies include Fixed Load Energy Absorbing (FLEA), Variable Load Energy Absorbing (VLEA), Variable Profile Energy Absorbing (VPEA), and Adaptive Energy Absorbing (AEA) [43].
A VLEA configuration was chosen because it supports a broad range of vehicle occupant weights, it is lightweight,

Table 12.1: Energy absorbing system tradeoffs for occupant seats

Energy Absorber	Load Adjustability	Additional Weight
FLEA	No	Minimal
VLEA	Finite	Minimal
VPEA	Finite	Minimal
AEA	Continuous	Heavy

and it also allows for stroking load adjustment. This seat exceeds FAR 29 requirements for a 50th percentile male occupant of 77 kg (170 lb). The VLEA seat attenuates lumbar loads to 12g or less for the entire anticipated occupant weight range of 5th percentile female to 95th percentile male. A wire bender system composed of an adjustable roller pin and steel wire is located in the seat structure. This simple design provisions for limit load adjustments to decrease the impedance of the wire stroking motion. The seat strokes 21 cm (8.3 in) under a 9.5g deceleration for a 5th percentile female, used to determine maximum available stroke to avoid bottoming out.

During a rescue or supply delivery, each pilot and crew chief occupy the VLEA seats. Wounded persons who are picked up and escorted to safety will occupy the litters or foldout seats. In the case of a VIP transport, VLEA seats may be provided for all personnel.

12.2.2 Seat Comfort

Disruptive vibration levels introduce physical fatigue through whole body vibration (WBV), create discomfort, and may disorient the pilots and crew. The use of magnetorheological (MR) fluid dampers have been introduced in series with the VLEA system to isolate occupant seat vibration throughout the frequency spectrum through a semi-active control strategy. Modern enhancements made to the seats include a lightweight magnetorheological energy attenuation system (LMEAS) that has demonstrated a 79% attenuation improvement of rotor induced vibration over an unmodified Black Hawk seat [44]. This technology also provides additional safety in the event of a crash such that a 30–50% load reduction can be achieved for low and medium speed impact.

12.3 Airframe

The airframe is designed to maximize energy absorption in the event of a crash to minimize vehicle damage and protect crew and passengers. Anti-plow beams under the cockpit floor and vehicle nose design help keep the underbelly structure smooth in a crash to prevent a sudden deceleration. Heavy mass items, including the rotor, transmission, and engines, are restrained to the inertial loads: forward, 20g; upward, 20g; downward, 20g; lateral, 18g. A buoyancy estimation determined that the vehicle will remain afloat for 30 minutes in Sea State 3 with the use of floats deployed after initial water contact, as per the requirements of FAR 29.563 (2).

12.4 Proprotor Blades

The composite blade structure undergoes a soft failure mode in the event of a violent blade impact. The multiple load-paths provided by the composite fibers will allow the blades to ”broomstraw,” effectively disintegrating the blades before causing additional damage to the aircraft.

12.5 Fire Suppression

Solid propellant gas generator (SPGG) technology is used for dry bay fire suppression against flammable aviation fuel, hydraulic fluid, and lubrication oil. SPGGs were selected over halon-based solutions for powerplant-type compartments because they are a lightweight, non-ozone depleting solution. While the likelihood of a cabin fire is minimal because of the use of self-extinguishing materials for compartments and insulation, the crew has immediate access to at least two fire extinguishers.

12.6 Emergency Egress

Emergency exits are designed to be openable from inside or outside the vehicle according to FAR 29.809, but are also jetisonable if necessary and have backup latching if the primary latching mechanism fails. They are designed not to jam under inertial forces according to FAR 29.783 (d). The aircraft is designed such that all passengers and crew may exit in under 60 seconds through either the side door, the rear ramp, or three designated window exits. In the unlikely event that the vehicle lands on its side, passengers and crew may exit through the rear ramp via the jetisonable doors.

13 Avionics

This section describes all avionics equipment to be included on the *HeliX*. The comprehensive list details systems included to address the high-priority categories for the aircraft design, as discussed in Section 1.4. Organization of the cockpit avionics is shown in Fig. 13.1.

13.1 Autopilot

Despite having made the minimization of pilot workload a high priority in the design of the *HeliX*, pilots inevitably have to manage several tasks simultaneously. Pair the numerous responsibilities with degraded visual environments and operation in devastated areas, and even these routine responsibilities can push pilots toward the dangerous extreme of task saturation. For these reasons, the design of the *HeliX* has included an Auto Pilot Module (APM) and a Stability Augmentation System (SAS). Pilots can use these systems in conjunction with the Flight Control Panel (FCP) and Flight Director (FD) to bring the aircraft, and its precious cargo, safely home in any weather conditions.

13.2 Communications

Communication is critical to the success of any mission because the process, from start to finish, requires many different people to have the ability to communicate, often simultaneously. The pilot needs to be able to contact Air Traffic Control (ATC), the co-pilot and crew/persons in cabin, ground crew/persons waiting to be rescued, and other vehicles within the fleet. Standard communication equipment for the *HeliX* includes transmitters and receivers such as FM, HF, UHF, and VHF. A flight crew intercom system allows communication between the cockpit and cabin. The cockpit is also fitted with a voice recording system to satisfy the FARs. However, not all communication directly involves the pilots. An automatic altitude reporting system works with ATC transponders via a datalink to aid in fleet management. Periodic contracts relay location and altitude information every few minutes to ATC without any pilot involvement. This system increases flight safety and effectiveness, while helping to manage a fleet of vehicles operating in potentially close proximity over a disaster zone during relief efforts.

13.3 Electric Power

A generator onboard the aircraft supplies the electric power to run its many flight control and health monitoring systems. Also installed are a voltmeter, ammeter, and a transformer.

13.4 Equipment / Furnishings

Various equipment are needed to keep the crew and passengers safe, such as crashworthy seats and shoulder harnesses. Rescues with equipment including a hoist and a sling are provided as standard. An oxygen system is standard because of the higher altitude capabilities of the *HeliX*. Fire extinguishers are installed, as required. To further aid the rescue mission, equipment for making sound signals and a megaphone are onboard to facilitate communication with persons on the ground. In the unfortunate case of an aircraft accident, emergency flotation and multiple emergency location transponders are installed.

13.5 Fuel Gauges

The function and status of the fuel system needs to be closely monitored by the flight crew. Fuel tank quantity indicators are made clearly visible to both pilots, and an avionics suite with a fuel flow meter and fuel pressure indicators provide the status of fuel system health. If the aircraft were to experience a fuel issue, low fuel and low fuel pressure

caution lights are used to alert the pilots.

13.6 Air Conditioning

Air vents, fans, and heat are included in the *HeliX* out of necessity, not luxury. It is critical to monitor the cockpit/cabin temperature to ensure proper cooling of the important avionics housed there, especially those which ensure safety of flight, as well as providing a comfortable environment for the pilots especially during extended missions. This monitoring is handled by temperature probes, and in the event the air conditioning system fails to maintain an internal temperature within the required range, an overheating detector will trigger warning messages, and in extreme cases, an alarm. As for the equipment bays housing avionic and electrical components, it is sufficient to cool them in flight by using engine bleed air. To assist with cooling on the ground, fans have also been installed in the avionics bays.

Injuries resulting in significant blood loss often lead to some degree of hypothermia. In most medical rescue situations, heated blankets are kept on board to keep patients warm, but these can be bulky and hinder possible treatment. For this reason, the *HeliX* does not keep heated blankets on board, but rather uses the air vents to provide critical patients with directed heat, alleviating associated supply costs and providing for a better work environment for the crew.

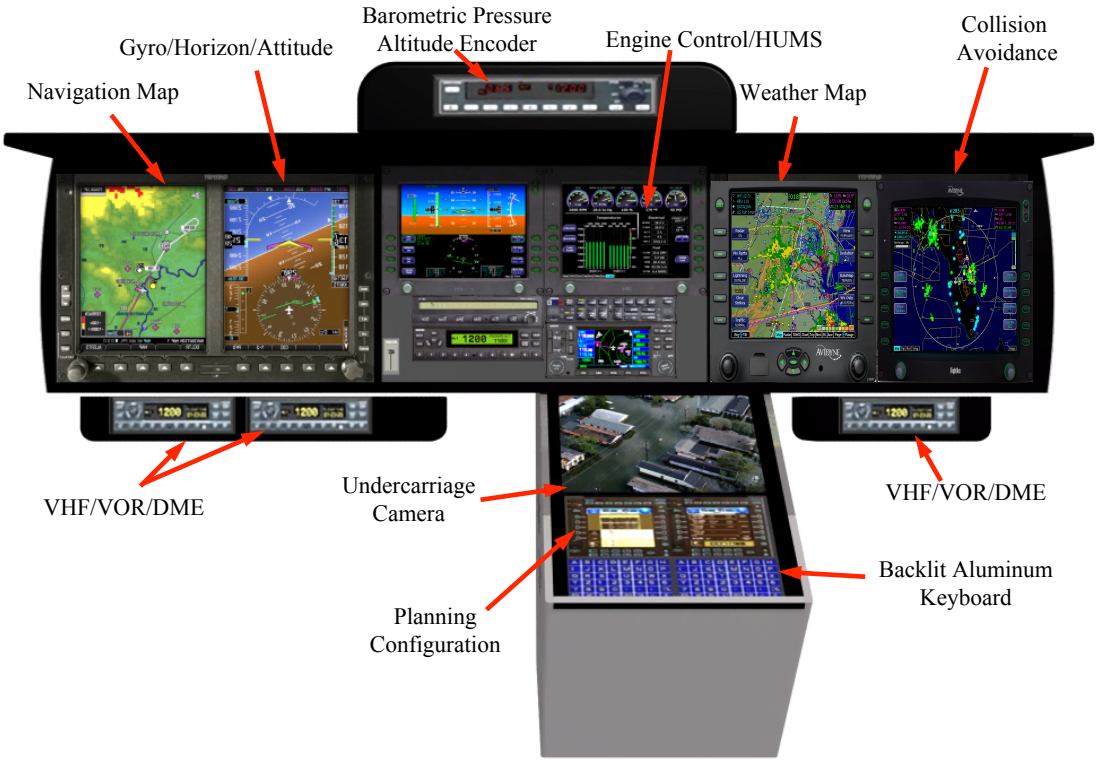

Figure 13.1: Cockpit avionics placement

13.7 Ice and Rain Protection

Ice, and even rain, can be a problem for all aircraft surfaces such as blades, engine inlets [45], pitot tubes, and windshields. The *HeliX* employs on-blade de-icing [17]. The main rotor is fitted with a de-ice slip ring, which delivers power to de-icing mats on the blades. The pitot tubes are fitted with heaters and feature a failure indication system.

The engine inlets contain recessed infrared lamps that warm the incoming air and help to prevent icing [17]. In the event of rain, windshield wipers are installed on the *HeliX*. Electric windshield de-icing is also provided.

13.8 Indicating Systems

For safety, the *HeliX* features a variety of flight safety indication systems. The many components of the aircraft can be monitored from the cockpit, with a main console that offers ramp and door status indicators and engine monitoring. A Vehicle and Engine Management Display (VEMD) and Health and Usage Monitoring System (HUMS) keeps the pilot informed about the health of the engines and transmission at all times.

13.9 Landing Gear

The tricycle landing gear used on the *HeliX* includes a parking brake and landing gear actuating system. The deployment of the landing gear is aided by a landing gear position indicating system, and an alarm sounds in the event that the landing gear fails to extend properly.

13.10 Rotors and Gearboxes

The proprotors on the *HeliX* are fitted with brakes, each having its own braking position caution light. Indicators monitor oil pressure and temperature in the main and auxiliary gearboxes and are also equipped with caution lights.

13.11 Lights

Lights are extremely important as they ensure the people onboard can see inside the aircraft and also see the ground below, as well as ensuring that people on the ground below and in the surrounding air can see them, especially in fleet operations. A Helicopter Emergency Egress Lighting System (HEELS) safely guides passengers and crew to the nearest exit in an emergency situation. Cabin lighting is essential for providing care to the wounded. Position lights and anti-collision lights make the aircraft visible to others within the fleet. For the search and rescue application, a powerful searchlight is installed in the *HeliX*, which can rotate 360° to illuminate stranded persons anywhere in the vicinity of the aircraft.

Figure 13.2: Example of iPad mount configuration

13.12 Navigation

HeliX is equipped with a state-of-the-art navigation suite. A Traffic Collision Avoidance System (TCAS) enables all aircraft in the fleet to safely work close together during relief efforts. An Enhanced Ground Proximity Warning System alerts pilots to any obstacles that may be unanticipated or not visible in the degraded visual environment (DVE) that may occur in a devastated area. A panel-mounted GPS is fitted, but pilots can also choose to interface with an iPad, shown in Fig. 13.2, as an auxiliary source of navigation, and a standby magnetic compass is available as a back-up. A weather radar system with an XM satellite backup is used to aid in strategic route planning.

13.13 Equipment Power Estimates

Table 13.1 includes the varying power required estimates for the equipment previously mentioned.

Table 13.1: Minimum equipment list

Required Avionics	Manufacturer and Model	Weight (lb)	Dimensions (in)	Energy Consumption
Radio-communication transmitters and receivers: FM, HF, UHF, VHF	Rockwell Collins RT-1939	12.2	5.6 x 5 x 9.85	28 VDC
Health and Usage Monitoring System (HUMS)	Honeywell Zing HUMS	4.3	3 x 5.75 x 7.58	10-40 VDC (18 W)
Cockpit voice recorder	Universal Avionics Solid State cockpit voice records	13	N/A	27.5 VDC (14 W)
Flight crew intercom system	Becker Avionics DVCS6100	1.8 + 6.2	5.74 x 2.98 x 3.6 + 13.14 x 2.24 x 7.68	28 VDC
Surface Navigation System (GPS)	Rockwell Collins 60J-5 Airborne GEM V	0.8	5.88 x 5.7 x 0.57	3.0 W
Terrain Awareness and Warning System (TAWS) / Enhanced Ground Proximity Warning System (EGPWS)	Honeywell MK XXII	3.9	12.1 x 3.0 x 6.2	15 W
Airborne Collision Avoidance System (ACAS) / Traffic Collision Avoidance System (TCAS)	Southeast Aerospace TCAS 791	18.8	7.62 x 6.39 x 15.08	20 VDC (120 W)
Auto Pilot Module (APM)	Rockwell Collins	N/A	N/A	N/A
Flight Control Panel (FCP)	Rockwell Collins Athena 611 Integrated Flight Control System	9.7	N/A	18.5 W
Weather Radar System	Honeywell Primus 660	31	4.2 x 6.1 x 11.49 + 1.875 x 5.75 x 6.5	28 VDC

14 Health and Usage Monitoring Systems (HUMS)

Health and Usage Monitoring Systems (HUMS) continuously determine the status of flight critical systems and analyze the information to determine the overall health of the aircraft. Because of the large number of flight critical dynamic components on the *HeliX*, including the blade retraction mechanism, wing extensions, tilting nacelles, transmission, and engine systems, it is important to diagnose any problems effectively and quickly.

The HUMS aboard *HeliX* is comprised of two elements: the on-line element and the off-line element. The on-line processing element relays information directly to the pilot; this data, such as average torque usage or flight regime characteristics, is typically not heavily processed and may be easily condensed. This intuitive display informs the pilot of the current aircraft status and necessary warnings. The off-line element saves pertinent data from the various sensors onboard the aircraft to the flight data recorder and determines the next necessary hard-time overhaul of components. The suite of warning sensors is coupled with software that has knowledge of the physical and temporal limits of the mechanical components to allow for a comprehensive life-cycle analysis to be conducted in real-time, thereby reducing the mean time between failure and mean time to repair, which improves the safety of the aircraft dramatically. Safe life limits of a part are automatically tracked by cycles or hours of operation. The HUMS can notify ground crew of a part approaching its life expectancy and creates a diagnostic report that can be used by ground technicians.

There are three distinct processes of the maintenance schedule:

- Hard-time: Preventive maintenance is required at fixed intervals of time.
- On-condition: A less rigorous maintenance of suspect components is performed and the aircraft is approved for continued operation.
- Condition monitoring: A non-preventative process where data from all components and systems are assimilated and corrective measures are applied where necessary.

14.1 Proprotor

Continuous monitoring of the proprotor system health is vital to the operation of *Helix*, especially because of the numerous added components associated with the variable diameter proprotor system. A series of strain gauges and accelerometers are implemented on the rotor system to continually provide vibration and loads data to the HUMS system. The HUMS system monitors the number of extension/retraction cycles, hours of operation and the loads placed on critical components such as the Kevlar straps and spooling assembly. The data from the sensors is compared to a pre-existing database of potential risks and failure modes that are compiled during the flight testing and certification phase. If the observed sensor data exhibits characteristics that indicate a potential failure mode or that a part has reached its life cycle limit, the system alerts flight crews and creates a diagnostic report to be examined by maintenance technicians. During maintenance, ground crews can utilize acoustic methods to monitor the health of the electric spooling motor and harmonic drive system. These systems have been designed for ease of access for maintenance. Proprotor track and balance is performed using an infrared (IR) camera in conjunction with the data from the strain gauges and accelerometers to ensure optimal rotor performance.

14.2 Engine

The engine performance assessment monitors engine torque and temperatures at the inlet, compressor, combustor, turbine, and exhaust. The system also records the time spent above operational torque limits, oil filter and temperature, average flight performance data, and fault monitoring. The HUMS also monitors the health of the Full Authority Digital Engine Control (FADEC) systems that govern the engine fuel flow and power. Dual FADECs are used in the aircraft and the HUMS can automatically override a faulty FADEC.

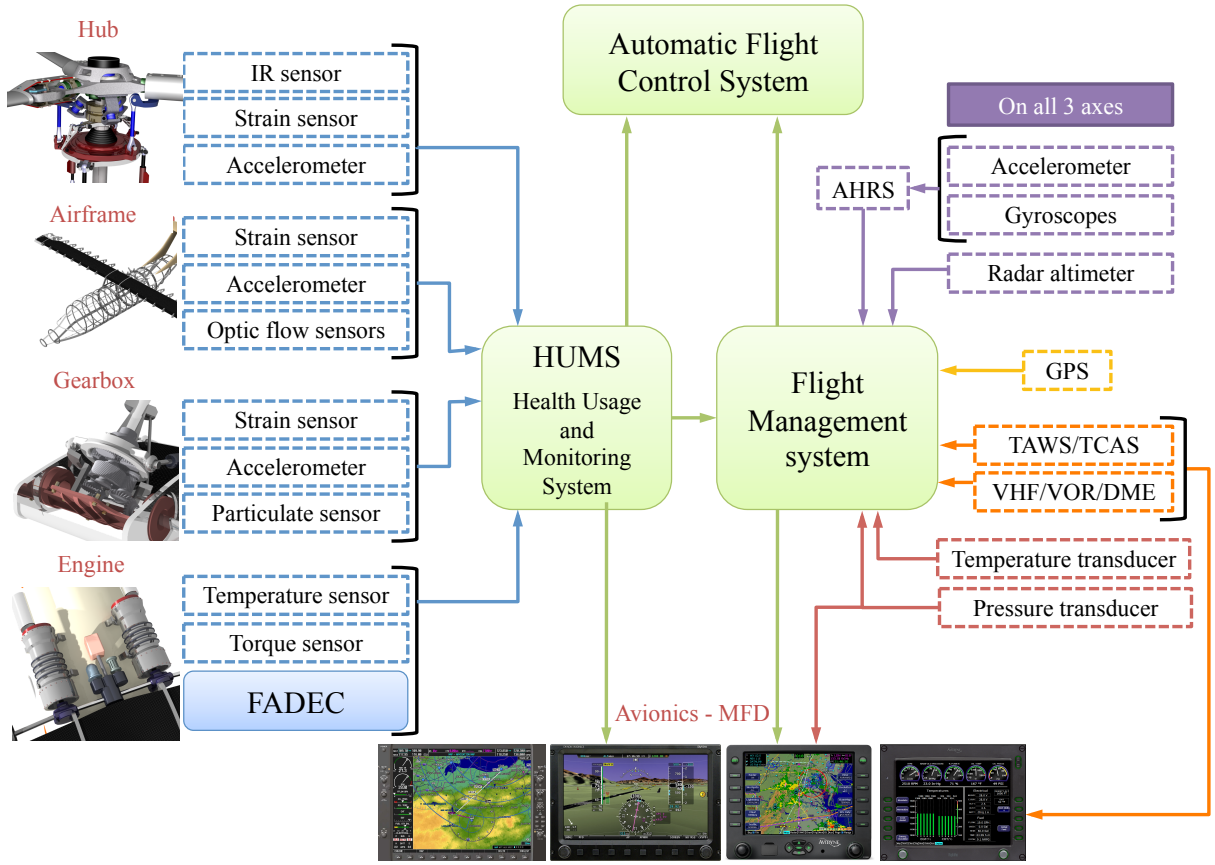

Figure 14.1: Automatic flight control system dependency schematic

14.3 Gearbox

The gearbox contains an accelerometer and a tachometer that are mounted to each proprotor shaft and are connected to a gear. The vibrations observed are time-synchronously averaged using the tachometer pulse train and any anomaly is recorded and preventive action is taken by the flight management system. In-line inductive oil debris monitors are installed to monitor oil leak and debris accumulations.

14.4 Structure

Accelerometers are embedded in the pilot seats to monitor lateral and vertical acceleration ensuring acceptable levels of vibration. Strain gages are mounted at critical stress points of the main load-bearing structures throughout the aircraft. Optic fibers are used as sensors and are embedded in, or bonded onto, the aircraft's composite structures. When fractures, cracks, or delaminations occur in the airframe, they destroy the fibers and so interrupt the light flow, allowing the anomaly to be isolated.

15 Flight Control System

15.1 Control Mixing

The *HeliX* uses the collective, cyclic, and anti-torque controls in helicopter mode, and uses the throttle, flaperons, elevator, and rudder when operating in airplane mode. Extensive and continuous control mixing is employed to ensure a seamless transition between the two primary flight modes. The control actions of the *HeliX* in both helicopter and airplane mode are shown in the flight control system foldout. In helicopter mode, thrust/power change is obtained through simultaneous collective pitch of both proprotors. Aircraft pitch/fore-aft is obtained through symmetric longitudinal cyclic in both rotors. Similarly, yaw control is achieved through differential longitudinal cyclic. Finally, aircraft roll control is achieved through a differential collective coupled with the application of symmetric lateral cyclic. In airplane mode, the pilot stick inputs induce traditional fixed-wing control surface responses, in which thrust/power is applied through throttle control, aircraft pitch through elevators, yaw control through rudder, and roll control is achieved through the flaperons.

All controls, with the exception of collective in helicopter mode, throttle in airplane mode, and yaw, are achieved using a right-handed joystick. Yaw is achieved through foot pedals and collective and throttle are achieved through an innovative design, shown in the foldout. In times of duress, a pilot will tend resort to his or her previous training, either as a helicopter or an airplane pilot. To avoid accidental control inputs, the collective/throttle is designed such that it is in a typical helicopter up-down moving collective configuration when the vehicle is in helicopter mode, and then transitions to a typical fore-aft moving throttle configuration when in forward flight, as depicted graphically in the foldout.

15.2 Dynamics and Stability

While a well designed control input method is helpful, it is important to ensure that the vehicle is stable during normal modes of flight. Poor handling qualities can make it difficult for a pilot to control the aircraft, driving up the pilot's workload. To increase this vehicle's autonomy, it was important to minimize stability concerns. A simplified linear flight model, RAPiD [46], was used to carry out the stability and control analysis for the *HeliX*.

A linear model, defined by the equation $AX = Bu$ was used at all trim points. This is a classical equation where A and B are the stability derivative matrix and control derivative matrix, respectively. X is the state vector, and u the control input vector.

15.2.1 Stability in Hover

As helicopters are inherently unstable vehicles, the first study was done on the *HeliX* in hover. In order to be considered stable, the real part of a pole must lie in the left hand plane. As shown in Fig. 15.1, the *HeliX* has two unstable modes, with positive real parts, and a neutrally stable heading mode, where the pole is zero. The unstable modes, a phugoid and sideslip/roll mode, have long enough time constants that they can be controlled by the flight control system. Figure 15.1 also shows hover stability modes of two tiltrotor concepts, the XV-15 and UMD *Excalibur*, and the UH-1H Huey, a SMR helicopter.

15.2.2 Stability in Forward Flight

The forward flight trim analysis was performed for the *HeliX* at the cruise speed dictated by the RFP. By evaluating the A matrix, defined in Section 15.2, key stability modes were identified and are shown in Fig. 15.2. Based on this methodology, the open-loop stability of the aircraft could be predicted. Based on the data shown, it is apparent that the *HeliX* has instabilities that are similar to both the XV-15 and the UMD *Excalibur*. However, these instabilities demonstrate slow and long enough time constants that they can be easily controlled by the flight control system as well.

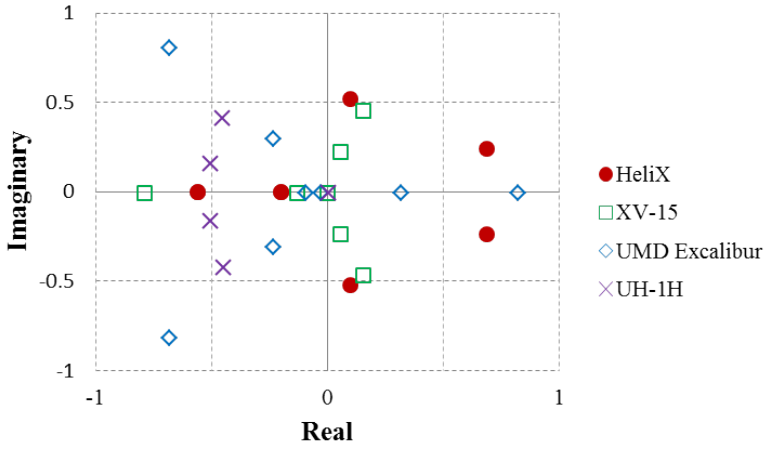

Figure 15.1: Pole diagram characterizing hover stability modes

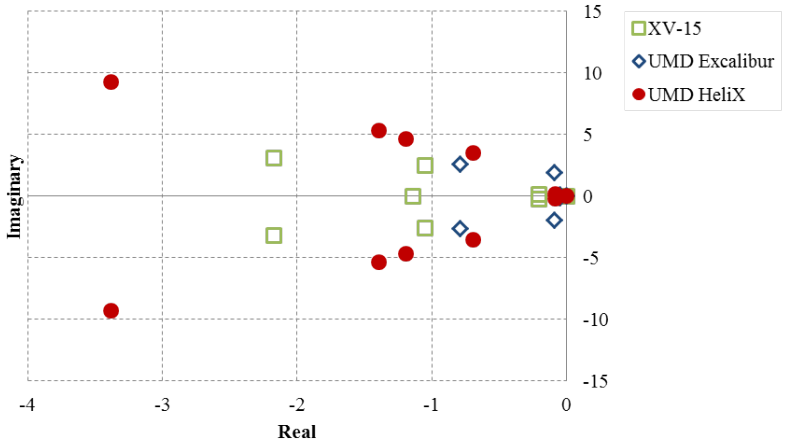

Figure 15.2: Pole diagram characterizing forward flight stability modes

The six stability modes shown in Fig. 15.2 were determined to be a heading hold, wing rocking, spiral, Dutch roll, short period, and phugoid mode.

15.3 Digital Fly-by-Wire Architecture

Figure 15.3 shows the schematic of the digital flight control system architecture. Each of the subsystems are designed with safety and redundancy in mind. Four separate data channels from sensors to the FCS ensure redundancy in the FCS design. The input-output processor (IOP) and the two Primary Flight Control Processors (PFCP), collectively called the flight control computers (FCC), form the backbone of the architecture. The Automatic Flight Control Processor (AFCP) is responsible for handling threads tied to the Automatic Flight Control System (AFCS). The functional split between the PFCP and AFCP maximizes safety and reliability by partitioning the flight-critical and mission-critical control laws, respectively. The AFCP computes enhanced flying qualities, which vary according to the mission profile.

Data from various onboard sensors are sent to HUMS (see Section 14), which is linked to an Air Data Computer (ADC). Because the FCC is also coupled to the HUMS system, violation constraints are applied to prevent the pilot

from performing maneuvers that could structurally damage the vehicle, or to steer the aircraft out of regions where aeroelastic instabilities (such as whirl flutter) may occur. The FCC contains all control laws and gains that have been obtained through flight tests and system identification techniques. The ADC also receives information from GPS and onboard navigational equipment through the AHRS and passes it on to the Flight Management Computer (FMC). Information regarding other aircraft in the fleet is used by AFCP to provide autonomy while working together with other aircraft, reducing pilot workload. Failure logics are implemented and coupled to sensors from the VDR and OWE systems that are activated automatically if an anomaly is detected.

15.4 Task Automation

The AFCS is designed to improve handling qualities and reduce the pilot workload while increasing safety, redundancy, and reliability. Specifically, the system is capable of rate command attitude hold and attitude command attitude attitude hold compliant with ADS-33E-PRF. A model-following architecture (shown in Fig. 15.4) provides inherent stability augmentation and gust rejection. The avionics suite installed onboard the aircraft extends the capabilities of the AFCS to allow pilot-commanded way-point navigation to a specified latitude/longitude, airspeed hold, altitude hold, close proximity terrain avoidance, hover holds, and to conduct auto-search patterns.

The FCS of the *HeliX* is designed to be adaptive for pilots trained primarily in helicopters or airplanes exclusively. Each pilot is required to perform simulated maneuvers on the ground consisting of short period roll, pitch, and yaw. The input/output gains in the pilot transfer function are modified based on these tests. Each pilot needs to calibrate only once as the pilot dependent data can be transferred between separate aircraft. The fully-digital FCS restricts control authority to certain pilots by placing restrictions on the collective, cyclic, and engine torque so that the pilot will not unknowingly put the vehicle in a dangerous flight condition. Special attention has also been given to the design of pre-flight procedures. The *HeliX* is capable of all pre-flight system checks apart from those requiring a visual/walk-around inspection, thereby significantly reducing the pre-flight time.

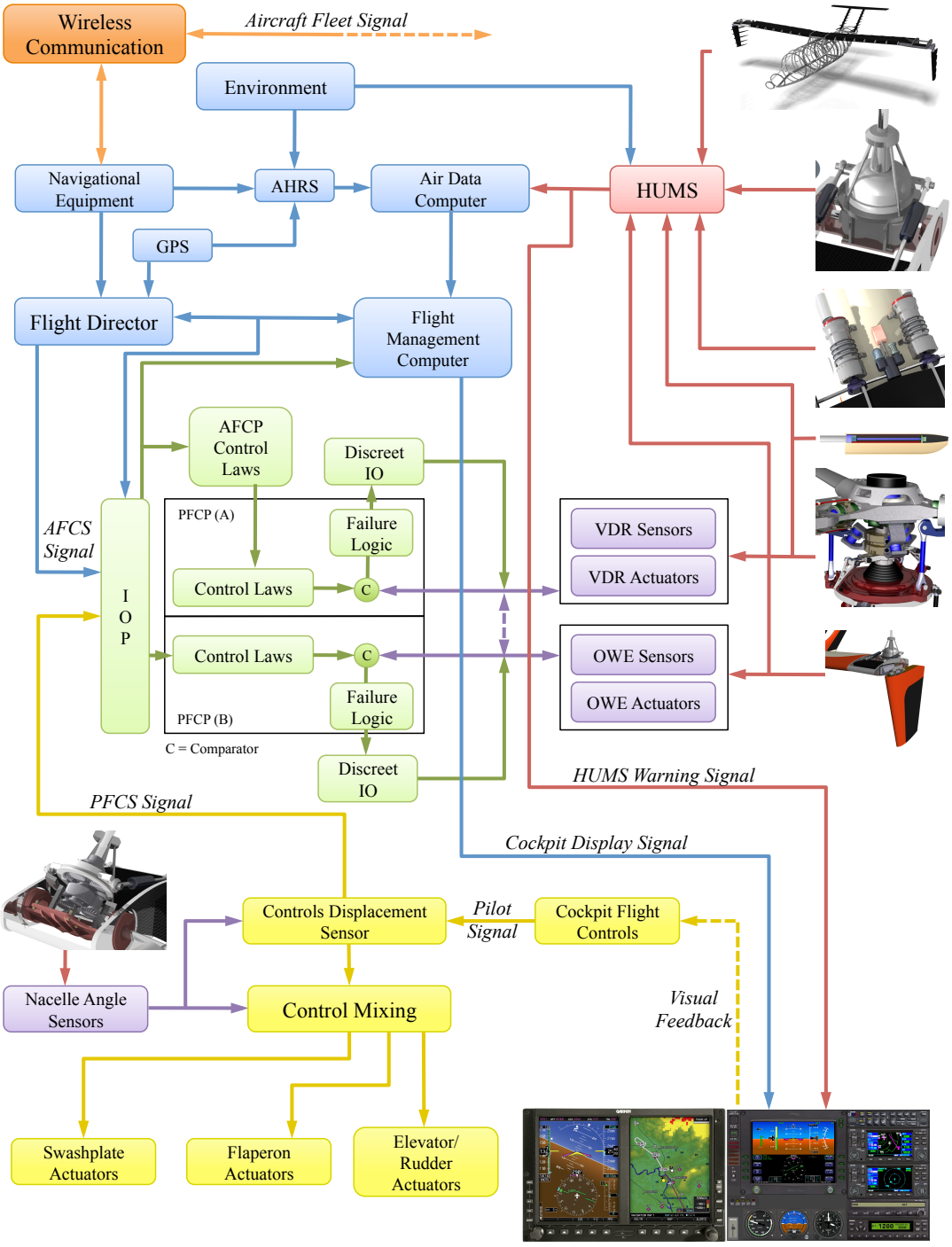

Figure 15.3: Flight Control System architecture

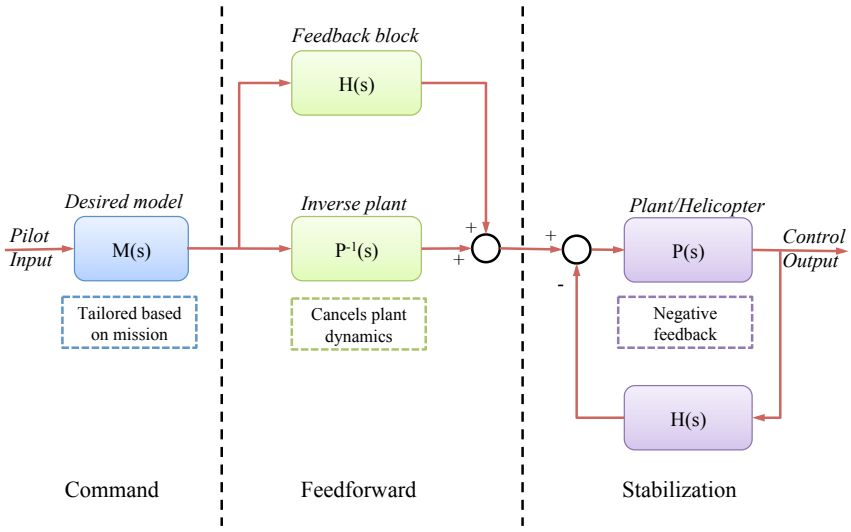

Figure 15.4: Model following flight control system

Control Mixing

Swashplate actuator movement

Helicopter controls	P_1	P_2	P_3	SB_1	SB_2	SB_3	Airplane controls
δ_{coll}	+1	+1	+1	+1	+1	+1	Thrust
δ_{long}	0	+1	-1	0	+1	-1	Pitch
δ_{lat}	-1	-1	-1	+1	+1	+1	Roll
δ_{ped}	0	-1	1	0	+1	-1	Yaw

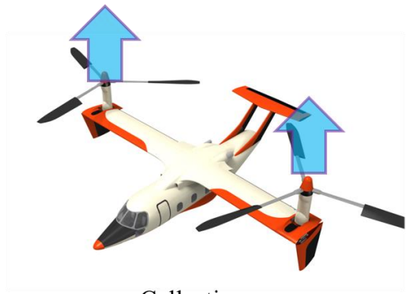

Collective

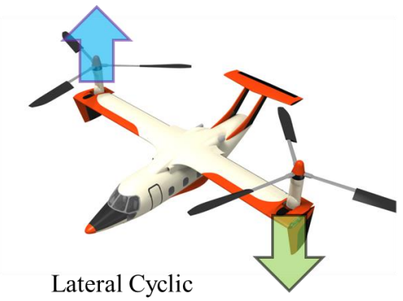

Lateral Cyclic

Longitudinal Cyclic

Directional

Pilot Controls

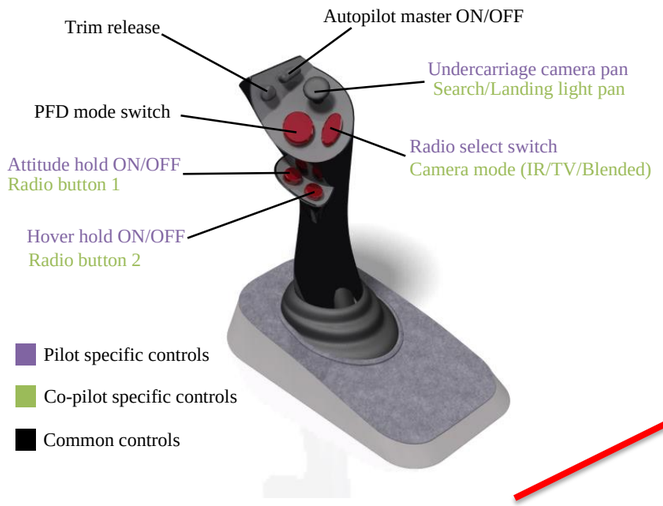

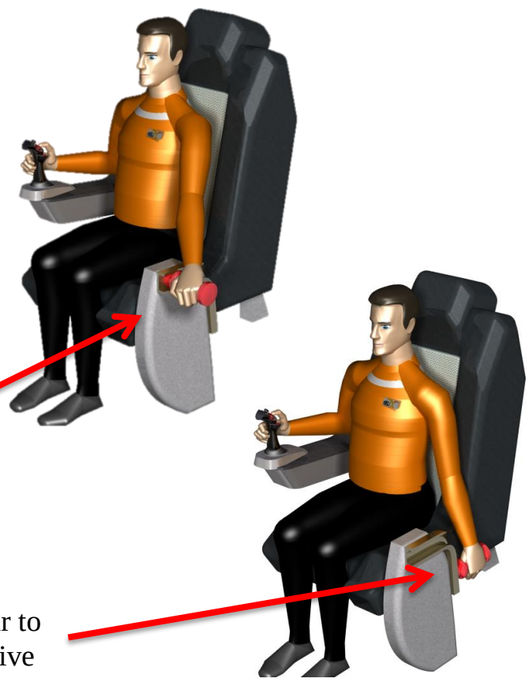

Positioning similar to airplane throttle

Positioning similar to helicopter collective

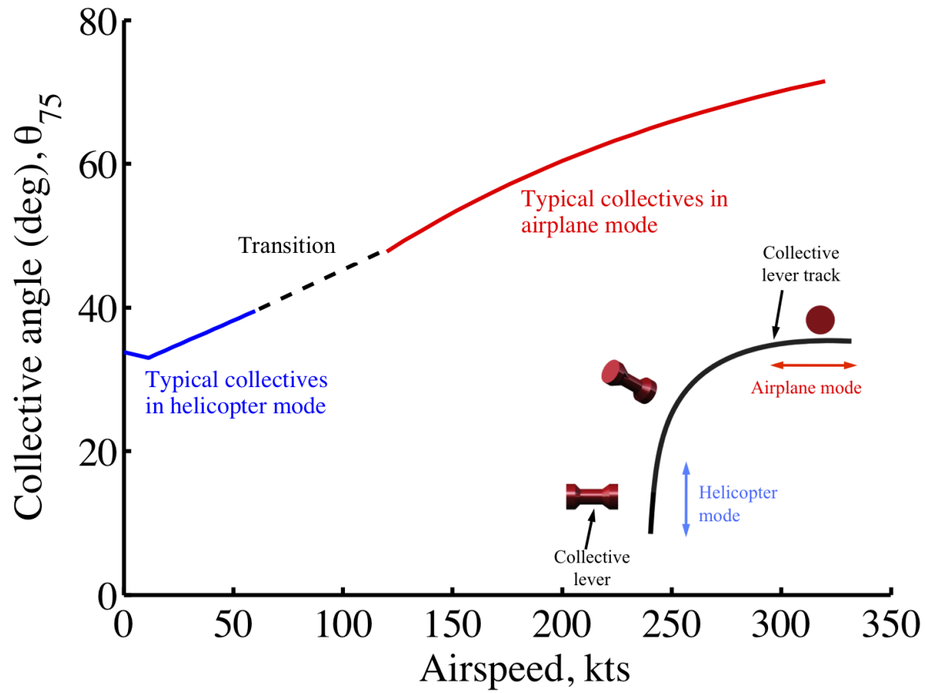

16 Acoustics

16.1 Internal Noise

Because the *HeliX* is an unconventional tiltrotor with the engines mounted inboard on the fuselage, provisions must be made for adequate soundproofing of the cabin. Similar to soundproofing methods used in the Bell 430 [47], the *HeliX* is built with a sound blocking material consisting of two sound absorption mats with a foil layer between. The mat is made of alternating layers of lead foil, fiberglass batting, and sound attenuating composite foam. To prevent other possible sound paths, access panels and bulkhead passages for wiring and ducting are sealed. This setup incurs only a minimal weight penalty.

16.2 FAA Regulations

The Federal Aviation Administration (FAA) has recently adopted noise certification standards for tiltrotor aircraft. The Federal Aviation Regulations (FARs) provide uniform noise certification standards for tiltrotors certified in United States and harmonizes U.S. regulations with the Annex 16 standards from the International Civil Aviation Organization (ICAO). Tiltrotors, when tested in accordance with the FAA noise regulations, shall not exceed certain noise levels at the overflight reference points. The regulation defines the overflight reference noise measurement points as:

- A flight path reference point located on the ground 150 m (492 ft) vertically below the flight path.
- Two other points on the ground symmetrically disposed at 150 m to both sides of the flight path and lying on a line through the flight path reference measurement points.

Figure 16.1 shows the reference noise measurement points, A, B, and C.

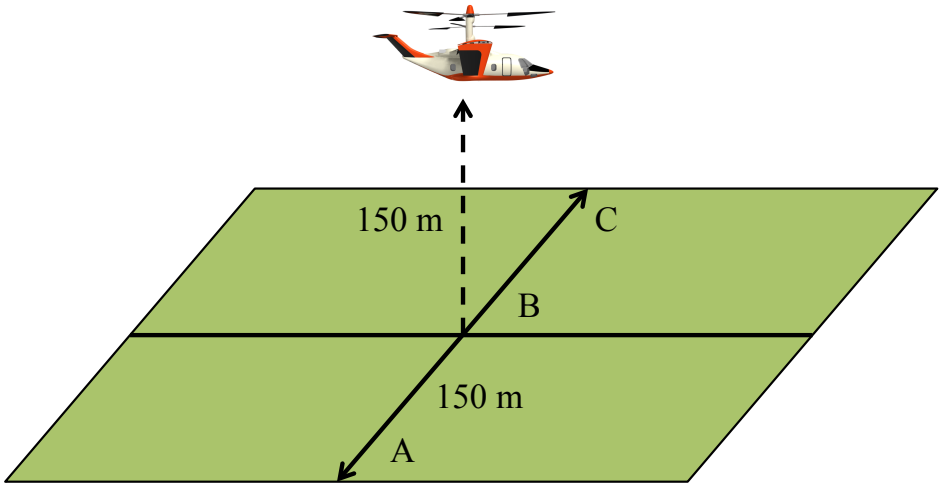

Figure 16.1: Overflight reference noise measurement points

16.3 Overflight Reference Procedure

The noise level limit is defined for a tiltrotor in helicopter or transitional flight mode with a MGTOW of 80,000 kg and over. The noise level cannot exceed 108 EPNdB (effective perceived noise level in dB). The noise requirement decreases linearly at a rate of 3 EPNdB per halving of vehicle weight down to 88 EPNdB, after which the limit remains constant. This requirement is shown graphically in Fig. 16.2. Because the *HeliX* has a maximum weight of approximately 15.3 tons, the value of n in this case is 2.415. Therefore, the noise level limit is 100.8 EPNdB. The effective

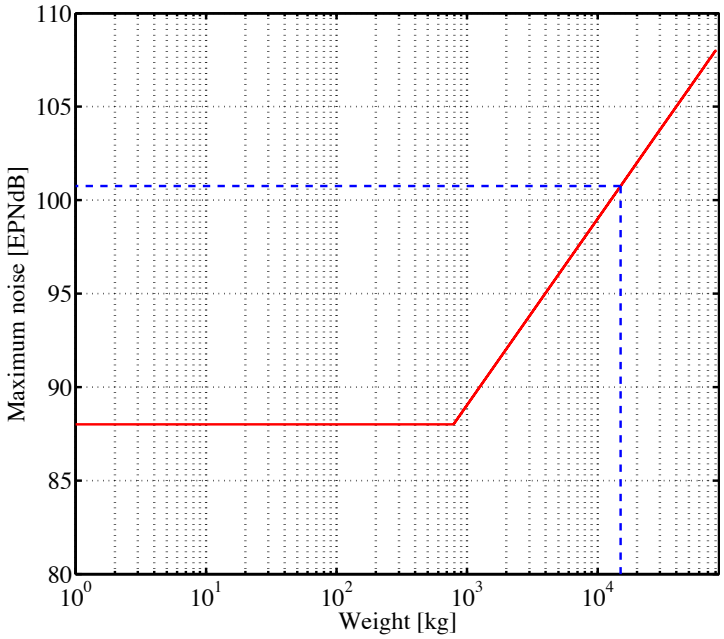

Figure 16.2: Maximum noise levels versus takeoff weight

perceived noise level in decibels (EPNdB) is a scale that gives good measure of annoyance. Another way to account for annoyance is the usage of A-weighted averaged SPL. A-weighted averages are generally higher than EPN levels, but lower than SPL levels for lower audio frequencies. The procedure computes a weighting for each pressure level based on its frequency content. The human ear is less sensitive to low audio frequencies, therefore the A-weighting is used to reduce the noise levels (negative gain) corresponding to low frequencies and increase the levels for the noise with higher frequency content (positive gain).

16.4 Noise Measurement

Rotor noise estimations were obtained using an acoustics analysis developed at the University of Maryland based on Farasatt's Formulation-1A of the Ffowcs Williams - Hawkings equation. This analysis computes both the thickness noise and loading noise from the rotor blades. Thickness noise, caused by the unsteady displacement of the air, is mainly governed by the thickness of the blades and is directed mostly in the plane of the rotor. Loading noise is largely dependent on blade loading and is mostly directed downward below the rotor plane.

16.4.1 Helicopter Mode

For the initial analysis, sound pressure levels (SPL) in decibels were calculated on a hemisphere of 50 m (164 ft) centered around the vehicle. This radius is approximately equal to 8 times the main rotor radius. Figure 16.3 shows the thickness noise contours along the surface of the sphere. The corresponding loading noise levels in hover along the surface of the hemisphere are shown in Fig. 16.4. As expected, the thickness noise levels are maximum in the plane of rotor while the maximum loading noise occurs below the rotor planes. In helicopter mode, the noise signature is symmetric about the plane perpendicular to the line joining two hubs.

Sound pressure levels were also calculated at reference measurement points, defined in Section 16.2, to ensure that the noise levels for *HeliX* satisfy the FAA requirements. Combining both thickness and loading noise levels, the noise levels at points A, B, and C were all found to be below 89 dB; the expected EPN decibels level will also be low for reasons previously mentioned. The estimate EPNdB levels can be obtained by computing the A-weighted SPLs. The

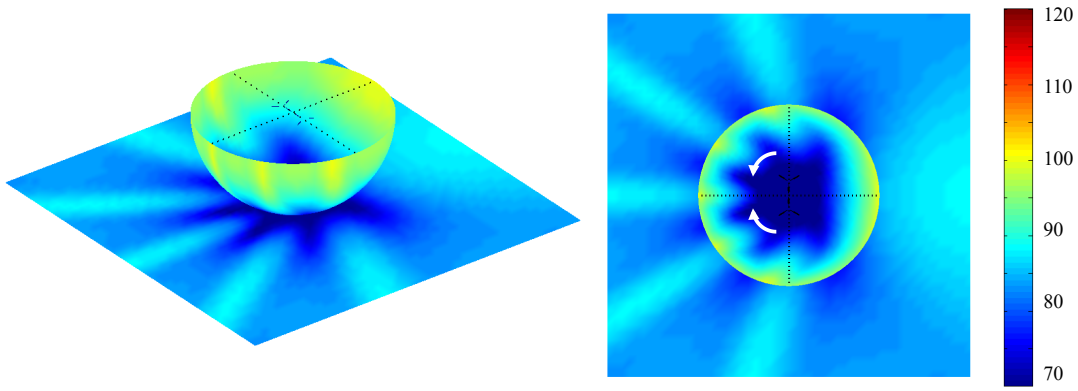

Figure 16.3: Thickness noise sound pressure levels in hover

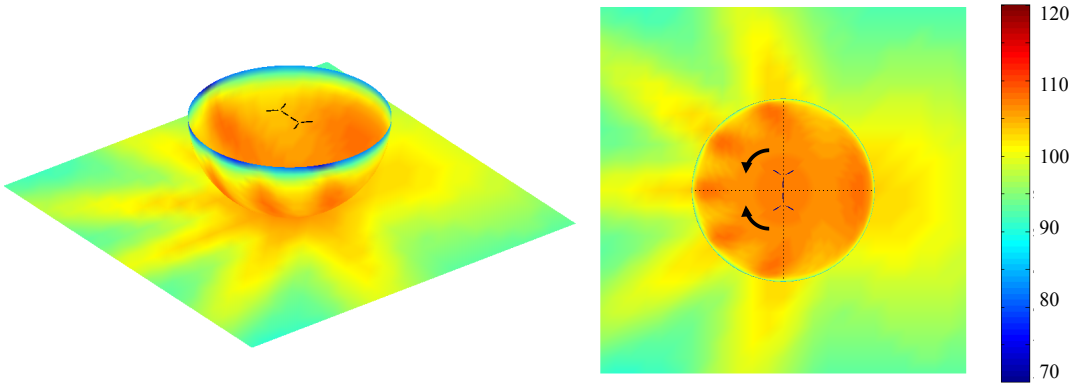

Figure 16.4: Loading noise sound pressure levels in hover

A-weighting is applied in an effort to account for the relative loudness perceived by the human ear. The A-weighting is also a good measure of annoyance level because it results in positive weighting for sound levels with frequencies that human ears are most sensitive to. Generally the A-weighted SPLs are higher than the EPNdB levels. Therefore, if the noise regulations are satisfied by the A-weighted values, the EPNdB values will generally also satisfy the noise regulations.

Table 16.1: Total sound pressure levels of vehicle in helicopter mode

Reference Point	Total Noise (dBSPL)	Total Noise (dBA)
A	91.8	88.9
B	88.4	85.3
C	91.8	87.9

16.4.2 Airplane Mode

Another acoustic analysis was conducted for the vehicle in airplane mode with the same overflight condition. In airplane mode, the nacelles are oriented at the down stop position (shaft tilt angle of 90°) and the cruise speed is 0.9 V_{MCP}. Note that V_{MCP} is the maximum operating limit airspeed corresponding to maximum continuous power (MCP) available for ISA conditions. V_{MCP} for the *HeliX* is 283 kts, as shown in Section 3.4. Therefore noise measurements were conducted at a cruise speed of 211 kts (90% of V_{MCP}) in airplane mode. Although the FARs do not specify a

maximum noise level limit in airplane mode, the noise levels in this configuration are lower than when in helicopter mode.

16.5 Effect of Blade Tip Sweep on Noise

A parametric study was conducted to investigate the effect of tip sweep on the acoustics produced by the vehicle, and it was found that the noise levels were almost unaffected by tip sweep. Two points were chosen for the study: 1) Point P, in the plane of the rotor where thickness noise is dominant in helicopter mode, and 2) Point Q, located well below the plane of the rotor, where loading noise is dominant in helicopter mode. As shown in Tables 16.2 and 16.3, the noise levels remain nearly unaffected by tip sweep. Although not presented here, the noise at Points P and Q in airplane mode were much lower than those in helicopter mode.

Table 16.2: Proprotor tip sweep analysis results at Point P in helicopter mode

Sweep Angle (deg)	Thickness Noise (dB)	Loading Noise (dB)	Total Noise (dB)
3.5	96.20	82.38	95.18
15	96.23	82.37	95.23
20	96.23	82.37	95.23
25	96.24	82.36	95.25

Table 16.3: Proprotor tip sweep analysis results at Point Q in helicopter mode

Sweep Angle (deg)	Thickness Noise (*dB*)	Loading Noise (*dB*)	Total Noise (*dB*)
3.5	88.37	107.28	107.20
15	88.39	107.28	107.17
20	88.39	107.28	107.17
25	88.42	107.27	107.14

17 Cost Analysis

17.1 Unit Acquisition Cost

In general, the cost of an aircraft can be separated into three major parts: development cost, production cost, and operational cost. The sum of the aforementioned costs adds up to the total life-cycle cost of the aircraft. However, the customer is initially concerned with only two aspects of the cost of the aircraft: the unit acquisition cost and the operating cost. In the case of the *HeliX*, the focus went toward minimizing the acquisition and operating cost of the design while still meeting all of the requirements of the RFP. This focus was especially important given the fact that tiltrotor designs have historically higher costs in comparison to conventional helicopter designs of comparable size and/or weight.

To estimate the unit acquisition cost of the *HeliX*, the empirical model developed by Harris and Scully [48] was utilized. This model is based on historical data available for 120 helicopters and 2 tiltrotors. The Consumer Price Index [49] was applied to account for annual inflation rates and to update the predicted acquisition from 2008 U.S. dollars to 2013 U.S. dollars.

It should be noted that while the Harris and Scully model has proven to be an effective means of estimating the acquisition price of conventional helicopters, its ability to accurately predict the acquisition cost of tiltrotors is yet unproven, partly because there is only one tiltrotor in current production. Regardless, the Harris and Scully empirical model is a widely accepted method to predict the acquisition cost of rotorcraft and so was used in the acquisition cost estimation of the *HeliX*. Using the Harris and Scully empirical model, updated to 2013 U.S. dollars, it was possible to compare the

Table 17.1: Comparison of tiltrotor unit acquisition costs

Baseline Cost (in millions of $)	BA-609	V-22	*HeliX*
Calculated Baseline Price	13	32.6	25.3
Actual Baseline Price	12.3*	67	N/A

* Predicted

acquisition price of the *HeliX* to that of two other tiltrotors. As shown in Table 17.1, the Harris and Scully empirical formula can adequately predict the acquisition cost of various tiltrotors except for the V-22. This is primarily because of the steep increase in production and development costs that the V-22 program has incurred throughout its 25-year development timeline.

Based on the Harris and Scully model, the $25.3 million acquisition cost of the *HeliX* is not much greater than that of other rotorcraft in the same weight class. However, given the advanced technology utilized by the *HeliX*, especially in the VDR concept, it is expected that the actual acquisition cost of the aircraft would be higher. This is a result of the increase in research and development costs required to prove and validate the VDR concept, as well as the wing extensions. It is important to keep in mind that the hover and minimum useful load requirements of the RFP drive up the respective installed power and empty weight of the vehicle and, in turn, have a large impact on cost. Had the *HeliX* been designed for operations at a lower altitude and temperature, and thus required a smaller installed power, the acquisition cost would have been commensurately reduced.

The operating costs of the *HeliX* were estimated using the cost models developed by Conklin and de Decker [50]. Like the acquisition cost model developed by Harris and Scully, the operating cost models are based on historical data for over 100 rotary-wing vehicles. When estimating the operating costs of the *HeliX*, a 40% penalty was applied to costs associated with the rotor system, transmission system, and wing. This penalty was derived from the results of a study comparing the estimated operating cost of tiltrotors to conventional aircraft [51] and was adjusted to account for the variable diameter rotor system, wing extensions, and novel transmission system that are unique to the *HeliX*.

The 25.3 million dollar acquisition cost of the *HeliX* is greater than that of other rotorcraft in its weight class. It is

important to note, however, that the hover and minimum useful load requirements of the RFP drive up the respective installed power and empty weights of the vehicle and, in turn, have a large impact on cost.

17.2 Direct Operating Cost, DOC

Direct operating costs (DOCs) are the costs related to the operation of a given aircraft that vary in direct proportion to the number of flight hours. DOCs cover the cost of fuel, additives, lubricants, maintenance labor, and inspections as well as the cost of replacing various parts of the aircraft. Figure 1(b) shows a percentage breakdown of how each component of the DOC contributes to the overall DOC of the *HeliX*.

As a base of comparison, the *HeliX* was compared to two conventional helicopter designs within the same weight class, namely the AW-101 and the S-92. As per the requirements of the RFP, the *HeliX* was also to be compared to the UH-60 Black Hawk with upgraded T700-GE-710C engines. Given that the Black Hawk is a U.S. military aircraft, detailed operating cost data for that particular vehicle are not available. However, it was possible to determine the operating costs of the Sikorsky S-70 with CT7-2C engines, the commercial variant of the UH-60 that was specified. Given its similarity to the Black Hawk, the operating cost data of the S-70 was used for comparison to the *HeliX*.

Table 17.2 shows a comparison of the DOC of the aforementioned conventional helicopter designs calculated using the Conklin and de Decker model alongside that of the *HeliX*, while Fig. 17.1(a) and Fig. 17.1(b) show a breakdown of the direct maintenance costs and direct operating costs of the *HeliX*, respectively. As shown in Table 17.2, it is

Table 17.2: Comparison of DOC

Direct Operating Costs	Average $/FH over 20 years			
	S-92	AW-101	S-70	*HeliX*
Takeoff Weight, tons (lb)	12.0 (26,500)	14.6 (32,180)	10.0 (22,000)	15.1 (33,331)
Fuel and Additives	1,601	1,898	1,457	1,583
Maintenance and Labor	612	843	799	1,093
Parts	857	1,138	1,112	1,114
Engine Overhaul	345	426	283	393
Life Limited/Overhaul/ Inspections	90	1,118	157	1,316
Total DOC	**3,505**	**5,423**	**3,808**	**5,499**

apparent that the *HeliX* provides a lower fuel cost compared to other conventional designs in its weight class. The tiltrotor design is more fuel efficient in comparison to conventional helicopter designs because of the reduced power consumption and fuel burn in cruise flight. Given that fuel costs are the number one contributor to the total direct operating cost, greater fuel efficiency is imperative for decreasing the operating cost of the aircraft. The main reason behind the higher DOC of the *HeliX* over conventional designs is its use of advanced technology. The retractable blades, blade retraction mechanism, advanced hub design, and wing extension mechanisms all add to the cost of parts, labor, and life-limited part overhauls. From Figure 17.1(a), it can be seen that part and overhaul costs make up over 80% of the maintenance cost associated with the aircraft and combined with labor cost, constitute over 60% of the total direct operating cost of the *HeliX*.

17.3 Indirect Operating Cost, IOC

Indirect operating costs (IOCs) encompass the cost of daily operations and fixed costs associated with operating the aircraft. Included in the IOCs are the pilot and crew salaries, hangar fees, hull and liability insurance, and other miscellaneous costs. Table 17.3 provides a comparison of the IOC of the of the *HeliX* to the chosen conventional helicopter

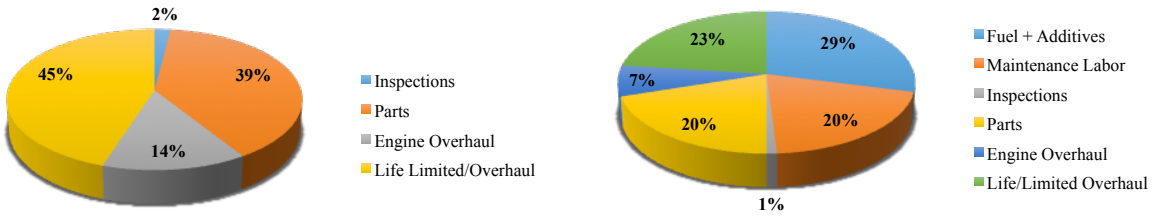

(a) Breakdown of maintenance costs (b) DOC breakdown

Figure 17.1: Maintenance and operating cost breakdown

designs.

The indirect operating cost of the *HeliX* appears noticeably higher than that of the other conventional rotorcraft designs to which it is compared. However, this is mainly because of the pilot and crew salaries and the hull insurance costs. The RFP requires that the *HeliX* operate with a crew of three, as opposed to a crew of two (common to other designs) thereby increasing the crew salaries. However, if that requirement were relaxed to two crew, the crew costs for the *HeliX* would be on par with other designs.

Along with crew salaries, hull insurance costs constitute a large fraction of the total IOC. Hull insurance costs are based on a set percentage of the purchase price and for newly introduced families of rotorcraft, a hull insurance rate of 2.5% to 3% is typical. As the *HeliX* accrues more service hours and the safety and reliability of the design gets demonstrated, it is expected that the hull insurance cost would decrease. While both the direct and indirect operating costs of the *HeliX* are higher than those of conventional helicopters, the values are within an acceptable cost range compared to other rotorcraft. This outcome shows that through the use of best practice maintenance and operation programs, future tiltrotor systems can provide a cost-effective alternative to conventional designs with a mission capability that is unmatched by other current, commercial VTOL aircraft.

Table 17.3: Comparison of IOC

Indirect Operating Costs	Average $/year over 20 years			
	S-92	AW-101	S-70	*HeliX*
Pilot/Crew Salary and Benefits	291,835	291,835	291,835	358,205
Hangar	20,959	19,750	16,391	20,959
Hull Insurance	380,888	282,139	349,315	505,835
Liability Insurance	29,222	29,222	29,222	29,222
Miscellaneous	136,336	140,584	123,644	143,008
Total DOC	**859,239**	**763,529**	**810,407**	**1,057,228**

18 Multi-Role/Multi-Mission Capability

18.1 Configurability

A key design feature of the *HeliX* is the configurability of the cabin. Based on the requirements of the RFP, it was important to ensure that components within the vehicle could be removed and added with relative ease and speed. To make this possible, everything in the cabin can be installed by using reconfigurable tie-down fittings. These fittings can either be rings with the ability to swivel freely for quickly snapping things into place, or female bolt fittings that accommodate different screw-in or snap-in attachments. All fittings are recessed into the floor when not in use. The only items that will not use these fittings are the stretchers, described in Section 18.4, which have specific attachment points in different areas of the vehicle. The universal fittings are located approximately every 0.5 m along the floor and every 0.25 m up the interior side wall so as to allow for maximum configuration flexibility.

18.2 Mission 1 – Aerial Triage

There are no major requirements associated with Mission 1. Because of this, and the low TOW weight for this mission, as discussed in Section 2, provisions for the other missions can be included if necessary, as detailed in the following sections.

18.3 Mission 2 – Aid Distribution

The second mission requires that the crew be able to deliver 2 tons of relief material with small parachutes. Based on the provided relief density of 1.5 g cm^{-3}, the 2 ton material can fit into a 1.33 m^3 package. With a three person crew, one of the important design considerations was to make it easy for three people to move 2 tons of cargo or other material into the vehicle with limited equipment. To this end, the *HeliX* is equipped with a dual-operation winch/hoist system. Because winches are typically employed for pulling heavy loads slowly, and hoists for lifting lighter loads much more quickly, internal gearing is required to make provisions for both uses. As shown in Fig. 18.1, the winch cable can be re-directed such that it can pull in the cargo, loaded on wheeled pallets, with limited need of crew. To avoid backlash in the event the winch cable breaks, the winch is built with a clutch.

The possibility of using rollers similar to the Chinook Cargo On/Off Loading System (COOLS) was also considered. In addition to weight considerations, after consultation with a SAR pilot it was decided that this system would not be ideal for victim rescue operations as all the additional parts would be more difficult to keep clean and smoothly running. With all of the potential blood and dirt from the disaster zone, it was important to avoid any unnecessary crevices in which these contaminants could get caught. The relief material is easily held in place using cargo netting that hooks onto the aircraft using the universal fittings. Distribution of the relief aid is done using small parachutes. Once the vehicle reaches the desired relief drop point, braking parachutes are released and pulled from the vehicle by a drogue chute. The braking parachutes pull the load from the vehicle to the ground within the drop zone. The main parachutes are sized to stop the movement of the load sliding on the ground within the required space, and are not intended to control the descent of the load to the ground. Once the drop is completed, the aircraft can climb to the required altitude and return to base. These procedures, whether done for the entire load at once, or for several smaller portions, are completed easily and quickly by a minimum number of crew.

18.4 Mission 3 – CASEVAC

The third mission required is possibly the most demanding of all three in regards to configurability requirements. The *HeliX* has only a three person crew and yet is required to land and recover six wounded persons within a thirty minute timeframe.

Because it is unknown if patients are ambulatory or not, the Team decided that it would be necessary to install at least six supine stretchers. One problem with positioning the patients in a supine position, however, is that it subjects the

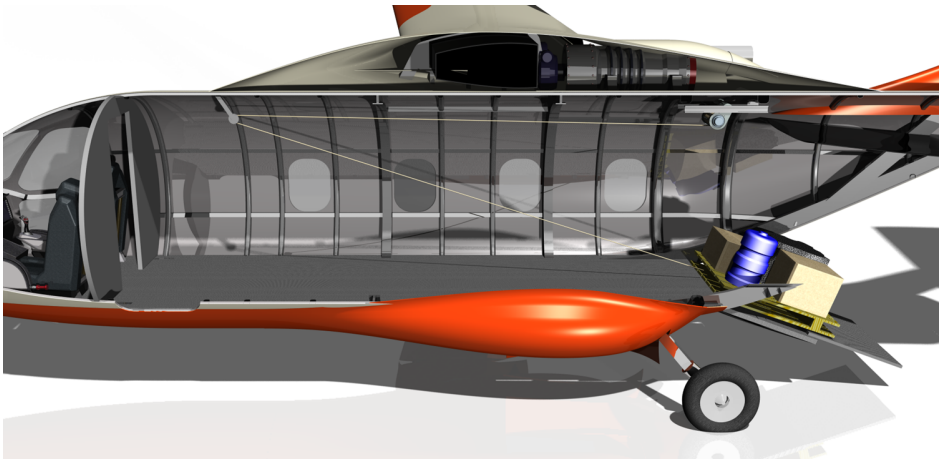

Figure 18.1: Redirection of winch cable for cargo loading

patient to undesirable vibrations that could accelerate bleeding and worsen the patient prognosis [52]. To combat the negative effects of unwanted vibrations, the team decided to use the NODIN Aviation AS NT-620 stretcher rack for individual damping of vibration, jolt, and shock. These stretchers comply with the NATO standard, STANAG 2040 as well as 3204AMD, annex E.

One of the reasons this stretcher system was chosen was the ability to set up the system quickly and efficiently. Stretchers are stored folded in a 0.035 m^3 package, and take only one person to unfold. Additionally, the rack for stacking patients is compact, and can be attached to preinstalled anchoring points quickly and by one person. This setup allows the vehicle to change its role into a casualty evacuation (CASEVAC) vehicle within 5 minutes. NODIN even claims that the setup and loading of three patients can be done within 2 minutes of landing. If this time were doubled to account for unforeseen problems on the ground, and then doubled for the installation of 6 victims, the 8 minutes required is far less than the 30 minute requirement in the RFP. As shown in Fig. 18.2, these stretchers can be stacked three-high as long as the floor and ceiling anchor points are 1.85 m apart. Because of the easy and quick configurability, as well as

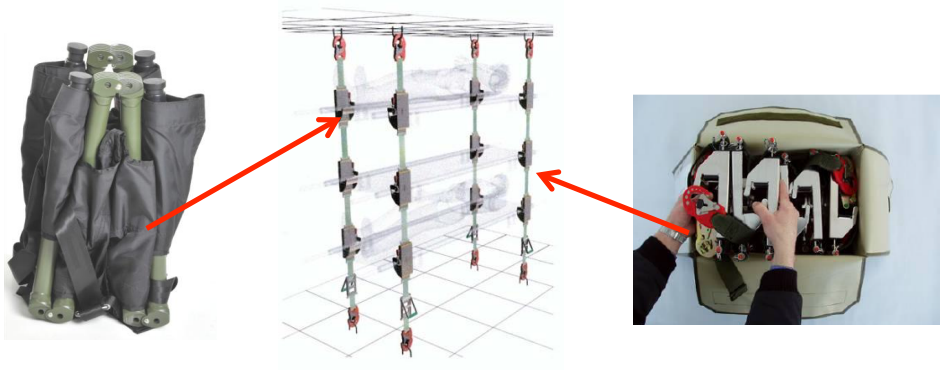

Figure 18.2: NODIN vibration supressing stretcher rack

the relatively low weight of the entire system, the *HeliX* does not necessarily need to return to base to be reconfigured for a CASEVAC mission. If one of the vehicles within the fleet were to complete its mission early, or even had extra fuel on board (which could be possible with the fuel tank capacities installed), the vehicle could be configured by the third crew member and used to evacuate more victims.

Other equipment that would be needed on board for a CASEVAC mission are detailed in Table 18.1. Because the

HeliX has a limited crew, the equipment required is also limited. Only one of items such as the laryngoscope, AED, or lab analyzer, which is capable of monitoring multiple patients, is required, but there may be multiple indicated in the table to account for situations in which batteries may not be fully charged or malfunctioning. All equipment is certified for use in aircraft.

Table 18.1: CASEVAC mission equipment

Equipment	Manufacturer	Number Required	Total Weight,kg (lb)
Stretchers/Attachment Rack	NODIN Aviation	6/2	58.1 (128)
Head/Neck Stabilizers	Ambu Ace Adult and Child Collar	10	3.31 (7.3)
Portable EKG and Lab Analyzer	TEMPUS IC	2	5.44 (12)
Defibrillator	MEDAire AED	3	4.76 (10.5)
Medical Dressings	MEDAire Emergency Medical Kit	1	10.0 (22)
Intubation Equipment	McGrath Video Laryngoscope*	1	0.45 (1)
Isotonic Crystalloids+	Moore Medical	10 x 2 L of fluid	21.1 (46.5)
Foldout seating	ORO Manufacturing Company	4	18.1 (40)

* Comes with replaceable blades for use on multiple patients

+ Intravenous (IV) fluid for maintaining osmotic pressure

In the event that a rescue needs to take place without landing, the *HeliX* can use the winch/hoist, as described in Section 18.3. A HF digital camera is installed such that the pilot can see a rescue happening on one of the multi-functional displays in the cockpit, and adjust vehicle position as needed. However, to offload some work from the pilot, the winch operator has been given limited capability to override the hover position while the aircraft is in an autopiloted hover. It should be noted that all rescues will require the use of two people, so if the *HeliX* only has three crew, the co-pilot will not be in the cockpit during these missions.

As shown in Fig. 18.3, the stretcher racks have four different possible positions: two anchor point sets along each side of the cabin. If some of the victims are ambulatory, the *HeliX* also is equipped to have four ORO Manufacturing Company certified foldout seats. These seats, the same as those found on the C-130, are described in Table 18.2 and each seat up to 2 people; this increases the available seating for wounded from 6 to 14. If all patients are ambulatory, the *HeliX* can transport up to 18 patients. It should be noted that the foldout seats are not crashworthy.

Table 18.2: Foldout seats

Seat Section	Measurement, m (in)
Seat Depth	0.38 (15)
Back Height	0.76–1.19 (30–47)*
Bench Width	0.91 (36)
Leg Separation	0.51 (20)

* Adjustable

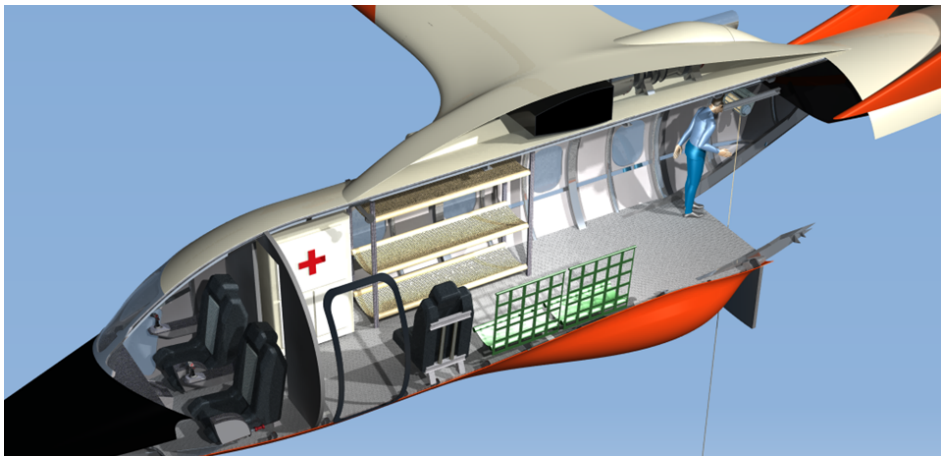

Figure 18.3: Possible internal configuration during SAR operations

18.5 Alternate Vehicle Configurations

Because of its size, the *HeliX* is capable of performing a variety of other tasks. The high range and speed capabilities make it ideal for VIP transport applications. As mentioned in Section 18.1, the UAFs make installing a variety of equipment simple. *HeliX* can hold up to an additional 12 crashworthy seats for passenger transport missions.

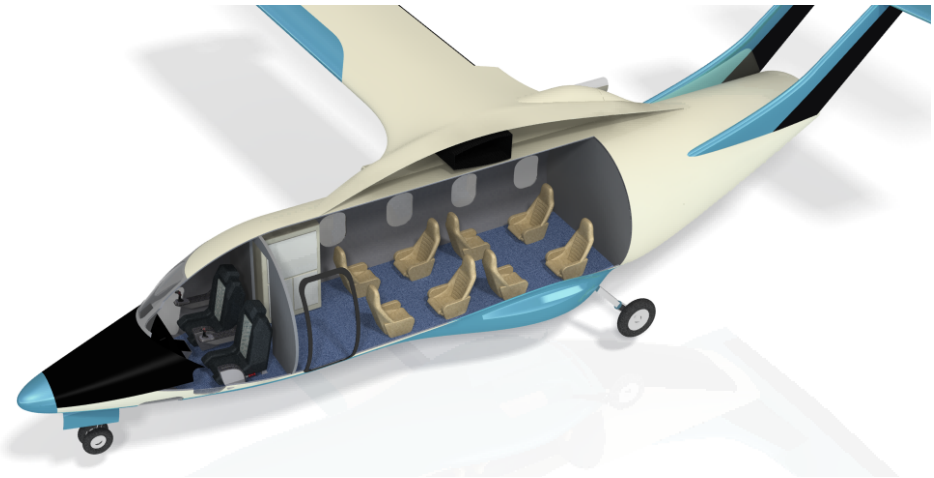

Figure 18.4: Possible VIP transport configuration

19 Search and Rescue Scenario Simulation

This section describes a realistic disaster situation to evaluate how the *HeliX*, and a fleet of such aircraft, would perform. The performance and effectiveness of the *HeliX* is then compared against helicopters in current use by the U.S. Coast Guard for such disaster scenarios.

19.1 Motivation

The RFP outlines requirements for a fleet of highly autonomous aircraft to perform reconnaissance, aid distribution, and SAR tasks. To demonstrate that the *HeliX* can fulfill this requirement with ease and proficiency, a real-world, well-known natural disaster was selected as a model. This simulation employed optimized path planning to route a small fleet of two aircraft out to rescue several groups of stranded, injured people spread over hundreds of square miles of the Gulf coastline, spanning three states.

The ability of the *HeliX* to navigate the disaster zone is second to none, shown clearly by the evaluation of well-defined comparison metrics. Flight paths are defined by priorities to rescue critically-injured persons while minimizing fuel consumption. Ultimately, these metrics are used to estimate the performance of the *HeliX* in a disaster of a large magnitude.

19.2 Scenario Description

Hurricane Katrina was selected as the natural disaster for the simulations. Katrina caused catastrophic damage including more than 1,800 casualties in the New Orleans area and along the Gulf Coast, severely challenged those tasked with providing relief. The group of responders to perform most impressively was undeniably the U.S. Coast Guard, who rescued 33,500 people out the overall 60,000 stranded people in the New Orleans area alone.

In light of these statistics, the simulation was also executed employing Eurocopter's Dolphin helicopter and also Sikorsky's Jayhawk to provide basis for comparison with the capabilities of the *HeliX*. To realistically model a SAR scenario, data were collected on the areas affected by the far-reaching hurricane. The simulated disaster zone was populated with hundreds of widespread distress locations from which groups critically or non-critically injured people were awaiting rescue and transport to medical facilities. These coordinates were selected from maps of the Gulf Coast fitted with overlays of location-specific data, which indicated regions of Katrina's destruction and flooding.

In the simulation, a small fleet of homogeneous helicopters cruise to priority destinations, hovering at these locations for the duration of their rescue. Because of the prevalence of flooding associated with this specific disaster, all rescues were assumed to be performed via hoist while the aircraft was in hover. All parts of the flight profile associated with takeoff, climb to altitude, and landing have been neglected for simplicity. The duration of the rescue was determined by multiplying the number of stranded people at a given location by a factor of difficulty (from easily manageable, average, and most difficult) and also by a factor defined as the assumed hoist time per person. The time required to unload passengers once they were transported to a medical center outside the boundaries of the disaster zone and the time required to refuel a vehicle once it has arrived at an airfield outside the disaster zone were accounted as factors. However, the hoist, unload, and refuel durations were assumed to be constant, independent of the platform.

19.3 Routing the Fleet

A high degree of autonomy within the fleet is achieved via global mobile satellite communications. Vehicles tasked with reconnaissance are sent out to canvas the devastated area, scouting for people in distress. These first responders compile a database of intelligence, including location, status, and number of people to be rescued. This information can be relayed between vehicles by using a real-time datalink. The scouting aircraft can initiate a periodic contract

with the members of the SAR fleet, which allows the scouts to request from each of the fleet aircraft its current coordinates, fuel level, number and status of victims, as well as the elapsed time since having been identified as needing rescue of any all patients onboard. This exchange of information occurs without any pilot interaction. Updating position information with such ease and frequency not only makes it possible to safely deploy a greater number of vehicles within limited airspace, it also helps to reduce pilot workload.

In the simulation, this periodic exchange of information and route assignment is modeled with discrete time steps. At each new time, new information comes in to update the scout's database, and the queue of victims waiting to be rescued is prioritized. Among the critically-injured, priority is given to the those who have been waiting the longest in an attempt to increase the chances of getting them to the medical attention within the golden hour. The next highest priority is the remaining critically-injured, not having the greatest elapsed time, and finally the non-critically injured are targeted. Considering the current condition of each aircraft in the fleet, a flight path optimized to maximize chance of survival and minimize fuel burn is assigned to each, relayed via the datalink.

Aircraft are continually routed to rescue destinations to perform hoists until the maximum capacity of victims is reached. If the total number of victims at a destination exceeds the remaining capacity of the aircraft, as many as possible are rescued and that location remains in the queue and the number of victims needing rescued there is reduced appropriately; it will be revisited at a later time. To minimize the fuel burn, the route taken by the aircraft must be as close to optimal as possible. This goal was achieved by implementing a Modified Traveling Salesman Problem (MTSP), which weighed the viability of rescue targets based on injury status and elapsed time in addition to the distance between targets.

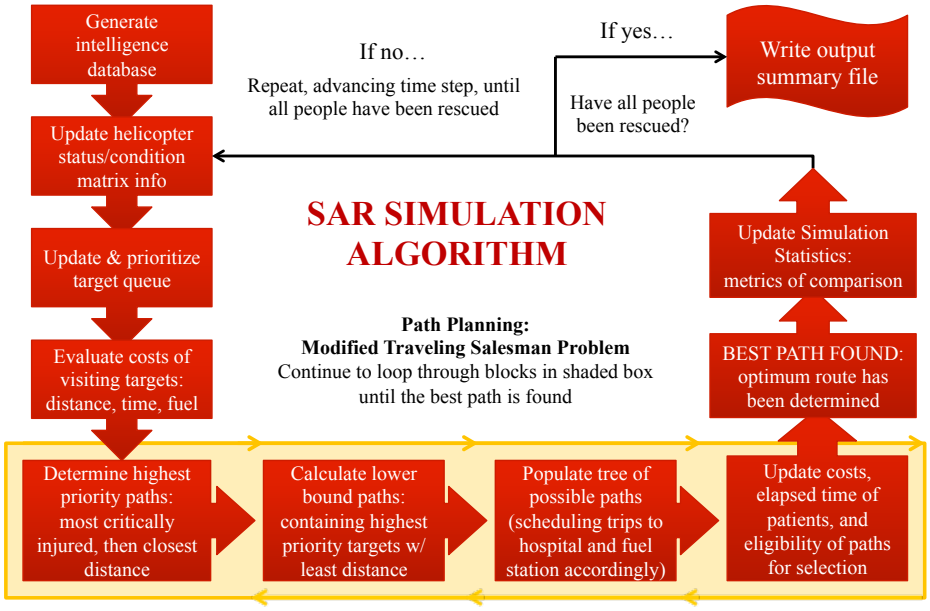

Figure 19.1: Modified Traveling Salesman Problen used to determine optimimum flight paths for fleet aircraft.

19.4 Metrics for Comparison

To evaluate proficiency of different vehicle platforms in navigating the SAR scenario, specific metrics of comparison were defined. The rescue rate is defined as the number of victims rescued per hour. In average distance per tour, a tour is defined as the journey from the medical center out to target(s) and/or the refueling location, and ultimately returning to the medical center. The total time and total fuel is a measure of efficiency, referring to the quantities required to complete the SAR scenario, which concludes when all of the victims have been rescued and transported to a medical center.

The golden hour ratios offer an assessment of mission success, with the critical golden ratio evaluating the number of critically-injured people who were transported to medical attention within one hour. Similarly, the total golden ratio relates the number of people being delivered to receive care within an hour of being discovered to the total number of people needing rescue throughout the simulation.

These metrics were evaluated for the *HeliX* with the minimum critically-injured PAX capacity as required by the RFP as well as for the maximum mixed PAX capacity (critical and non-critical casualties) the vehicle can accommodate. The *HeliX* is capable of transporting up to as many as 18 non-critically injured persons at a time, but this particular vehicle configuration was not simulated due to the likely abundance of critical casualties in such a situation.

Table 19.1: Simulation Results: Metrics for Comparison.

	Dolphin	*Jayhawk*	*HeliX*	*HeliX*
PAX Capacity	3	4	6	12
Rescue Rate [PAX/hr]	2.22	2.44	4.18	6.67
Avg Dist per Tour [km]	193	290	233	378
Total Time [hr]	38.5	42.0	25.0	16.5
Total Fuel [kL]	51.1	45.0	48.8	26.5
Critical Golden Ratio	0.30	0.37	0.71	0.79
Total Golden Ratio	0.55	0.57	0.74	0.86
Relative Productivity [PAX/hr/L]	1.00	1.17	1.86	5.45

Table 19.2: Scaled Results: Potential impact for a full-scale disaster of Katrina-magnitude.

	Dolphin	*Jayhawk*	*HeliX*	*HeliX*
PAX Capacity	3	4	6	12
Total Fuel [kL]	9,085	7,571	8,517	4,542
Relative Fuel Consumption	1.00	0.83	0.93	0.50
Fuel Cost [US dollars]	8.4 Million	7.0 Million	7.8 Million	4.2 Million

19.5 Conclusions from Simulation

For the same vehicle platform, namely the *HeliX*, it was shown that doubling the PAX capacity yielded a 46% reduction in fuel cost and a 34% reduction in total time to complete the simulation. Additionally, this extra capacity resulted in approximately a 10% increase in the golden hour ratios, for both critical and non-critical passengers. Comparing the simulation results across platforms, the *HeliX*, when configured to accommodate its maximum capacity of 12 critical and non-critical passengers, rescued 200 casualties in approximately 40% of the total time and for just over half the fuel. This result more than doubled the critical golden hour ratios of the U.S. Coast Guard models, which were the most successful in the Katrina relief effort.

Overall, the *HeliX* outperformed the stars of the most daunting hurricane relief effort in the history of the United States. Considering the public opinion that Katrina relief was poorly organized and executed far too slowly, this is a profound result. Reflecting back on such loss and tragedy prompts one to also look forward with hopes of a realizable, feasable, and affordable aircraft, capable of getting more people the help they need more quickly, and going farther and faster to do so. Scaling the simulation results by a factor of 175, to be comparable to a disaster of Katrina's magnitude, reveals a fuel cost savings for the *HeliX*, in this configuration, of \$2.8–4.2 *million*. This also comes with the added benefit of rescuing more people per hour and delivering more of them to medical care within the golden hour. This savings could then be put toward meeting the many other needs of affected communities, helping them to rebuild their lives.

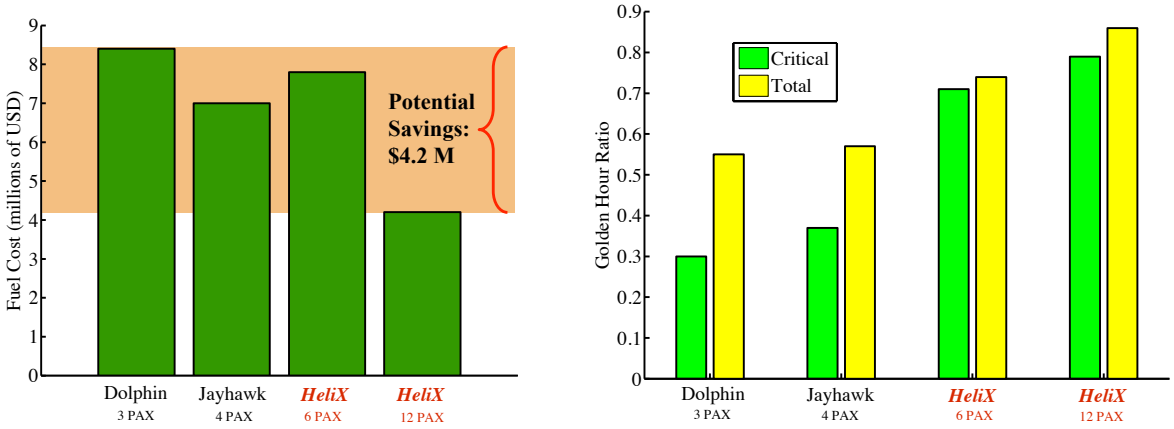

(a) Fuel costs

(b) Golden ratio

(c) Lag stiffness

(d) Relative productivity

Figure 19.2: Search and Rescue comparison metrics

20 Summary

The University of Maryland Graduate Team has designed the *HeliX* variable diameter tiltrotor to meet each of the vehicle and operational requirements mandated by the 2013 AHS Student Design Competition RFP, including the completion of fast deployment and SAR coordination, aid distribution, and evacuation missions. The mission capability of the Helix is unmatched by other current, commercial VTOL aircraft. This proposed design concludes:

1. Innovative technologies used in the design, such as the variable diameter rotor system and the outboard wing extensions (OWEs), increased forward flight and hover performance and efficiencies and improved fuel economy, thereby allowing for significant cost savings. The VDR system substantially reduced downwash velocities in hover by lowering disk loading, making this tiltrotor a much more viable solution for SAR. The pilots are unencumbered by the extension of the OWEs, as they are activated automatically by sufficient lift generation in forward flight. When they are not deployed, hover download is not exacerbated because of their vertical profile. Advantages such as these clearly benefit the customer because they directly contribute to satisfying the RFP requirements by increasing vehicle autonomy, efficiency, and performance.

2. The *HeliX*'s use of advanced technology increased its overall performance but also lowered its Direct Operating Cost to $5,499 per flight hour, comparable to other rotorcraft in its weight class. Its acquisition cost of $25.3 million ensured the customer received an affordable aircraft that is easily reconfigured for a variety of SAR mission types and deployed quickly around the world, while achieving levels of performance unprecedented in the rotorcraft community.

3. Large vehicle autonomy is also achieved by a state-of-the-art navigation suite, including a Traffic Collision Avoidance System and Enhanced Ground Proximity Warning System to assist during flight in degraded visual environments. A simulation algorithm automatically prioritized distress locations during stressful disaster conditions in a preliminary optimization study designed to reduce pilot workload. An Automatic Flight Control System (AFCS) architecture ensured a smooth flight mode transition, from helicopter to airplane mode and back, through responsive and continuous control mixing. The use of a Datalink allowed enhanced fleet operations in close quarters, minimizing pilot workload by tracking vehicle locations to safely share a confined airspace.

4. An SAR simulation, using real disaster data from Hurricane Katrina in 2005, evaluated the *HeliX* against the rescue aircraft that responded to each distress location. The superiority of the *HeliX* is evident in the scaled simulation result, saving more lives each hour with its greater range, speed, and PAX capacity, while providing an approximate fuel cost savings of $2.8–4.2 million.

These conclusions strongly support the assertion that the proposed HeliX design is ahead of the curve.

References

[1] Tishchenko, M. N., and Nagaraj V. T., "ENAE634 Helicopter Design Lecture Notes," University of Maryland, College Park , 2010.

[2] Johnson, W. "NDARC – NASA Design And Analysis of Rotorcraft Validation and Demonstration," AHS Aeromechanics Specialisists Meeting, San Francisco, CA, Jan. 20–22, 2008.

[3] "24th Annual AHS Student Design Competition 2007 Request for Proposal (RFP), sponsored by Sikorsky Corporation and AHS International,", 2007.

[4] *Environmental Protection, Vol. 1, Aircraft Noise* International Civil Aviation Organization, Fifth Edition, July 2008.

[5] Roskam, J. *Airplane Design: Preliminary Configuration Design and Integration of the Propulsion System* Design, Analysis and Research Corporation, Lawrence, KS, 2004.

[6] Raymer, D. P. *AMC Engineering Design Handbooks, AMCP-706 Series* USA DoD, Alexandria, VA, 1974.

[7] Yeo, H. and Johnson, W. with image courtesy to Harris, F. D. "Aeromechanics Analysis of a Heavy Lift Slowed-Rotor Compound Helicopter," *AIAA Journal of Aircraft*, Vol. 44, No. 2, 2007, p. 501.

[8] Prouty, R. W. *Helicopter Performance, Stability, and Control* Kreiger Publishing Company, Malabar, KS, 1995.

[9] Keys, C. N. "Rotary-Wing Aerodynamics, Volume II - Performance Prediction of Helicopters," NASA CR - 2083, 1979.

[10] Ward, T. A., *Aerospace Propulsion Systems* Wiley, 2010.

[11] Stahlhut, C. and Leishman, J. G. "Aerodynamic Design Optimization of Proprotors for Convertible-Rotor Concepts," 68th Annual Forum of the American Helicopter Society, Ft. Worth, TX, May 1–3, 2012.

[12] Celi, R. "Helicopter Rotor Blade Aeroelasticity in Forward Flight with an Implicit Structural Formulation," *AIAA Journal*, Vol. 30, No. 9, Sept. 1992.

[13] Davis, S. J., Fradenburgh, E. A., Moffitt, R. C., and Visintainer, J. A. "Variable Diameter Rotor Having an Offset Twist," United Technologies Corporation, Patent US 1993/5253979 A, June 1, 1992.

[14] Nixon, M. *Aeroelastic Response and Stability of Tiltrotors with Elastically Coupled Composite Rotor Blades* PhD thesis, University of Maryland College Park, 1993.

[15] Matuska, D. G., Gronenthal, E. W., and Jepson, D. "Torque Tube/Spar Assembly for Variable Diameter Helicopter Rotors," Sikorsky Aircraft Corporation, Patent US 5636969, March 28, 1995.

[16] Sheet, T. D., "Polyurethane Protective Tape 8542HS," 3M Corporation , November 2011.

[17] Palacios, J., Smith, E., and Rose, J. "Investigation of an Ultrasonic Ice Protection System for Helicopter Rotor Blades," Proceedings of the 64th Annual American Helicopter Society Forum, 2008, April 29–May 1, 2008.

[18] "Stanyl Polyamide 46 Typical Properties Data Sheet," DSM Corporation , 2005.

[19] Madison, R. K. "Pitch Change Bearing System," Bell Helicopter Textron Inc., Patent US 5110259, Sep. 10, 1990.

[20] Neathery, W. D., Broekhuizen, W., and Schellhase, E. C. "Constant Velocity Elastomeric Bearing Joint," Bell Helicopter Textron Inc., Patent US 4729753, Nov. 4, 1985.

[21] Fradenburgh, E. A., et al. "Drive System for Changing the Diameter of a Variable Diameter Rotor," United Technologies Corporation, Patent US 5299912, Apr. 1994.

[22] Walker, T. D. and Baskin, B. K. "Drive Mechanisms for Variable Diameter Rotor Systems," Sikorsky Aircraft Corporation, Patent US 20110206513 A1, Dec. 22, 2010.

[23] Prabhakar, T., Gandhi, F., and McLaughlin, D. "A Centrifugal Force Actuated Variable Span Morphin Helicopter Rotor," 63rd Annual AHS Forum and Technology Display, Virginia Beach, VA, May 1–3, 2007.

[24] Matuska, D. G., et al. "Reaction/Extension Mechanisms for Variable Diameter Rotors," Sikorsky Aircraft Corporation, Patent US 5642982, July 1997.

[25] Gmirya, Y. Z. "Harmonic Drive System for the Retraction/Extension of Variable Diameter Rotor Systems," Sikorsky Aircraft Corporation, Patent US 6454532, Jan. 23, 2001.

[26] Toshiba "Toshiba 2013 Motor Catalog," http://www.toshiba.com/ind/data/tag_files/LVM_Catalog.pdf, 2013.

[27] Federici, F. D. "Blade Lock System for Variable Diameter Rotor Systems," Sikorsky Aircraft Corporation, Patent US 6398497, Nov. 4, 1985.

[28] Sikorsky "Full-size helicopter runs on 100% electric power," http://www.dvice.com/archives/2010/07/sikorsky.php, 2010.

[29] Sikorsky "Project Firefly: Sikorsky Unveils Electric Helicopter Technology demonstrator," http://www.gizmag.com/sikorsky-project-firefly/15993/, 2010.

[30] GIGA, "Lithium Ion Battery - 45 Ah, 3.6 V," http://www.gaia-akku.com/fileadmin/user_upload/downloads/en/Handling_HP602030NCA-45Ah.162Wh.pdf, 2009.

[31] Boeing "V-22 Osprey," http://www.boeing.com/boeing/rotorcraft/military/v22/v22spec.page, 2013.

[32] Flightglobal, http://www.flightglobal.com/cutaways/, 2012.

[33] Brigade, 1. A. "United States Army Aviation Warfighting Center UH-60A Auxiliary,".

[34] Brigade, 1. A. "United States Army Aviation Warfighting Center UH-60A Powertrain/Rotor System,".

[35] Honeywell International Inc., "Honeywell Generators," http://honeywell.com/sites/aero-technology/Key-Technologies/Documents/generators.pdf, 2006.

[36] Rashidi, M. and Krantz, T. *Dynamics of a Split Torque Helicopter Transmission* Scholarship Collection, 1992.

[37] Bellocchio, A., "Drive System Design Methodology for a Single Main Rotor Heavy Lift Helicopter," Master's thesis, Georgia Tech, 2005.

[38] Dudley, D. W. *Handbook of Practical Gear Design* Technomic Publishing, Boca Raton, 2002.

[39] Peyran, R. J. and Rand, O. "The Effect pf Design Requirements on Conceptual Tiltrotor Wing Weight," 55th Annual Forum of the American Helicopter Society, Montreal, Quebec, Canada, May 25–27, 1999.

[40] Johnson, W. "Dynamics of Tilting Proprotor Aircraft in Cruise Flight," NASA TN D-7677, 1974.

[41] Nixon, M., Piatak, D., Corso, L., and Popelka, D. "Aerodynamic Tailoring for Stability Augmentation and Performance Enhancements of Tiltrotor Aircraft," 55th Annual Forum of the American Helicopter Society, Montreal, Quebec, Canada, May 25–27, 1999.

[42] Nixon, M. "Aeroelastic Response and Stability of Tiltrotors with Elastically Coupled Composite Rotor Blades," Master's thesis, University of Maryland College Park, 1993.

[43] Desjardins, S. "The Evolution of Energy Absorption Systems for Crashworthy Helicopter Seats," *Journal of the American Helicopter Society*, Vol. 51, No. 2, 2006.

[44] Hu, W., Wereley, N. M., Ngatu, G., Hiemenz, G. J., and Woodhouse, J. "Lightweight Magnetorheological Energy Attenuation System for Rotorcraft Seats," American Helicopter Society 68th Annual Forum, Ft. Worth, TX, 2012.

[45] Ritland, P. "System and method for heating an air intake of turbine engine," United Technologies Corporation, Patent US 2006/0090472 A-1, May 4, 2006.

[46] Rand, O. "RaPID," Rand Technologies and Engineering, Computer Program, 2013.

[47] Bell Helicopter Textron Inc. "Bell 430 Product Data," `http://www.eas-helicopter.de/downloads/430_Data.pdf`, 2003.

[48] Harris, F. D. and Scully, M. P. "Helicopters Cost Too Much," American Helicopter Society 53rd Annual Forum, Virginia Beach, VA, April 1997.

[49] " U.S. Department of Labor, Consumer Price Index, Bureau of Labor Statistics," `www.bls.gov/home.htm`, 2010.

[50] Conklin & de Decker "Life Cycle Cost: Helicopters," .

[51] U.S. Congress, Office of Technology Assessment "New Ways: Tiltrotor Aircraft and Magnetically Levitated Vehicles," OTA-SET-507 1991.

[52] Carchietti, E, A Cecchi, F Valent, and R Rammer. "Flight Vibrations and Bleeding in Helicoptered Patients with Pelvic Fracture.," *Air Medical Journal*, Vol. 32, No. 2, 2013, pp. 80–83.